

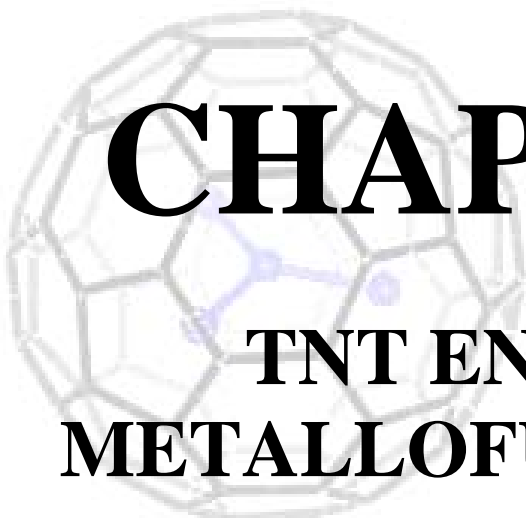
PART II. RESULTS

Chapter 4 TNT endohedral
metallofullerenes 63

Chapter 5 Heterohedral metallofullerenes
..... 153

Chapter 6 $M(\text{PH}_3)_2$ exohedral
metallofullerenes 233

Chapter 7 Final conclusions 273



CHAPTER 4

TNT ENDOHEDRAL METALLOFULLERENES

Fullerenes containing a trimetallic nitride template (TNT) within the cage are a particularly interesting class of endohedral metallofullerenes (also termed incarcerated fullerenes). Hereafter, they will be referred to as TNT endohedral metallofullerenes. Not only are the cage properties modified by the presence of the incarcerated group but, almost uniquely amongst endohedral metallofullerenes, they are quite stable. Furthermore, they can be produced in multimilligram quantities, and these amounts should increase in the future. The electronic effect of the TNT group is such that some fullerenes of sizes and symmetry that are otherwise relatively unstable become available for investigation. Classical endohedral metallofullerenes contain a large variety of stoichiometries that are the combination of fullerene cages with different numbers and varieties of incarcerated metals. In C_{28} , for example, there is only one metal atom whereas in the higher C_{84} fullerene there are as many as three. TNT endohedral metallofullerenes are the first time that a four-atom metal unit has been encapsulated inside a fullerene cage. These TNT metallofullerenes mostly have the following stoichiometries: $Sc_{3-n}M_nN@C_k$ ($n = 0-3$, $M = Y, La$ and lanthanides; $k = 68, 78, 80$). They are prepared using a modified Krätschmer-Huffman arc generator under N_2 atmosphere. The main advantage they have over classical endohedral metallofullerenes is that the structure can be determined by a single crystal X-ray diffraction study. This is an important advance because crystallization has long been a bottleneck in the structural determination of classical endohedral metallofullerenes, whose metals can present different oxidation states and geometrical positions in a single

stoichiometry. Also, because these TNT endohedral metallofullerenes can be synthesized in high yields and consequently they have already been fully characterized. Now they are about to be exohedrally functionalized. So, these new endohedral metallofullerenes have attracted special interest as new spherical molecules with novel properties ever since they were first detected in 1999.

This chapter is structured in the same way as chapters 5 and 6. All three chapters consist of four different parts. They start with an introduction to the experimental and theoretical studies which provide valuable information about the aspects that will be dealt with in the future sections and then go on to discuss the kind of metal bond between the metal unit and the carbon cage. Subsequently they describe their isomerism, properties and reactivity, and the chapters end with a section of concluding remarks.

In this chapter, section 4.1 starts with a comprehensive review of all the experimental and theoretical studies of the $Sc_3N@C_k$ ($k = 68, 78, 80$) complexes. Section 4.2 uses the fragment molecular orbital method to conclude that an ionic bond between the TNT unit and the cage explain the most important electronic behavior and geometry of these new endohedral metallofullerenes. Section 4.3 deals with the rapid motion of the TNT unit inside the cage and studies several isomers of $Sc_3N@C_k$ ($k = 78, 80$) constructed by the Sc_3N rotation. Section 4.4 compares the physical properties of the $Sc_3N@C_k$ ($k = 68, 78, 80$) complexes with those of free fullerenes and classical endohedral metallofullerenes. The wide variety of TNT units encapsulated inside the fullerene cages is discussed in section 4.5. We pay particular attention to the effects of increasing the ionic radii and decreasing the electronegative character when Sc atoms are replaced progressively by Y and La atoms. Section 4.6 is the biggest step forward in this area: it describes an easy way of determining which fullerenes will be capable of encapsulating TNT units. At the end of the chapter, we investigate the exohedral reactivity of these TNT endohedral metallofullerenes via $[4 + 2]$ cycloaddition reactions (section 4.7) and hydrogenation/fluorination reactions (section 4.8).

4.1 INTRODUCTION	67
4.1.1 <i>Experimental part</i>	67
4.1.2 <i>Theoretical part</i>	69
4.2 IONIC BOND BETWEEN THE FULLERENE AND THE TRIMETALLIC NITRIDE TEMPLATE (TNT)	70
4.2.1 <i>Structures of Sc₃N@C_k (k = 68, 78, 80)</i>	70
4.2.2 <i>Ionic model</i>	76
4.2.3 <i>Electron charge transfer</i>	78
4.2.4 <i>Decomposition of the encapsulation binding energy (EBE)</i> ..	80
4.3 ISOMERISM	84
4.3.1 <i>Sc₃N@C₇₈</i>	84
4.3.2 <i>Sc₃N@C₈₀</i>	90
4.4 PHYSICAL PROPERTIES	91
4.5 EXTENDED FAMILY: M₃N@C_k (M = La, Y; k = 78, 80)	93
4.5.1 <i>Experimental considerations</i>	93
4.5.2 <i>Geometry considerations</i>	95
4.5.3 <i>Electronic structure</i>	95
4.5.4 <i>Decomposition of the EBE</i>	97
4.6 GENERAL RULE FOR THE STABILIZATION OF CAGES ENCAPSULATING TNT UNITS	99
4.6.1 <i>The stability can be predicted</i>	99
4.6.2 <i>Bond resonance energy (BRE) method</i>	100
4.6.3 <i>LUMO+3–LUMO+4 gap method</i>	101

4.7 EXOHEDRAL REACTIVITY (I): [4 + 2]	
CYCLOADDITION	103
4.7.1 <i>Experimental and theoretical considerations</i>	104
4.7.2 <i>Effects of TNT encapsulation on exohedral reactivity</i>	105
4.7.3 <i>[4 + 2] cycloaddition on $Sc_3N@C_{80}$</i>	115
4.7.4 <i>Clues about [4 + 2] cycloaddition on $Sc_3N@C_k$ ($k = 68, 78$)</i>	119
4.8 EXOHEDRAL REACTIVITY (II): FLUORINATION	
OF $Sc_3N@C_{80}$	124
4.8.1 <i>Experimental part</i>	124
4.8.2 <i>Hydrogenation binding energies (HBE) for I_h-C_{80}</i>	124
4.8.3 <i>HBE for $Sc_3N@C_{80}$</i>	129
4.8.4 <i>Sc_3N encapsulation in free cages vs. hydrogenated fullerenes</i>	130
4.8.5 <i>Stabilities of $C_{80}H_{52}$ and $C_{80}F_{52}$ isomers</i>	132
4.8.6 <i>Stabilities of $Sc_3N@C_{80}H_{52}$ isomers</i>	134
4.8.7 <i>Geometric and electronic structure of $Sc_3N@C_{80}H_{52}:5$</i>	135
4.8.8 <i>Factors affecting the stabilization energies</i>	138
4.9 CONCLUDING REMARKS	141
REFERENCES AND NOTES	146

4.1 INTRODUCTION

4.1.1 Experimental part

Many fullerenes with encapsulated metals and nonmetals have been reported, but they are typically formed in low yields (< 0.5 %) with multiple isomers of low symmetry, which have prevented progress in the exploration of the chemical and physical properties. However, a new family of trimetallic nitride template (TNT) endohedral metallofullerenes have been reported recently in relatively higher yields with a general formula of $A_3\text{-}_nB_n\text{N}@C_k$ ($n = 0\text{-}3$; $A, B =$ group III, IV and rare-earth metals; $k = 68, 78, 80$). The archetypal examples, in the chronological order of their first reported synthesis are: $\text{Sc}_3\text{N}@C_{80}$,¹ $\text{Sc}_3\text{N}@C_{68}$ ^{2,3} and $\text{Sc}_3\text{N}@C_{78}$.⁴ These new endohedral metallofullerenes were prepared by the Krätschmer-Huffman arc fullerene preparation with graphite rods doped with A_2O_3 and B_2O_3 oxides in a dynamic atmosphere of helium and nitrogen in relative yields of 8:1:1, respectively. In fact, the first of these fullerenes, $\text{Sc}_3\text{N}@C_{80}$, is the third most abundant fullerene and is only exceeded by C_{60} and C_{70} . After the soot is produced, these TNT endohedral metallofullerenes are isolated through a three-step high-pressure liquid chromatography (HPLC) procedure.⁵

The macroscopic quantities of TNT endohedral metallofullerenes make them available for chemical and physical characterization. $\text{Sc}_3\text{N}@C_{80}$ has been characterized by ^{13}C , ^{14}N and ^{45}Sc NMR spectroscopy, UV/vis spectroscopy and single-crystal X-ray diffraction of the cocrystallized solid: $\text{Sc}_3\text{N}@C_{80}\cdot\text{Co}^{\text{III}}\text{-}(\text{OEP})\cdot 0.5\text{C}_6\text{H}_6\cdot 1.5\text{CHCl}_3$ (OEP is the dianion of octaethylporphyrin).^{1,6} ^{13}C NMR analysis revealed that the Sc_3N moiety is planar encapsulated in the highly symmetric $I_h\text{-C}_{80}$:**7** isomer. The cage is stabilized as a result of electron charge transfer between the TNT unit and the fullerene cage. The ^{13}C NMR results also suggested that internal motion of the Sc_3N unit yields a time-averaged electronic environment that preserves the overall I_h symmetry for the carbon cage. The encapsulated Sc_3N unit is not localized at any specific internal bonding sites. The ^{45}Sc NMR spectrum exhibited a single symmetric line which is also indicative of a dynamic structure.¹ On the other hand, the rotational modes from temperature-dependent Raman and infrared spectroscopy studies gave a

direct evidence of the formation of a $\text{Sc}_3\text{N}-\text{C}_{80}$ bond, which significantly reduces the symmetry.⁷ It is important to notice that the relaxation times of the vibrational excitations are shorter than those of the magnetic resonance methods. These UV/vis and Raman studies have been extended to a variety of $\text{M}_3\text{N}@\text{C}_{80}$ ($\text{M} = \text{Y}, \text{Tb}, \text{Ho}, \text{Er}$) complexes.⁸ Recently, the isolation of a new isomer of $\text{Sc}_3\text{N}@\text{C}_{80}$, which corresponds to the Sc_3N encapsulation inside the $D_{5h}\text{-C}_{80}$:**6** isomer, has been characterized by HPLC, mass spectroscopy and ^{13}C NMR.⁹ Neither of these C_{80} isomers has been isolated as empty fullerenes and are not even the most stable isomers among the 7 distinct isomers that satisfy the so-called isolated pentagon rule (IPR).¹⁰ In the case of $\text{Sc}_3\text{N}@\text{C}_{78}$ the ^{13}C NMR analysis revealed that the $D_{3h}\text{-C}_{78}$:**5** isomer encapsulates the planar Sc_3N . This isomer has not been calculated as the most stable or it has never isolated as an empty cage. It is very interesting to see that the empty fullerene isomers isolated so far are often different from the carbon cages found in isolable metallofullerenes. On the other hand, the $\text{Sc}_3\text{N}@\text{C}_{68}$ molecule is an exception to the IPR rule: it has three pentalenes (fused pentagons). The TNT unit in each complex is oriented differently with respect to the fullerene cage. Whereas in $\text{Sc}_3\text{N}@\text{C}_{78}$ the metals reside over the set of C27–C28 bonds, a pyracylene C–C bond type (Appendix A.5), the X-ray characterization for $\text{Sc}_3\text{N}@\text{C}_{80}$ and $\text{ErSc}_2\text{N}@\text{C}_{80}$ ¹¹ shows that the metals reside over individual carbons in the latter and near the center of 6:5 C–C bonds in the former. Pyracylene C–C bonds consist of 6:6 ring junctions abutted by two hexagons (see Appendix A.1 for the different C–C bond types in IPR fullerenes). Special attention has been paid to Lutetium-based TNT endohedral metallofullerenes, $\text{Lu}_{3-n}\text{A}_n\text{N}@\text{C}_{80}$ ($n = 0-2$; $\text{A} = \text{Ga}, \text{Ho}$), because they may prove useful as multifunctional contrast agents for X-ray, MRI and radiopharmaceuticals, thereby eliminating the need for three separate agents.¹²

The chemistry of the TNT metallofullerenes may become a substantial area of fullerene research, and it is particularly interesting not only because of the electronic effect of the incarcerated molecule, but because unusual C–C bonding characteristics may exist on the modified fullerene surface. Unfortunately, little is known about the exohedral reactivity of TNT endohedral metallofullerenes. Recently, however, the first organic derivative of the most common TNT endohedral metallofullerene,

$\text{Sc}_3\text{N@C}_{80}$, has been successfully synthesized and characterized by functionalizing the exterior of the cage via the [4 + 2] cycloaddition reaction with 6,7-dimethoxyisochroman-3-one.^{13,14} The addition product occurs across a 6:5 rather than a 6:6 C–C bond and has a mirror plane of symmetry as observed from the ^{13}C spectrum. The formation of water-soluble fullerlenols $\text{Sc}_3\text{N@C}_{80}(\text{OH})_n\text{O}_n$ ($n = ca. 10$) have also been reported (the value of n is very approximate as no structural characterization was obtained).¹⁵ Finally, experiments have been carried out with the hydrogenation and fluorination of $\text{Sc}_3\text{N@C}_{80}$ but the results about the number of H or F atoms added to the fullerene surface are unclear.¹⁶ The $\text{Sc}_3\text{N@C}_{78}$ has also been functionalized with a ^{13}C -labeled reagent to afford mono-, di- and triadducts. ^{13}C and ^1H NMR data about the monoadduct suggests that the addend is added to an asymmetric site in the C_{78} carbon cage.¹⁷

4.1.2 Theoretical part

The electronic distribution for $\text{Sc}_3\text{N@C}_{80}$ is $(\text{Sc}^{3+})_3\text{N}^{3-}\text{@C}_{80}^{6-}$. Electronic structure calculations showed that the stability of the $I_h\text{-C}_{80}:\mathbf{7}$ isomer increases markedly when six electrons are added to the cage.¹⁸ As a result, the I_h isomer becomes the most stable structure for C_{80}^{6-} .¹⁹ Seven isomeric structures of C_{80} (with symmetries and numbering: $D_{5d}\text{-C}_{80}:\mathbf{1}$, $D_{2\text{-}C}_{80}:\mathbf{2}$, $C_{2v}\text{-C}_{80}:\mathbf{3}$, $D_3\text{-C}_{80}:\mathbf{4}$, $C_{2v}\text{-C}_{80}:\mathbf{5}$, $D_{5h}\text{-C}_{80}:\mathbf{6}$ and $I_h\text{-C}_{80}:\mathbf{7}$) fulfill the IPR.²⁰ Two empty cage isomers, $D_2\text{-C}_{80}:\mathbf{2}$ and $D_{5d}\text{-C}_{80}:\mathbf{1}$, have been isolated²¹ and theoretical calculations have shown that the $I_h\text{-C}_{80}:\mathbf{7}$ structure is the least stable isomer overall.²² In contrast, in the TNT endohedral metallofullerenes, only the cages with I_h and D_{5h} symmetry have been found. $\text{Ti}_2\text{@C}_{80}$ has also been shown to have D_{5h} symmetry through electron energy loss and ^{13}C NMR spectroscopic studies.²³ In very recent theoretical work, Kobayashi et al. have shown that the I_h isomer is strongly stabilized by the presence of the TNT unit inside the cage and that in the series of $\text{Sc}_3\text{-}_n\text{La}_n\text{N@C}_{80}$ ($n = 0\text{-}3$) this stabilization decreases as the number of La atoms increases. The La_3N unit in these TNT endohedral metallofullerenes retains its pyramidal structure unlike Sc_3N in $\text{Sc}_3\text{N@C}_k$ ($k = 68, 78, 80$). Surprisingly, $\text{La}_3\text{N@C}_{80}$ has an electronic structure which is formally described as $\text{La}_3\text{N}^{8+}\text{@C}_{80}^{8-}$ according to Kobayashi et al..²⁴ For $\text{La}_2\text{@C}_{80}$,

calculations revealed that the I_h structure is favored with a formal $(\text{La}^{3+})_2@C_{80}^{6-}$ electron distribution within the molecule.²⁵

There are five IPR isomers for the empty C_{78} cage with the following symmetries and numbering: $D_3-C_{78}:\mathbf{1}$, $C_{2v}-C_{78}:\mathbf{2}$, $C_{2v'}-C_{78}:\mathbf{3}$, $D_{3h}-C_{78}:\mathbf{4}$ and $D_{3h'}-C_{78}:\mathbf{5}$.²⁰ Calculations carried out at different levels of theory for these empty cages suggest the following relative stability order: $C_{2v'}-C_{78}:\mathbf{3} > C_{2v}-C_{78}:\mathbf{2} > D_3-C_{78}:\mathbf{1} > D_{3h'}-C_{78}:\mathbf{5} > D_{3h}-C_{78}:\mathbf{4}$.²⁶ Three stable isomers of C_{78} have been separated and their symmetries identified as $C_{2v'}-C_{78}:\mathbf{3}$, $C_{2v}-C_{78}:\mathbf{2}$, and $D_3-C_{78}:\mathbf{1}$ through their ^{13}C NMR spectrum.²⁷ The X-ray structure of $\text{Sc}_3\text{N}@C_{78}$ corresponds to the encapsulation of the nitride moiety by the $D_{3h'}-C_{78}:\mathbf{5}$ cage, which is the second least stable empty cage isomer.

In conclusion, the wide range of novel TNT endohedral metallofullerenes, which can be prepared in reasonably high yields and purity, provide host-guest chemistry with new possibilities because of their unique structural, chemical and reactivity features. Experimental and theoretical studies of these new endohedral species are summarized in a very recent book by Nagase and Akasaka.²⁸

4.2 IONIC BOND BETWEEN THE FULLERENE AND THE TRIMETALLIC NITRIDE TEMPLATE (TNT)

4.2.1 Structures of $\text{Sc}_3\text{N}@C_k$ ($k = 68, 78, 80$)

Greater effort on resolving the geometric structure has been done on the $\text{Sc}_3\text{N}@C_{78}$ cluster. The $D_{3h'}-C_{78}:\mathbf{5}$ isomer is one of the five IPR isomers of C_{78} and therefore all C–C bonds involve 6:6 or 6:5 ring junctions. There are several kinds of 6:6 C–C bonds in $D_{3h'}-C_{78}:\mathbf{5}$, which range in distances from 1.372 to 1.470 Å. The shortest ones appear in the pyracylene C–C bonds (**A** type in Appendix A.1). On the other hand, the corannulene 6:5 C–C bonds (**D** type) have an average bond length of 1.44 Å. These values fall within the range of C–C distances reported in earlier theoretical studies.²⁶ A complete description of the different C–C bonds of $D_{3h'}-C_{78}:\mathbf{5}$ can be found in the Appendix A.5. There is no X-ray determinations for free C_{78} cages to check the computed geometries, but the present level of computation has demonstrated that is capable of reproducing the geometry of C_{60} very well. The computed distances for the two different C–C bonds in C_{60} are 1.397

and 1.452 Å (Appendix A.2), values that almost coincide with the experimental parameters of 1.391 and 1.455 Å from neutron powder diffraction²⁹ and of 1.401 and 1.458 Å from electron diffraction.³⁰

Although the free Sc₃N molecule is pyramidal with an optimized Sc–N bond length of 1.957 Å and a Sc–N–Sc angle of 99.1°, this fragment has a planar structure inside the cage of C₆₈, C₇₈ and C₈₀ fullerenes.^{1,2,4} A priori, several orientations of the Sc₃N unit inside the *D*_{3h}-C₇₈:5 fullerene are possible. However, the X-ray determination of Sc₃N@C₇₈ shows that the Sc₃N unit lies close to the original σ_h plane of the *D*_{3h}-C₇₈:5 cage. This most stable structure corresponds to the case in which the scandiums are over the set of C27–C28 bonds (pyracylene 6:6 C–C bond types) hereafter called as isomer **1**, Sc₃N@C₇₈:1. Such sites are completely analogous to the sites where metal units coordinate on the outside of fullerene surface in C₆₀, C₇₀ and C₈₄ (see Chapter 6). When a Sc₃N unit is encapsulated, there is a significant local distortion in the fullerene cage. This distortion results in the outward movement of the carbons closest to the scandium ions away from these ions. Thus this distortion resembles the distortions seen in the exohedral metallofullerene complexes, where binding to a metal center also results in an outward displacement of the fullerene carbons and an increase of the pyramidalization of the carbons bound to the external metal centers, see Chapter 6.³¹ A similar, but smaller, distortion has also been seen in the chemically modified endohedral, Sc₃N@C₈₀-C₈H₆(OCH₃)₂,¹³ see section 4.7. The Sc–N bond lengths were found to be 1.997 Å, a close value to the experimental one originally reported for Sc₃N@C₇₈, 1.983–2.125 Å. Nevertheless, a major discrepancy appears in the Sc–C bond lengths: hence, whereas the computed value of 2.255 Å is a common distance for Sc–C bonds, the experimental distances, which range between 2.024 and 2.107 Å in the original refinement with a fixed cage geometry, may be considered very short bond lengths for Sc–C bonds. Experimental and theoretical Sc–N and Sc–C distances are tabulated for the most stable TNT endohedral metallofullerenes in Table 4.1. The earlier X-ray crystallographic investigation of the structure of Sc₃N@C₇₈·Co(OEP)·1.5(C₆H₆)·0.3(CHCl₃) used rigid models for the fullerene cages to distinguish between the five possible IPR isomers for the C₇₈ cage and concluded that the *D*_{3h}-C₇₈:5 cage was present. The resulting model identified three different orientations of the *D*_{3h}-C₇₈:5 cage and three corresponding orientations of the Sc₃N unit.

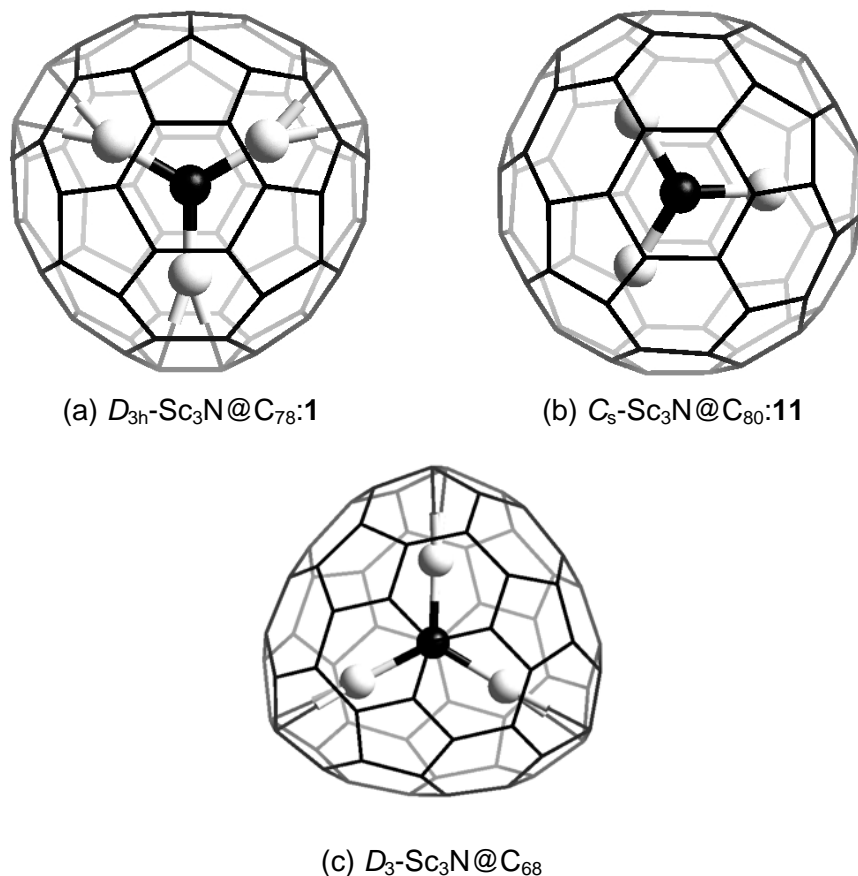


Figure 4.1 Optimized structures for $\text{Sc}_3\text{N}@C_{78}:1$ (a), $\text{Sc}_3\text{N}@C_{80}:11$ (b) and $\text{Sc}_3\text{N}@C_{68}$ (c). For more details see Figures 4.5 and 4.7.

With that model, the closest Sc–C contacts inside the cage were short (2.024 Å) and also quite far from the mean (2.430 Å) and shortest (2.204 Å) Sc–C distances obtained in an exploration of 73 examples in the Cambridge Structural Database.¹¹ Because of the orientational disorder, free refinement of the cage parameters that might have revealed any structural distortion of the cage by the Sc_3N unit could not be done as part of the original refinement. However, knowing that the Sc_3N unit produced a significant change in the dimensions of the C_{78} cage, it was appropriate to re-examine the crystallographic data. Consequently, the crystallographic data for $\text{Sc}_3\text{N}@C_{78}\cdot\text{Co}(\text{OEP})\cdot 1.5(\text{C}_6\text{H}_6)\cdot 0.3(\text{CHCl}_3)$ were re-refined by Balch and

co-workers using the optimized and computed structure of the C_{78} cage as a new model for the fullerene portion of the structure.³² Incorporation of this model in the structure into the three locations identified previously and further refinement, in which the orientations of these three groups were allowed to vary, produced a final structure in which the R factor decreased from 0.1107 to 0.0977. We consider this reduction in R to be significant and conclude that the computed structure is in better agreement with the experimental crystallographic data than was the formerly used rigid cage model. With this model, the Sc–C distances in the major site are Sc1–C34, 2.230(3); Sc1–C35, 2.281(3); Sc2–C27, 2.235(15); Sc2–C28, 2.206(15); Sc3–C41, 2.273(4); Sc3–C42, 2.239(4) Å. These values are within the range of Sc–C bond lengths found in the Cambridge Structural Database and are consistent with the calculated results reported. At the major site, the Sc–N distances are Sc1–N, 1.981(6); Sc2–N, 1.967(15); Sc3–N, 2.127(4). These values are similar to those obtained in the original refinement (Sc1–N, 1.988(7); Sc2–N, 1.983(15); Sc3–N, 2.125(5)).⁴ The Sc_3N unit is planar. The sum of the Sc–N–Sc angle is 360° . The individual Sc–N–Sc angles are Sc1–N–Sc2 130.1(5), Sc1–N–Sc3 114.0(2), and Sc2–N–Sc3, 115.9(6) (See Appendix A.5 for the carbon numbering system of the cage). The optimized structure of the most stable isomer of Sc_3NC_{78} is shown in Figure 4.1a. It is special to realize that the 6:6 C–C bonds linked to the three Sc atoms (C27–C28, C34–C35, C41–C42) increase their distances in 0.069 Å giving some clues about the kind of Sc–C₂ bond established in the $Sc_3N@C_{78}$ cluster.

The Sc_3N unit strongly stabilizes the icosahedral isomer of C_{80} , which is the most unstable of the seven structures that satisfy the IPR for the C_{80} stoichiometry. $I_h-C_{80}:7$ fullerene is spherical with almost non-differentiate C–C bonds, since this fullerene does not contain any pyracylene 6:6 C–C bond (**A** type), only corannulene 6:5 C–C bonds (**D** type) and **B** C–C bond types (Appendix A.1 and A.6). This geometry provokes that $I_h-C_{80}:7$ fullerene contains no high electron density π -bonds in contrast to the common fullerenes: C_{60} and C_{70} (compare bond orders in Appendix A.6, A.2 and A.3). In the case of $Sc_3N@C_{80}$ there is evidence from the ^{13}C NMR spectrum that the TNT may freely rotate inside the cage.¹ Thus, several different orientations of the TNT have been found for the slightly different TNT endohedral metallofullerenes of C_{80} :

Table 4.1 Comparison of some computed and experimental bond lengths for the most stable isomers of $\text{Sc}_3\text{N@C}_{68}$, $\text{Sc}_3\text{N@C}_{78}$ and $\text{Sc}_3\text{N@C}_{80}$ endohedral metallofullerenes^a

Complex	Method	Sc–N ^b	Sc–C ^c	Source ^e
$\text{Sc}_3\text{N@C}_{68}$	X-Ray	1.961-2.022	2.225	2
	DFT-BP	1.982	2.324	*
$\text{Sc}_3\text{N@C}_{78}:\mathbf{I}$	X-Ray	1.983-2.125	2.024	4
	X-Ray ^d	1.981-2.127	2.206	32
	DFT-BP	1.997	2.255	*
$\text{Sc}_3\text{N@C}_{80}:\mathbf{II}$	X-Ray	1.966-2.011	2.170	1
	DFT-BP	2.011-2.021	2.276	*

^a Distances in Å. ^b Range of Sc–N bond lengths. ^c Contact distances between Sc and the nearest neighbour carbon. ^d Re-examination. ^e * means data from this work.

$\text{ErSc}_2\text{N@C}_{80}$,¹¹ $\text{Sc}_3\text{N@C}_{80}$ ¹ and $\text{Sc}_3\text{N@C}_{80}\text{-C}_8\text{H}_6(\text{OCH}_3)_2$.¹³ However, we have chosen the most stable structure according to the calculations in order to study the bond between the nitride and the C_{80} cage. The differences among the most stable isomer are rather small, 0.00-0.10 eV, see subsection 4.3.2. In the theoretically most stable structure of $\text{Sc}_3\text{N@C}_{80}$ the three metal ions are oriented toward 6:5 C–C ring junctions, which indeed coincides with the X-ray structure observed for $\text{Sc}_3\text{N@C}_{80}\cdot\text{Co}^{\text{II}}(\text{OEP})\cdot 1.5\text{CHCl}_3\cdot 0.5\text{C}_6\text{H}_6$.¹ This isomer will be named as $\text{Sc}_3\text{N@C}_{80}:\mathbf{11}$. The mean Sc–C distances were found, again, higher than the experimental one, 2.276 Å versus 2.170 Å, but very close to the mean Sc–C distance in $\text{Sc}_3\text{N@C}_{78}$ (Table 4.1). It should be noted that the Sc–C distance of $\text{Sc}_3\text{N@C}_{80}$ is slightly shorter than those reported for other non-TNT endohedral metallofullerenes: mono- and dimetallofullerenes. For example, the shortest Sc–C distance has been estimated as 2.53 Å for Sc@C_{82} ³³ and 2.4 Å for $\text{Sc}_2\text{@C}_{84}$.³⁴ This agrees well with the calculated distances of 2.50 Å and 2.36 Å, respectively.³⁵ The cage radius is also slightly enlarged during the encapsulation process from 4.103 to 4.118 Å. Cage radius is defined as the average distance of all carbons to the center of the fullerene. The optimized structure of $\text{Sc}_3\text{N@C}_{80}$ is displayed in Figure 4.1b.

The third fullerene cage, which was capable of incarcerating four atoms, was the non-IPR D_3 - C_{68} :**6140**.^{2,36} The $Sc_3N@C_{68}$ complex is not the only non-IPR fullerene cage that has been seen to encapsulate metal units. Possible non-IPR structures have also been investigated for $Ca@C_{72}$, $La_2@C_{74}$,³⁷ $Ca@C_{74}$,³⁸ $Sc_2@C_{74}$ ^{38,39} and $Sc_2@C_{66}$.⁴⁰ C_{74} and C_{82} cages seem to contain heptagon rings. IPR fullerene cages cannot exist in the range from C_{60} to C_{70} .²⁰ It is interesting to notice that the only known violations of the IPR rule are in endohedral metallofullerenes. Subsequent studies by Aihara confirmed that the IPR could not be applied to charged fullerenes.⁴¹ For a C_{68} cage whose carbon surface consists solely of pentagons and hexagons, there are 6332 possible isomers, but the 12 ^{13}C NMR signals and a single ^{45}Sc NMR signal in the spectrum of $Sc_3N@C_{68}$ restricts these possibilities to only 11 isomers with either D_3 or S_6 symmetry.² On the basis of DFT calculations, isomers **6140** and **6275** emerged as the likely cage structure present in the TNT endohedral metallofullerene with D_3 symmetry.² Isomers **6140** and **6275** have only three fused pentagon pairs, which means that these are much more stable than other isomers that have more units like this.⁴² Finally, the detailed structural characterization of $Sc_3N@C_{68}$ showed that the carbon cage is the **6140** isomer.³⁶ This fullerene is significantly different from the other mentioned fullerenes. Unlike other cages, the D_3 - C_{68} :**6140** cage in $Sc_3N@C_{68}$ has a 5:5 ring junctions (*E* type in appendix A.1). The distance of this kind of C–C bond is computed to be 1.436 Å. As in the D_{3h} - C_{78} :**5** cage, pyracylene C–C bonds are found in this isomer of C_{68} . The average computed distance for this type of C–C bond is 1.396 Å, similar to the 6:6 C–C bond lengths in C_{60} and C_{78} . C_{78} and C_{80} are spherical, so all carbons are approximately at the same distance from the center: the cage radius is 4.052 Å and 4.103 Å, respectively. Nevertheless, the cage radius of C_{68} is not only considerably shorter (3.783 Å) but also distorted, with only one plane which can encapsulate the TNT unit guest (Figure 4.1c). In this plane, the scandiums are directly connected to 5:5 ring junctions and the N–carbon cage distances are similar to those found in C_{78} and C_{80} cages. So, the internal structure of the nitride is planar, although only one position is possible inside the C_{68} cage. Consequently, only one isomer will be possible. Although the cavity of the C_{68} is smaller, it encapsulates the Sc_3N unit very efficiently and even has a Sc–C distances of 2.324 Å, which is longer than its $Sc_3N@C_{78}$ and $Sc_3N@C_{80}$ analogues. The experimental

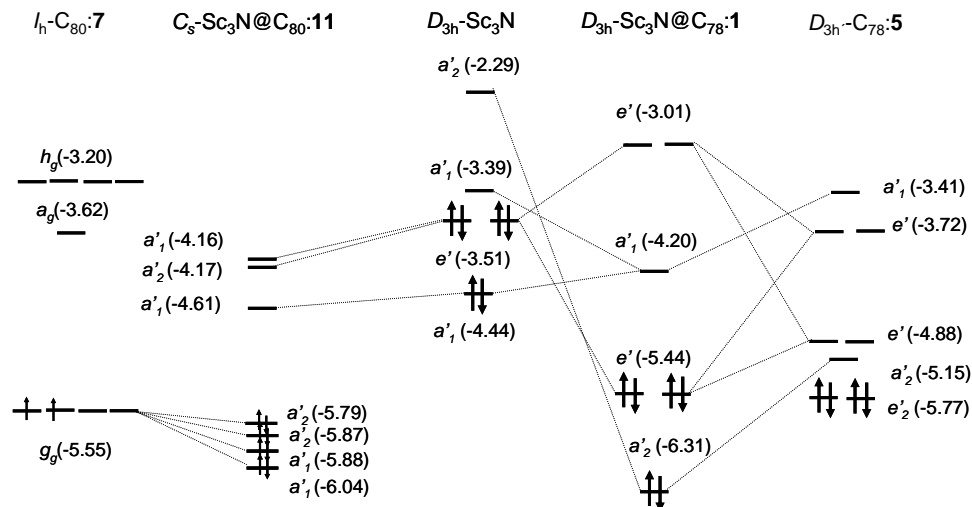


Figure 4.2 Orbital interaction diagram for $\text{Sc}_3\text{N}@C_{78}:1$ and $\text{Sc}_3\text{N}@C_{80}:11$. Only the most important orbitals that participate in the bond have been drawn. The $I_h\text{-C}_{80}:7$ fullerene has the open shell configuration $\dots(t_{1g}+h_u)^{16}(g_g)^2(h_g+a_g)^0\dots$ meanwhile the $D_{3h}\text{-C}_{78}:5$ fullerene has the closed shell configuration $\dots(e_2)^4(a'_2)^0\dots$

distance (2.225 Å) also confirms this trend (Table 4.1).³⁶ The mean Sc–N distance is found to be 1.982 Å, slightly shorter than the distance found in $\text{Sc}_3\text{N}@C_{78}$ (1.997 Å) and $\text{Sc}_3\text{N}@C_{80}$ (2.014 Å). The TNT encapsulation causes a similar geometrical deformation of the cage for $\text{Sc}_3\text{N}@C_{68}$: the 5:5 C–C bond lengths linked to Sc atoms increase by 0.009 Å and the aforementioned C–C bond displaces outward from the fullerene surface.

4.2.2 Ionic model

The bond between the nitride and the cage is markedly defined by the ionic model $\text{Sc}_3\text{N}^{6+}@C_k^{6-}$. A total of six electrons formally go from the highest occupied nitride orbitals to the lowest unoccupied cage orbitals. $\text{Sc}_3\text{N}@C_{78}$ is the most symmetric endohedral complex (D_{3h}) and thus it will be a suitable model to explain the bond between both units. The $D_{3h}\text{-C}_{78}:5$ isomer has a closed-shell ground state with three low unoccupied orbitals of symmetries a'_2 (–5.15 eV) and e' (–4.88 eV) that are π antibonding orbitals basically centered in the set of C27–C28 bonds, a pyracylene C–C bond

type (see Appendix A.5). These unoccupied orbitals can receive six electrons from the three highest occupied orbitals of the TNT unit as the orbital interaction diagram of Figure 4.2 of $\text{Sc}_3\text{N}@C_{78}$ shows. The Sc_3N degenerate orbital of symmetry e' mixes with the lowest unoccupied fullerene orbitals of the same symmetry. The lowest one is the HOMO and is essentially a fullerene orbital. The most important orbitals involved in the charge transfer are drawn in Figure 4.4. The mixing of orbitals of e' symmetry leads to a formal transfer of four electrons from the Sc_3N unit to the carbon cage. Orbital a'_1 can also interact with C_{78} orbitals but the lowest a'_1 orbital in the empty fullerene is ~ 1.7 eV higher than the LUMO that is of a'_2 symmetry. Consequently, there is a transfer of two additional electrons from the metal orbital of symmetry a'_1 to the cage orbital of symmetry a'_2 . The a'_1 orbital of the Sc_3N fragment becomes the LUMO in the endohedral cluster. In summary, we concluded that formally six electrons are transferred from the nitride unit to the fullerene.

Like in C_{78} , the encapsulation of Sc_3N into the $I_h\text{-C}_{80}:7$ results in a formal transfer of six electrons from the scandiums to the fullerene orbitals. Previous theoretical calculations have shown that the $I_h\text{-C}_{80}:7$ isomer has the open shell configuration: $\dots(t_{1g} + h_u)^{16} (g_g)^2 (h_g + a_g)^0 \dots$. Moreover, $I_h\text{-C}_{80}:7$ may deform to lower symmetries by Jahn-Teller effect.⁴³ It represents an electronic configuration with only 2 electrons in a four low-lying degenerate orbitals, -5.55 eV, which can easily accept 6 electrons. So, as a consequence of this electron charge transfer, the resulting endohedral has a closed shell configuration, Figure 4.2. From an electronic point of view, $D_3\text{-C}_{68}:6140$ has got a closed-shell ground state with HOMO-LUMO gap of 0.5 eV and with three low unoccupied orbitals of symmetries e' (-5.38 eV) and a_1 (-4.79 eV) which can easily accept six electrons as the other two fullerenes do. Indeed, a high stabilization appears due to electron charge transfer from the three HOMOs of Sc_3N to $D_3\text{-C}_{68}:6140$ cage, which is hugely stabilized since the final endohedral complex has a higher HOMO-LUMO gap of 1.27 eV. A similar gap was found for endohedral complexes of C_{78} and C_{80} : 1.24 and 1.18 eV, respectively. These electronic considerations seem to have the key to rationalize why only some cages can encapsulate metal units (in section 4.6 these ideas will be developed further).

Table 4.2 Mulliken populations for the Sc₃N unit in several TNT endohedral metallofullerenes

Molecule/Symmetry.	Sc				N	Elec- tron charge transfer ^c	
	Net charge	s	p	d	Net charge		
Sc ₃ N ^a	C _{3v}	+0.38	1.00	6.23	1.39	-1.14	--
Sc ₃ N ^b	D _{3h}	+0.46	1.20	6.21	1.13	-1.38	--
Sc ₃ N ^{6+ b}	D _{3h}	+2.59	0.00	5.93	0.48	-1.77	--
Sc ₃ N@C ₆₈ ^a	D ₃	+0.75	0.12	6.46	1.67	-1.36	0.89
Sc ₃ N@C ₇₈ : I ^a	D _{3h}	+0.88	0.12	6.39	1.61	-1.41	1.23
Sc ₃ N@C ₈₀ : II ^a	C _s	+0.86	0.15	6.43	1.56	-1.44	1.14

^a Optimized structure. ^b Planar structures with Sc–N distance from distance found in Sc₃N@C₇₈:**I**. ^c Electron charge transfer from the Sc₃N unit to the fullerene cage (calculated from Mulliken net charges).

4.2.3 Electron charge transfer

In spite of the formal transfer, the Mulliken populations given in Table 4.2 suggest that the electron charge transfer is not so important. The atomic populations for the neutral nitride indicate that this molecule is a polar molecule with a strong negative charge localized on N (−1.14 *e*) and a positive charge on each Sc of +0.38 *e*. Taking as reference the planar form of Sc₃N, the encapsulation by C₇₈ induces a lowering of 1.08 electrons in the *s* orbitals in each Sc. However, the populations of *p* and *d* orbitals increase by 0.18 and in 0.48 *e*, respectively, and the total charge of each Sc atom in the C₇₈ endohedral is +0.88 *e*. The charge on the Sc atom in the endohedral is positive, but far from +2.59 *e*, the positive charge of the metal ion in a free Sc₃N⁶⁺ unit. Notice in values of Table 4.2, that in spite of the electron charge transfer between the neutral nitride and the fullerene, the nitrogen atom increases its negative charge up to −1.41 *e*. Globally, there is a electron charge transfer between the two units of 1.23 *e*. Mulliken population analysis given in Table 4.2 shows that the electronic population on the nitride unit and the electron charge transfer between the two moieties for the analogous Sc₃N@C_k (*k* = 68, 80) clusters are almost identical to those found

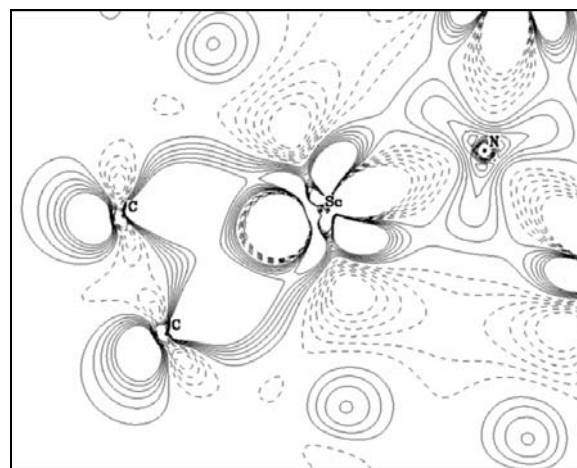
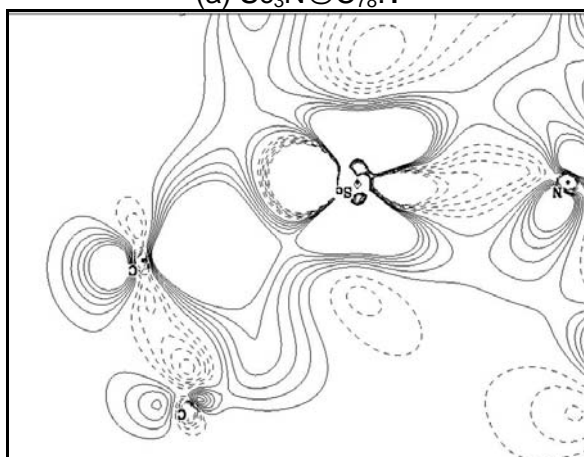
(a) $\text{Sc}_3\text{N}@C_{78}:1$ (b) $\text{Sc}_3\text{N}@C_{80}:11$

Figure 4.3 Electron density deformation map (EDDM) for $\text{Sc}_3\text{N}@C_{78}:1$ (a) and $\text{Sc}_3\text{N}@C_{80}:11$ (b). The electron density that has been computed as the difference $\rho(\text{complex}) - [\rho(\text{nitride}) + \rho(\text{cage})]$ is represented in a plane containing Sc_3N and two carbons.

for $\text{Sc}_3\text{N}@C_{78}$. The Mulliken population indicates that s orbitals of Sc lose this electronic density which is spread equally for all carbons in the carbon cage.

The analysis of the electron density deformation maps (EDDM) is a useful tool to characterize chemical bonds in large molecules.⁴⁴ An

Table 4.3 Decomposition of the encapsulation binding energy (EBE) for the most stable $\text{Sc}_3\text{N}@C_k$ ($k = 68, 78, 80$) isomers ^a

Complex	Isom.	ΔE_{ST}	ΔE_{ORB}	ΔE_{INT}	ΔE_{DE} ^b		EBE ^c
					Sc_3N	Cage	
$\text{Sc}_3\text{N}@C_{68}$	--	29.04	-42.04	-13.00	0.65	0.54	-11.81
$\text{Sc}_3\text{N}@C_{78}$	1	23.43	-35.34	-11.91	0.72	1.49	-9.70
	1^d	-81.62	-54.98	-136.60	--	0.72	--
$\text{Sc}_3\text{N}@C_{80}$	11	20.07	-33.04	-12.97	0.79	0.58	-11.60

^a Energies are in eV. ^b Deformation energy (ΔE_{DE}) is the energy necessary to modify the fragments from its optimal geometry to the structure that have in the complex. ^c $\text{EBE} = \Delta E_{DE} + \Delta E_{INT}$. ^d Decomposition of the EBE with respect to the ionic fragments Sc_3N^{6+} and C_{78}^{6-} . The deformation energy for the Sc_3N unit was not determined since we were unable to find a minimum for the cation.

important property of the EDDMs is that they are less dependent on the basis set than the Mulliken populations. Figure 4.3 contains contour lines in the σ_h plane associated to accumulations and depletions of charge density when the electron density of $\text{ScN}_3@C_k$ ($k = 78, 80$) is calculated with respect to its subunits Sc_3N and C_k ($k = 78, 80$). The electronic density exhibits accumulations close to carbons directly bonded to Sc atoms that may be associated to electronic transfers from Sc_3N to the π_{C-C}^* orbitals. The accumulations near the Sc atoms show that there is a reorganization in the Sc orbitals that shows that $3d$ orbitals take an active part in the formation of the cluster. This reorganization is fully consistent with the Mulliken populations. Roszak and Balasubramanian investigated the metal–ligand bond in the simple molecule ScC_2 and concluded that the interaction between Sc and the C_2 unit is highly ionic with a strong transference to the σ C–C bond that does not occur in the present case.⁴⁵

4.2.4 Decomposition of the encapsulation binding energy (EBE)

The bond between the C_k ($k = 68, 78, 80$) cage and the Sc_3N unit is also analyzed using the extended transition method developed by Ziegler and Rouk⁴⁶ and that is an extension of the well-known decomposition scheme of Morokuma.⁴⁷ According to this method, the binding energy (BE) between two fragments can be decomposed into several contributions. If BE

is related to an encapsulation process we will use the term encapsulation binding energy (EBE):

$$(4.1) \quad \text{EBE} = \Delta E_{\text{DE}} + \Delta E_{\text{ST}} + \Delta E_{\text{ORB}}$$

The first term, ΔE_{DE} , the deformation energy, is the energy necessary to convert the fragments from their equilibrium geometries to the conformation they assume in the optimized structure of the overall complex. Since the fragments have been considered in the same closed shell state both in the complex and as free molecules, this term corresponds simply to the sum of the fragment relaxation energies. ΔE_{ST} represents the steric repulsion between the two deformed fragments with the electron densities that each fragment would have in the absence of the other fragment. This term consists of two components; the first is the electrostatic interaction (ΔE_{elstat}) of the nuclear charges and the unmodified electronic charge density of one fragment with those of the other fragment and the second component is the so-called Pauli repulsion (ΔE_{Pauli}), which is essentially due to the antisymmetry requirement on the total wave function. ΔE_{ORB} known as the orbital interaction term represents the attracting orbital interactions that give rise to the energy lowering upon coordination. This term may be broken up into contributions from the orbital interactions within the various irreducible representations of the overall symmetry group of the system, according to the decomposition scheme proposed by Ziegler. The sum $\Delta E_{\text{ST}} + \Delta E_{\text{ORB}}$ is known as the fragment interaction energy and represented by ΔE_{INT} . Recently, Sgamellotti and co-workers have used this method to rationalize the C_{60} -metal bond in organometallic derivatives of C_{60} .⁴⁸

The encapsulation process of the TNT unit into a C_{78} cage is a strongly exothermic process that yields a EBE of -9.70 eV for $\text{Sc}_3\text{N}@C_{78}:1$. Decomposition of the EBE with respect its components are given in Table 4.3. A free Sc_3N unit has a pyramidal geometry in which the Sc-N bond distance is computed to be 1.957 Å at the present level of theory. The ΔE_{DE} necessary for Sc_3N to achieve the planar structure with a Sc-N distance of 1.997 Å, the optimal distance in $\text{Sc}_3\text{N}@C_{78}:1$, is 0.72 eV whereas 1.49 eV is the ΔE_{DE} that the fullerene cage requires to accommodate the Sc_3N unit in its interior. The interaction between the two fragments amounts -11.91 eV, term that is dominated by the orbital contribution ($\Delta E_{\text{ORB}} = -35.3$ eV). The

other component to ΔE_{INT} is the steric repulsion that was found to be very positive, $\Delta E_{\text{ST}} = +23.4$ eV. The large computed value for the orbital term corroborates that when two neutral fragments are put together there is an important electronic reorganization as we have seen through the orbital diagram in Figure 4.2 and the EDDM in Figure 4.3.

The formal transfer of six electrons between the two moieties makes also convenient the analysis of the EBE with respect to the ionic fragments Sc_3N^{6+} and C_{78}^{6-} (Table 4.3). The interaction energy between these two fragments to give $\text{Sc}_3\text{N}@C_{78}:\mathbf{1}$ is -136.6 eV, a large energy difference which is dominated by the classical electrostatic interaction between the two highly charged ions. The electrostatic interaction is much larger than the Pauli repulsion. Consequently the steric term, that is the sum of these two terms, is very negative; $\Delta E_{\text{ST}} = -81.6$ eV. These two large energies are totally consistent with the high charge located on each fragment. Nevertheless, the very large contribution to the stabilizing energy associated with the orbital term is unexpected. The ΔE_{ORB} term was found to be -54.9 eV, value that is even larger than the corresponding term when the fragments are neutral. After the encapsulation of Sc_3N^{6+} by C_{78}^{6-} there is an important *orbital mixing* and consequently an important electronic reorganization that induces a transfer of charge (in this case from the anionic cage to the cationic nitride) and a polarization of each unit. Both fragment polarization and charge transfer occur simultaneously, and unfortunately they are not easy to separate. In the ionic decomposition, the ΔE_{DE} term is almost negligible in comparison to ΔE_{INT} .

The incorporation of Sc_3N into the $I_h\text{-C}_{80}:\mathbf{7}$ is somewhat more exothermic than in the case of formation of $\text{Sc}_3\text{N}@C_{78}:\mathbf{1}$, since the EBE was found approximately 1.9 eV more stabilizing. The energetic difference between these two encapsulation processes essentially arises from the larger Sc–C bond distances in the larger fullerene (Table 4.1). Two factors contribute to the lengthening of Sc–C bond when going from C_{78} to C_{80} : a moderate increase of the cage radius from 4.052 Å to 4.103 Å and the different framework of these two cages. The direct consequence is that the steric repulsion (ΔE_{ST}) is less destabilizing in $\text{Sc}_3\text{N}@C_{80}:\mathbf{11}$, and this lower steric repulsion is accompanied by a minor deformation energy on going from the empty cage to the endohedral geometry (Table 4.3). The orbital interaction term (ΔE_{ORB}) is also very important but somewhat minor in the

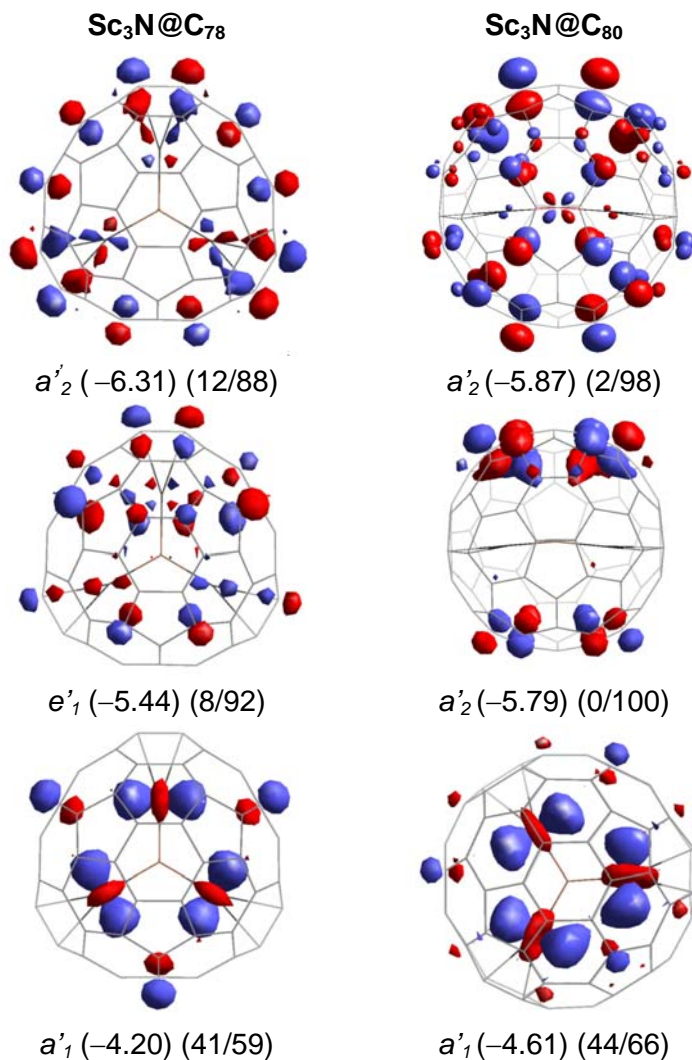


Figure 4.4 3D representations, symmetries, energies (in eV) and composition (% Sc₃N / % cage) of the most important molecular orbitals (MOs) involved in the electron charge transfer and the ionic metal bond for the Sc₃N@C₇₈:**1** and Sc₃N@C₈₀:**11** optimized complexes.

C₈₀ cluster when it is compared with the most stable endohedral of C₇₈. Notice from the orbital interaction diagram in Figure 4.2 and orbital composition in Figure 4.4 that the quadruply degenerate g_g orbitals of I_h -

C_{80} :**7** are less stable than the corresponding frontier orbitals in C_{78} due to *lower mixing* with the Sc orbitals. The higher EBE for the larger cluster may be associated to the smaller steric repulsion between the two fragments and to the lower energy necessary to deform the larger fullerene (Table 4.3). The EBE for $Sc_3N@C_{80}$ is computed to be -11.6 eV, a value that is quite similar to the energy reported (-10.73 eV) very recently by Kobayashi and co-workers who studied the energetics of several isomers of $Sc_3N@C_{80}$.²⁴

The EBE has also been decomposed for $Sc_3N@C_{68}$. The decomposition is quite similar to that of $Sc_3N@C_{80}$. The EBE, -11.81 eV, is even higher than for $Sc_3N@C_{80}$:**11**, -11.60 . The slight advantage comes from the ΔE_{ORB} and ΔE_{DE} terms. Although the steric repulsion term of C_{68} is higher (29.04 eV) because of its smaller size, the higher stabilization in the orbital interaction (-42.04 eV) largely compensates for this destabilization. The low deformation energy (1.19 eV) also shows that this non-IPR fullerene encapsulate efficiently. The ΔE_{DE} is a little smaller than in $Sc_3N@C_{80}$:**11** (1.37 eV) and much smaller than in $Sc_3N@C_{78}$:**1** (2.21 eV). So, the final order of the EBE is: $C_{68} \approx C_{80} > C_{78}$.

4.3 ISOMERISM

4.3.1 $Sc_3N@C_{78}$

A priori, several orientations of the Sc_3N unit inside the fullerene are possible. Since the X-ray determination of $Sc_3N@C_{78}$ shows that the Sc_3N unit lies close to the original σ_h plane of the D_{3h} - C_{78} :**5** cage, only isomers that retain this symmetry plane were studied. In the following discussion and in Figure 4.5 and 4.6 we consider that the Sc_3N unit is within the xy plane. The σ_h (or xy) plane crosses three pyracylene C–C bonds that are linked by hexagons as Figure 4.5 shows. By considering four additional orientations of the Sc_3N unit within the C_{78} cage, the five isomers shown in Figure 4.5 were studied. The most stable isomer, $Sc_3N@C_{80}$:**1**, which has been fully described in the first section, corresponds to the case in which the scandiums are over the pyracylene 6:6 C–C bonds, whereas in isomer **4**, the metals are over 6:5 C–C bonds. In isomer **2** the metal ions are directly connected to individual carbons. In the other two isomers, each metal is placed at the center of a pentagon (isomer **3**) or a hexagon (isomer **5**).

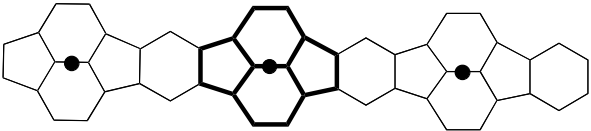
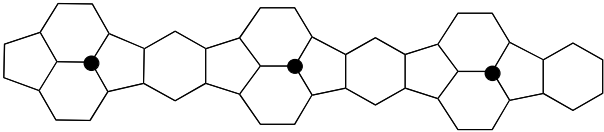
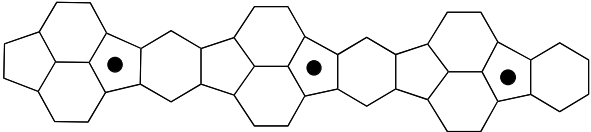
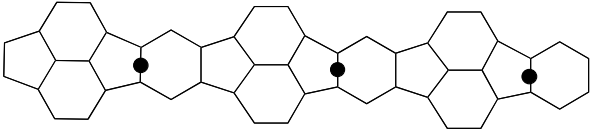
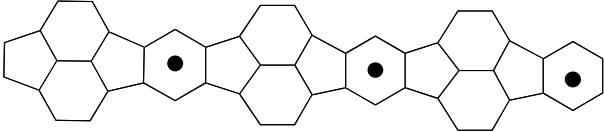
2D Scheme	Sym.	Isom.	RE
	D_{3h}	1	0.00
	C_{3h}	2	+0.10
	C_{3h}	3	+1.12
	C_{3h}	4	+0.79
	D_{3h}	5	+0.97

Figure 4.5 Carbon chains, symmetries, isomer number and relative energies (RE, in eV) with schematic positions of the scandiums with respect to the pyracylene C–C bond types for the $\text{Sc}_3\text{N}@C_{78}$ optimized isomers. Bold lines show the pyracylene patch in one of the 2D drawings. In the $\text{Sc}_3\text{N}@C_{78}:\mathbf{1}$ isomer the Sc_3N unit lies on the σ_h symmetry plane and the scandiums (represented by black dots) are over the set of pyracylene C27–C28 bonds (Fig. 4.14b and App. A.5). The rest of isomers correspond to rotations of the Sc_3N unit keeping the symmetry plane.

The fully optimization of these five isomers yields five structures with different stability. The relative energies (REs) for isomers **1–5** are collected in Figure 4.5. Isomer **1**, with the three scandiums bonded to the pyracylene 6:6 C–C bonds, gives the best orientation for the trimetallic unit inside the cage, an orientation that is 0.79 eV more stable than when the

Table 4.4 Decomposition of the encapsulation binding energy (EBE) for the $\text{Sc}_3\text{N}@C_{78}$ optimized isomers^a

Isomer	ΔE_{ST}	ΔE_{ORB}	ΔE_{INT}	ΔE_{DE} ^b		EBE ^c
				Sc_3N	Cage	
1	23.43	-35.34	-11.91	0.72	1.49	-9.70
2	22.88	-34.54	-11.66	0.67	1.37	-9.62
3	21.60	-31.86	-10.26	0.62	1.05	-8.59
4	21.76	-32.69	-10.93	0.62	1.38	-8.93
5	21.47	-32.15	-10.68	0.65	1.29	-8.74

^a Energies are in eV. ^b Deformation energy (ΔE_{DE}) is the energy necessary to modify the fragments from its optimal geometry to the structures that have in the endohedral cluster. ^c $\text{EBE} = \Delta E_{DE} + \Delta E_{INT}$.

three metals are over the 6:5 ring junctions (isomer **4**). The RE of isomers **3** and **5** with respect to **1** are +1.12 and +0.97 eV, respectively. These values clearly indicate that the nitride unit *can not freely rotate* inside the fullerene cage. However, a rotation of the Sc_3N unit by only 10 degrees in isomer **1** yields structure **2** in which the metals are linked to a unique carbon atom. Since the energy difference between these two isomers is only 0.1 eV, the conversion of **1** to **2** is nearly barrierless. This fact suggests that, although the rotation of the Sc_3N unit is hindered, the structure of the complex may fluctuate dynamically between these two forms. Several attempts have been made to obtain a C_{3v} complex with a pyramidal Sc_3N unit inside the fullerene. However, the optimization process always yielded a geometry with a planar Sc_3N unit.

Table 4.4 contains the decomposition energy terms of the EBE for isomers **1-5**. The values for isomer **2** are very similar to those of isomer **1** since both structures are very close. For the other three isomers **3-5** the repulsive steric term and the stabilizing orbital term are smaller in magnitude than in **1** but the decrease is larger in the orbital term. Consequently, ΔE_{INT} is less stabilizing when the scandium ions are focusing other sites than those close to carbons that form 6:6 ring junctions. In other words, when the Sc ions are over 6:6 C-C bonds the mixing of orbitals between the two fragments is maximized. Nevertheless, the *intrinsic* electronic and steric properties of the different fullerene sites are better

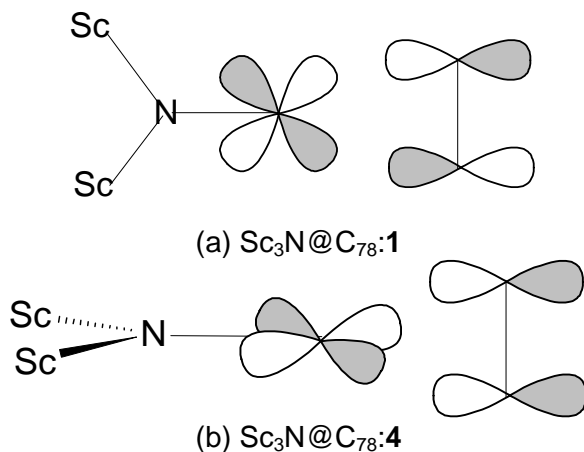


Figure 4.6 In-plane bonding interaction between a Sc metal and a 6:6 C–C bond in $\text{Sc}_3\text{N}@C_{78}:1$ isomer (a) and non-bonding interaction between a Sc metal and a 6:5 C–C bond in $\text{Sc}_3\text{N}@C_{78}:4$ isomer (b).

understood if fixed fragment geometries are used in the energy decomposition analysis. This process allows us isolate the changes in ΔE_{INT} from the effects due to changes in the geometry of the fragments. This procedure has been effective in identifying ligand donor and acceptor properties in organometallic complexes.⁴⁹ We have studied the interaction between a planar Sc_3N unit with the Sc–N distance equal to 1.975 Å—an intermediate value between 1.966 and 1.983 Å, the most frequent observed Sc–N bond lengths in these endohedral clusters—and a carbon cage with the geometry of the free fullerene.

Using these unrelaxed fragments we have searched the best orientation of a fixed planar Sc_3N unit in a rigid C_{78} cage for the five orientations described in Figure 4.5. Roughly, the REs obtained with the unrelaxed structures (Table 4.5) are quite similar to those found for the optimized clusters (Figures 4.5). Notice that in these model structures the deformation energy is only due to the Sc_3N fragment and has the same value for all orientations. This contribution has not been included in Table 4.5. Because of the similar environment that scandium ion has in **1** and **4**, the steric term is not very different in these two isomers. Therefore, the higher stabilization when Sc ions reside over a 6:6 C–C bond arises from the

Table 4.5 Decomposition of the interaction energy (ΔE_{INT}) for the $\text{Sc}_3\text{N}@C_{78}$ model complexes^a

Isomer	ΔE_{ST} ^b	ΔE_{ORB} ^c	ΔE_{INT} ^d
1	26.76	-34.91	-8.15
2	26.58	-34.69	-8.11
3	26.42	-33.82	-7.40
4	26.85	-34.02	-7.17
5	25.69	-33.18	-7.49

^a Energies are in eV. ^b Steric energy (ΔE_{ST}) includes Pauli repulsion + classical electrostatic interaction. ^c The orbital interaction term (ΔE_{ORB}) accounts for the stabilization produced when fragment orbitals of each subunit Sc_3N and C_{78} mix for giving the endohedral cluster. ^d Fragment interaction energy ($\Delta E_{\text{INT}} = \Delta E_{\text{ST}} + \Delta E_{\text{ORB}}$) is the resulting stabilizing energy associated to the interaction between the planar Sc_3N ($d_{\text{Sc-N}} = 1.975\text{\AA}$) and $D_{3h}C_{78}$:**5** at its optimal free geometry.

orbital contribution. The larger contribution of the ΔE_{ORB} term to ΔE_{INT} in **1** may be attributed to the effective overlap between the cage orbitals of symmetries e' and a_2' and the Sc d_{xy} type orbitals (Figure 4.6). This overlap does not occur when Sc atoms reside over 6:5 C–C bonds, as in isomer **4**, since the e' and a_2' cage orbitals in the 6:5 ring junctions regions are perpendicular to the Sc_3N plane (Figure 4.6). When the Sc ions are placed at the center of a pentagon (isomer **3**) or a hexagon (isomer **5**), the ΔE_{ST} and ΔE_{ORB} terms are smaller in absolute values than in **1**, because the Sc–C distances are larger. The longer Sc–C distances create less effective fragment orbital overlap but smaller steric repulsions. The loss of overlap effectiveness is higher than the diminution of the steric repulsion. Consequently, ΔE_{INT} in **3** and **4** are smaller than in **1**. In other words, when the scandium orbitals, localized in the symmetry plane, interact with the cage orbitals there is a gradual stabilization of the interacting cage orbitals. This effect reaches a maximum in isomer **1**. In summary, the analysis on the model structures clearly shows that Sc_3N is trapped in specific position due to an *orbital* effect.

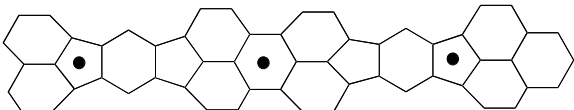
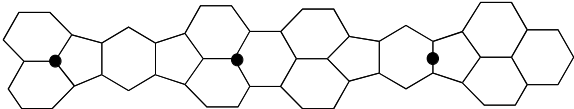
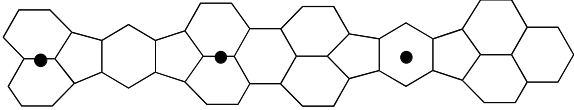
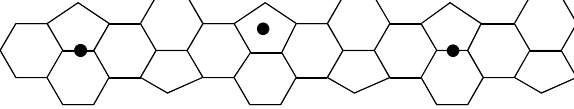
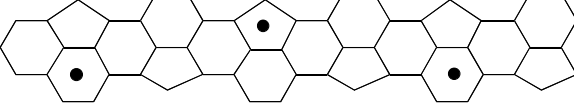
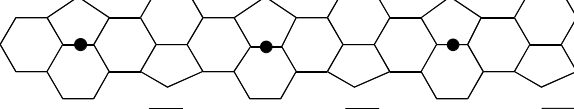
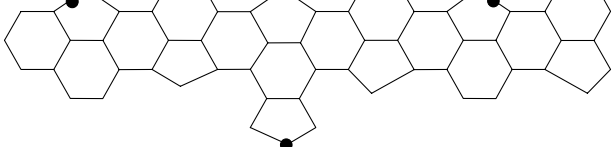
2D Scheme	Sym.	Isom.	RE
	C_{2v}	6	+0.23
	C_s	7	+0.06
	C_s	8	+0.08
	C_s	9	+0.07
	C_s	10	+0.04
	C_s	11	0.00
	C_s	12	+0.01

Figure 4.7 Carbon chains, symmetries, isomer number and relative energies (REs, in eV) with schematic position of scandiums in a 2D representation for the $Sc_3N@C_{80}$ optimized isomers. In isomer **6** the Sc_3N unit lies on one of the symmetry planes that retains the endohedral. Isomers **7** and **8** are simply rotations of the Sc_3N unit with respect **6**. Isomers **9**, **10**, **11** and **12** have also C_s symmetry but in these isomers the symmetry plane contains the nitrogen atom and only one of the metals. Like in Figure 4.5 the relative position of scandiums with respect to the cage is represented by black dots in the 2D scheme. Isomer **11** is the most stable overall, the scandiums are facing the corannulene 6:5 C–C bonds: C24–C25, C31–C32 and C67–C68 (see Figure 4.12c and Appendix A.6).

4.3.2 $Sc_3N@C_{80}$

Following the same strategy used for C_{78} , we have studied several orientations of the TNT unit inside the fullerene. The orientations considered have always maintained one plane of symmetry in the endohedral. Figure 4.7 shows the seven structures we have considered. In three of them (**6-8**), the molecular plane of the Sc_3N unit coincides with the symmetry plane of the endohedral cluster. In the other four orientations (**9-12**) the plane of symmetry contains the N atom and one of the Sc atoms, the symmetry plane relates the other two Sc's.⁵⁰ With these seven isomers we have tried to cover a large number of the alternatives where the metals can be found inside the icosahedral isomer of C_{80} . In structure **6**, the three metals are directed toward the center of two pentagons and one hexagon. Isomers **7** and **8** represent slight rotations of the trimetallic unit in relation to **6**, whereas in **11** the three metal ions are oriented toward 6:5 ring junctions and finally structures **9**, **10** and **12** correspond to a slight change in relation to **11**. Indeed, this later structure is computed to be the most stable and coincides with the X-ray structure observed for $Sc_3N@C_{80}\cdot Co^{II}(OEP)\cdot 1.5CHCl_3\cdot 0.5C_6H_6$.¹ The geometry found for $ErSc_2N@C_{80}$ ¹¹ is better represented by isomer **7** whereas the orientation of Sc_3N inside the functionalized $Sc_3N@C_{80}-C_8H_6(OCH_3)_2$ ¹³ adjusts to isomer **12**. Like in the endohedral of C_{78} the theoretical Sc–C distances for $Sc_3N@C_{80}$ are longer than the experimental ones but the differences are smaller. On the other hand, our structures for isomers **8** and **9** almost coincide with those found by Kobayashi and co-workers using the B3LYP functional.²⁴ The geometries of the distinct isomers are in Table 4.6.

The energy difference between the distinct isomers is rather small, < 0.08 eV for the majority of the Sc_3N orientations (Figure 4.7) corroborating the variety of Sc_3N orientations found in the experimental complexes. Only in isomer **6**, in which the three ions are oriented toward the center of three polygons, is the RE of the cluster is somewhat higher, 0.23 eV with respect to **11**. These REs for the $Sc_3N@C_{80}$ isomers yield the conclusion that the Sc_3N unit may easily rotate inside the fullerene cage and there is not any preferred position for TNT unit inside the cage unlike the cases of $Sc_3N@C_k$ ($k = 68, 78$). The fast rotary motion of Sc_3N^{6+} is consistent with the observed ¹³C NMR spectrum consisting of only two resolved lines with an

Table 4.6 Comparison of some computed and experimental bond lengths for several Sc₃N@C₈₀ isomers ^a

<i>Isomer</i>	<i>Method</i>	<i>Sc-N</i> ^b	<i>Sc-C</i> ^c	<i>Source</i> ^d
7	X-Ray ^d	1.97-2.06	2.03	4
	DFT-BP	2.004-2.018	2.272	*
8	DFT-B3LYP	2.020-2.029	2.329	24
	DFT-BP	2.008-2.034	2.259	*
9	DFT-B3LYP	2.014-2.029	2.320	24
	DFT-BP	2.010-2.021	2.284	*
11	X-Ray	1.966-2.011	2.170	1
	DFT-BP	2.011-2.021	2.276	*
12	X-Ray ^e	2.021-2.032	2.244	13
	DFT-BP	2.008-2.019	2.258	*

^a Distances in Å. ^b Range of Sc-N bond lengths. ^c Contact distances between Sc and the nearest neighbour carbons. ^d Average values obtained for ErSc₂N@C₈₀. ^e Values obtained for Sc₃N@C₈₀-C₈H₆(OCH₃)₂. ^d * means data from this present work.

intensity ratio of 3/1, which preserves overall I_h symmetry for the carbon on the NMR time scale.¹

4.4 PHYSICAL PROPERTIES

Calculations were also carried out to calculate the vertical electron affinity (EA) and ionization potential (IP) of these TNT endohedral metallofullerenes (Table 4.7). In general, fullerenes, exhibit relatively large EAs, and this is related to the presence of low-lying unoccupied orbitals. Smalley and co-workers used photoelectron spectra to estimate an EA of *ca.* 2.60-2.80 eV for C₆₀.⁵¹ In the gas phase, C₆₀ can accept two electrons, which gives rise to the C₆₀²⁻ ion. In solution electrochemical studies have shown that C₆₀ can be easily reduced to form the ions C₆₀ⁿ⁻ ($n = 1-6$). At the present level of theory, the adiabatic and vertical EAs for C₆₀ are computed to be 2.88 and 2.85 eV, respectively. These values are in excellent agreement with

Table 4.7 Vertical ionization potentials (IPs) and electron affinities (EAs) for several optimized molecules ^a

<i>Molecule</i>	<i>Sym.</i>	<i>IP</i>	<i>EA</i>	<i>E(HOMO)</i>	<i>E(LUMO)</i>	<i>HOMO-LUMO gap</i>
<i>Sc₃N</i>	<i>C_{3v}</i>	5.05	1.27	-3.21	-2.92	0.29
<i>C₆₀</i>	<i>I_h</i>	7.57	2.85	-6.25	-4.59	1.66
<i>C₆₈</i>	<i>D₃</i>	7.11	3.71	-5.90	-5.39	0.51
<i>C₇₈:5</i>	<i>D_{3h}</i>	6.88	3.49	-5.77	-5.15	0.62
<i>C₈₀:7</i>	<i>I_h</i>	6.92	3.75	-5.55	-5.55	0.00
<i>Sc₃N@C₆₈</i>	<i>D₃</i>	6.63	2.47	-5.48	-4.21	1.27
<i>Sc₃N@C₇₈:I</i>	<i>D_{3h}</i>	6.53	2.55	-5.44	-4.20	1.24
<i>Sc₃N@C₈₀:II</i>	<i>C_s</i>	6.88	2.99	-5.79	-4.61	1.18

^aEnergies in eV.

the experimental data.⁵² The isolated *D₃-C₆₈:6140*, *D_{3h}-C₇₈:5* and *I_h-C₈₀:7* clusters have larger vertical EAs: 3.71, 3.49 and 3.75 eV, respectively. The formal transfer of six electrons from the Sc₃N unit to the cage reduces the EA of these three TNT endohedral metallofullerenes with respect to that of the free fullerenes. This can be seen in Figure 4.8. The computed EA for Sc₃N@C₈₀ (2.99 eV) completely agrees with the experimental value of 2.81 ± 0.05 eV estimated by Ioffe et al.⁵³ To our knowledge, no EA has been determined for Sc₃N@C₆₈ and Sc₃N@C₇₈. These electronic behavior differs from the behavior of the classical endohedral metallofullerenes such as M_n@C_k (M = Sc, Y, La, Gd; n = 1, 2). The EAs of the mono- and dimetallofullerenes are higher than those of the corresponding free fullerenes (between 3.2-3.4 eV). Nevertheless, the relatively large EAs calculated for Sc₃N@C_k (k = 68, 78, 80) suggest that these complexes, like C₆₀, should still be easily reducible. It is important to notice from the values in Table 4.7 that the EAs of the endohedral metallofullerenes are not compared to the EA of the most stable empty isomer.

The HOMOs in Sc₃N@C_k (k = 68, 78, 80) are somewhat less stable than are the HOMOs in C₆₀ and C_k (k = 68, 78, 80). Therefore, the IPs of these endohedrals are slightly smaller than those of free fullerenes. Another interesting feature is that these three TNT endohedral metallofullerenes have

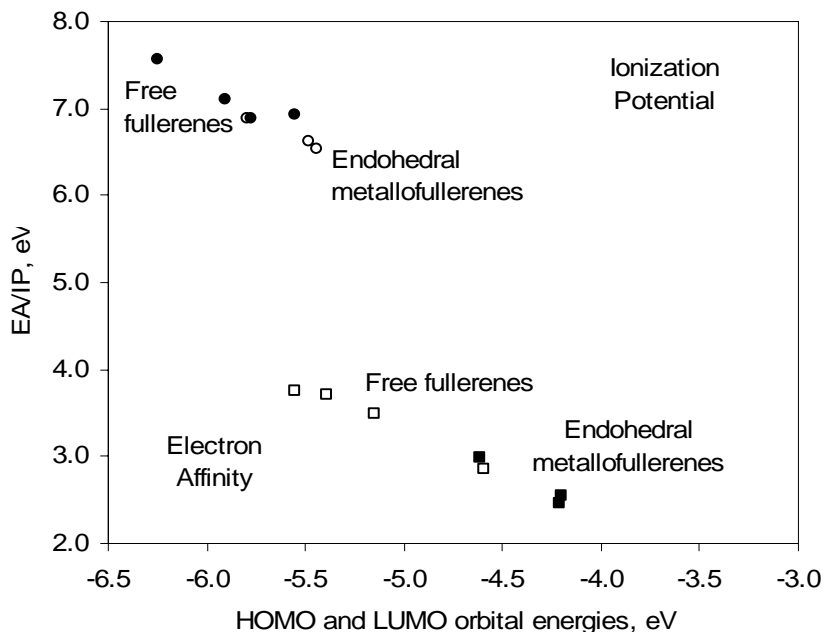


Figure 4.8 Vertical ionization potentials (IPs) and vertical electron affinities (EAs) versus HOMO and LUMO energies, respectively, for the free C_{60} , $D_{3h}-C_{78}$:**5**, I_h-C_{80} :**7** and their TNT endohedral metallofullerenes: $Sc_3N@C_{68}$, $Sc_3N@C_{78}$:**1** and $Sc_3N@C_{80}$:**11**.

moderately large HOMO-LUMO gaps, which explains their relative stability and abundance. In conclusion, TNT endohedral metallofullerenes are better electron donors and worse electron acceptors than the corresponding free fullerenes.

4.5 EXTENDED FAMILY: $M_3N@C_k$ ($M = La, Y; k = 78, 80$)

4.5.1 Experimental considerations

The Krätschmer-Huffman electric-arc generator has not only produced the previously studied TNT endohedral metallofullerenes ($Sc_3N@C_k$, $k = 68, 78, 80$) in relatively high yield but also a complete

Table 4.8 Geometric properties for several $M_3N@C_k$ ($M = \text{Sc, Y, La}$; $k = 68, 78, 80$) endohedral metallofullerenes ^a

<i>Complex</i>	<i>M</i>	<i>M-N</i> ^b	<i>M-C</i> ^c	<i>Pyram- idalization</i> ^d	<i>Cage radius</i>	<i>Electron charge transfer</i> ^e
$M_3N@C_{68}$	Sc	1.982	2.324	0.000	3.805	0.89
$M_3N@C_{78}:I$	Sc	1.997	2.255	0.000	4.069	1.23
	Y	2.056	2.350	0.502	4.087	2.14
	La	2.176	2.474	1.130	4.094	2.62
$M_3N@C_{80}:II$	Sc	2.014	2.282	0.122	4.118	1.14
	Y	2.076	2.380	0.337	4.129	1.72
	La	2.168	2.487	0.995	4.140	2.41

^a Distances in Å. ^b Mean distance. Free values for $C_{3v}\text{-Sc}_3\text{N}$: Sc-N 1.957 Å and pyr. 0.934 Å. $C_{3v}\text{-Y}_3\text{N}$: Y-N 2.097 Å and pyr. 0.596 Å. $C_{3v}\text{-La}_3\text{N}$: La-N 2.218 Å and pyr. 1.126 Å. ^c Contact distances between M and the nearest neighbour carbon. ^d Separation between the nitrogen atom at the center of the cage and the final optimal position in the TNT endohedral metallofullerene, see also note b. ^e

Electron transfer from the TNT unit to the cage calculated from the Mulliken net charges.

family of endohedral mixed-metallofullerenes: $A_nB_{3-n}N@C_k$ ($n = 0-3$, $k = 68, 78, 80$) where A and B are Sc, Y, La and rare-earth metals. These family members are prepared using graphite rods filled with A_2O_3 , B_2O_3 , powdered graphite and cobalt oxide under N_2 atmosphere. Some of these endohedral metallofullerenes with rare-earth metals have already been characterized spectroscopically^{8,12} and, the mixed $Sc_{3-n}La_nN@C_{80}$ ($n = 0-3$) clusters have also been fully described theoretically by Kobashi et al.²⁴ To complete our study about TNT endohedral metallofullerenes, we shall discuss the encapsulation of the Y_3N and La_3N TNT units inside the $D_{3h}\text{-}C_{78}:5$ and $I_h\text{-}C_{80}:7$ cages. Our primary concern is to reveal how the geometry and electronic structure differs from that of the previous analogous complexes and discuss some theoretical disagreements on the electronic structure of these non-scandium TNT endohedral metallofullerenes.

4.5.2 Geometry considerations

The most stable isomers for $M_3N@C_k$ ($k = 78, 80$; $M = Y, La$) complexes are found to be the same as those for $Sc_3N@C_{78}$ (isomer **1**) and $Sc_3N@C_{80}$ (isomer **11**). In the C_{78} cage, the M_3N ($M = Y, La$) TNT unit is also set in one position. In C_{80} , the encapsulation of Y_3N and La_3N units destabilises isomer **6** by 0.18 eV and 0.04 eV, respectively, with regard to the most stable isomer **11**. So, the nitride is allowed to rotate as the previous $Sc_3N@C_{80}$ complex does. The discussion will focus on the C_{80} because the C_{78} is not significantly different with respect to the higher fullerene. Unlike Sc_3N , both M_3N ($M = Y, La$) TNT units retain their original pyramidal structure inside the cages. The pyramidalization of M_3N unit increases in the order $Sc < Y < La$, as can be seen in the optimal structures in Figure 4.9. The pyramidalization of M_3N unit is calculated as the distance between the center of the cage and the final optimal position of the nitrogen atom. For example, the pyramidalization was calculated to be 0.122 Å, 0.337 Å and 0.995 Å for Sc, Y and La in $M_3N@C_{80}$:**11**. The behavior of the Y atom will always be between that of the Sc atom and the La atom because of the intermediate atomic radii and electronegative character. The non-planarization of the M_3N unit is due to the lack of space since the M–N and M–C ($M = Y, La$) distances are longer than the Sc–N and Sc–C distances. For example, the mean M–N distance increases from 2.014 Å ($M = Sc$) to 2.168 Å ($M = La$) and the mean M–C distance increases from 2.282 Å ($M = Sc$) to 2.487 Å ($M = La$) for $M_3N@C_{80}$:**11** (Table 4.8). Furthermore, the cage radius increases in the same order as pyramidalization does. The cage radius for the free C_{80} is computed to be 4.103 Å whereas $La_3N@C_{80}$:**11** has the highest value in these TNT endohedral metallofullerenes (4.140 Å). The lack of space causes the nitride to pyramidalize and the fullerene cages to undergo major deformation.

4.5.3 Electronic structure

The electronic structure can also be presented by the ionic model proposed for the Sc analogous complexes: $M_3N^{6+}@C_k^{6-}$ ($k = 68, 78, 80$; $M = Y, La$). In detail, the scandium-based TNT units in the endohedral complexes can even be explained as $(Sc^{3+})_3(N^{3-})$. Instead of this formal

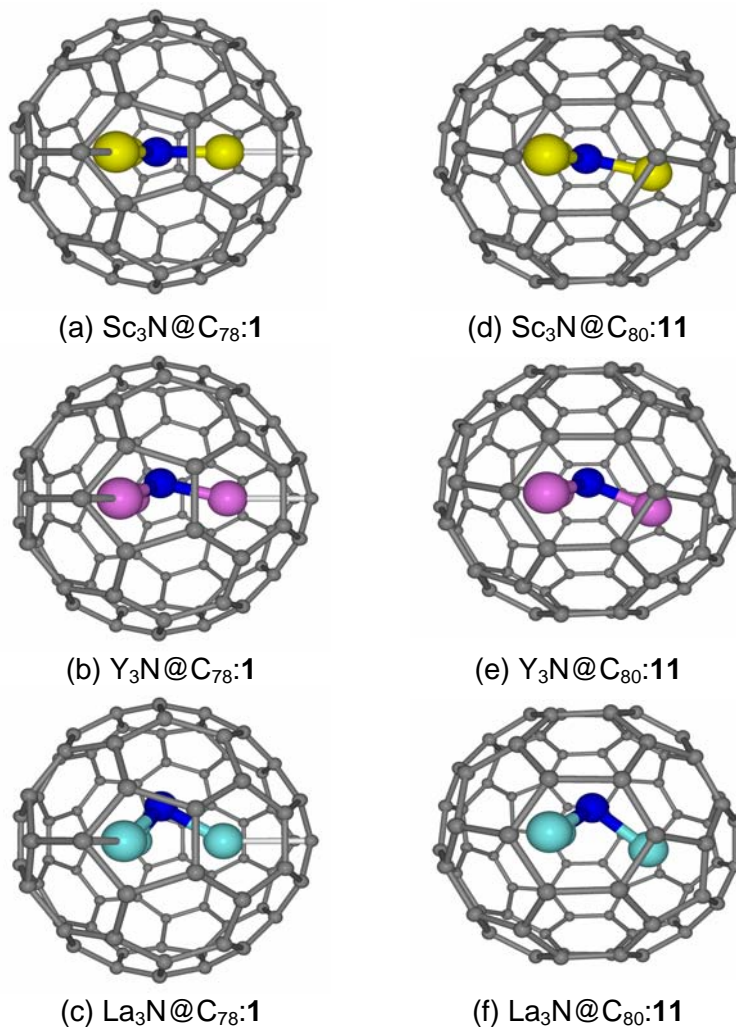


Figure 4.9 Optimized structures for $\text{M}_3\text{N}@C_{78}:1$ ($\text{M} = \text{Sc}$ (a), Y (b) and La (c)) and $\text{M}_3\text{N}@C_{80}:11$ ($\text{M} = \text{Sc}$ (d), Y (e) and La (f)).

charge of +3 on scandiums there is a more reliable Mulliken net charge of +0.86 e for $\text{Sc}_3\text{N}@C_{80}:11$. Electrons should be easier to remove from M_3N ($\text{M} = \text{Y}, \text{La}$) units than from Sc_3N . Indeed, the positive charges of +1.22 e

on Y and +1.12 e on La atoms are much larger than those of Sc atoms in $\text{Sc}_3\text{N}@C_{80}$:**11**. It is important to point out that the effect of these larger positive charges on the metals (Y and La) is that the electrostatic repulsion between metals is higher. This repulsion should be reduced by planarising the M_3N ($\text{M} = \text{Y}, \text{La}$) unit, as happened for Sc_3N . However, planarization is not permitted for M_3N ($\text{M} = \text{Y}, \text{La}$) units because of restrictions in cage size and the increase in $\text{M}-\text{N}$ and $\text{M}-\text{C}$ distances. For this reason, the M_3N ($\text{M} = \text{La}, \text{Y}$) unit is forced to maintain a pyramidal structure, which is as big as the $\text{M}-\text{N}$ and $\text{M}-\text{C}$ distances. The total Mulliken electron charge transfer from TNT unit to the cage is calculated in Table 4.8. This gradually increases from Sc to La TNT units. Despite these increases in the electron charge transfer, the description of $\text{La}_3\text{N}^{8+}@C_{80}^{8-}$ proposed by Kobayashi et al.²⁴ is not justified. This ionic model involves removing electrons from the highly stabilized nitrogen $2p$ shell, which (in the case of La) is 2.58 eV below the three donation occupied orbitals of La_3N . The $\text{M}_3\text{N}^{6+}@C_k^{6-}$ model only proposes the formal transfer of three electrons from the highest occupied orbitals of each metal: $3d^14s^2$ for Sc, $4d^15s^2$ for Y and $5d^16s^2$ for La, which are very predisposed since they are very destabilized (Figure 4.2). Furthermore, the $\text{La}_3\text{N}^{8+}@C_{80}^{8-}$ model would involve an open-shell electronic state that would lead to a higher reactivity than $\text{Sc}_3\text{N}@C_{80}$:**11**. Actually, the $\text{La}_3\text{N}@C_{80}$:**11** complex has a relatively big HOMO-LUMO gap of 1.422 eV, which confers the same stabilization as scandium-based TNT endohedral metallofullerenes.

4.5.4 Decomposition of EBE

The lack of space for the TNT units to expand freely makes $\text{M}_3\text{N}@C_k$ ($\text{M} = \text{Y}, \text{La}; k = 78, 80$) complexes less stable than the Sc analogous complexes. The decomposition of EBE for all non-scandium based TNT endohedral metallofullerenes is collated in Table 4.9. The decrease of the EBE follows the order of the group $\text{Sc} < \text{Y} < \text{La}$. The reduction for C_{78} is *ca.* 37 %, from -9.70 eV for Sc to -6.10 eV for La. In the case of C_{80} , the reduction is of 19 %. This reduction in the stability is consistent with the observation that the yield of $\text{La}_3\text{N}@C_{80}$ is one-fifth that of $\text{Sc}_3\text{N}@C_{80}$.⁵⁴ Actually, the lower yields for the $\text{Sc}_{3-n}\text{La}_n@C_{80}$ ($n = 0-3$) complexes are also consistent with the significantly higher increase in the

Table 4.9 Decomposition of the encapsulation binding energy (EBE) for $M_3N@C_k$ ($M = \text{Sc, Y, La; } k = 68, 78, 80$)^a

Complex	M	ΔE_{ST}	ΔE_{ORB}	ΔE_{INT}	ΔE_{DE} ^b		EBE ^c
					Sc_3N	Cage	
$M_3N@C_{68}$	Sc	29.04	-42.04	-13.00	0.65	0.54	-11.81
$M_3N@C_{78}:\mathbf{I}$	Sc	23.43	-35.34	-11.91	0.72	1.49	-9.70
	Y	30.57	-40.78	-10.21	0.04	2.70	-7.47
	La	35.57	-44.36	-8.79	0.06	2.63	-6.10
$M_3N@C_{80}:\mathbf{II}$	Sc	20.07	-33.04	-12.97	0.79	0.58	-11.60
	Y	27.11	-38.57	-11.46	0.01	1.17	-10.28
	La	28.76	-39.80	-11.04	0.11	1.53	-9.40

^a Energies are in eV. ^b Deformation energy (ΔE_{DE}) is the energy necessary to modify the fragments from its optimal geometry to the structures that have in the endohedral cluster. ^c $EBE = \Delta E_{DE} + \Delta E_{INT}$.

ionic radii of La (1.045 Å) than in those of Y (0.900 Å) and Sc (0.745 Å). The increment in the deformation energy (ΔE_{DE}) of the cage and also of the steric term (ΔE_{ST}) reduces the EBE. The La_3N TNT unit has the highest effects (just observe the ΔE_{DE} values for $M_3N@C_{80}:\mathbf{II}$ are 0.58 eV (Sc), 1.17 eV (Y) and 1.53 eV (La); and the corresponding ΔE_{ST} values are 20.07 eV, 27.11 eV and 28.76 eV). The deformation energy of the cage can be attributed to the increment in the cage radius. As expected, the energy involved in the deformation of the TNT unit is almost unappreciable: 0.01 eV for Y_3N and 0.11 for La_3N . On the other hand, the ΔE_{ST} increases because the electron transfer from the Y and La TNT units to the cage is higher, which in turn increases the repulsion between the charged fragments. In general, however, it is expected that the encapsulation of new TNT units containing a variety of metals will extend and enrich the research area of endohedral metallofullerenes.

4.6 GENERAL RULE FOR THE STABILIZATION OF CAGES ENCAPSULATING TNT UNITS

4.6.1 The stability can be predicted

The incorporation of a TNT unit into the fullerene results in an electron transfer from the metals to the carbon cage, in other words, the formation of a stable ion pair. Up to now, only four carbon cages have been capable of encapsulating TNT units: D_3 -C₆₈:**6140**, D_{3h} -C₇₈:**5**, D_{5h} -C₈₀:**6** and I_h -C₈₀:**7**. All these cages, except C₆₈, satisfy IPR. However, these fullerene isomers do not coincide with the most stable isomers for these stoichiometries: C_k ($k = 78, 80$). It is interesting to see that the empty fullerene isomers isolated so far are different from the carbon cages found in isolable endohedral metallofullerenes.⁵⁵ It should be noted that these fullerene cages are produced only when they are negatively charged by the encapsulated species. If a Sc₃N moiety is not encapsulated in these cages, they will possibly be very reactive in arc-discharge conditions. None of fullerene isomers that encapsulate TNT units have been isolated from fullerene soot as free fullerenes. Obviously, this is because the electron charge transfers from the metal units to the fullerene cages drastically change the relative stability of the fullerene isomers. Theoretical calculations indicated that the thermodynamic stability of a fullerene molecule depends heavily on the negative charge that resides on it.¹⁹ So, TNT units can stabilize unconventional cage structures. Consequently, the stability of TNT endohedral metallofullerenes cannot be predicted from the theoretical methods used for the empty fullerene molecules, such as the IPR. Which fullerene cages will be capable of encapsulating TNT units? How can the stability of the TNT endohedral metallofullerenes be predicted? Some answers to these questions are now available and have almost been accepted by the scientific community. Firstly, Aihara et al. proposed a method related to the kinetic stabilization of the empty cages: the bond resonance method (BRE). Secondly, the observation of the electronic structure of the precursor fullerene cage gives us new ideas on how to rationalize the stabilization of these TNT endohedral metallofullerenes.

4.6.2 Bond resonance energy (BRE) method

The bond resonance energy method has been applied satisfactorily not only to TNT endohedral metallofullerenes but also to classical endohedral metallofullerenes that generally contain one, two or three metals: $M_n@C_k$ ($n = 0-3$). The non-TNT endohedral metallofullerenes were first synthesized, studied and characterized. The increase in the stability of the fullerene that contains positive charged units can be attributed to two main factors: first, the π -electronic systems of the fullerene shell are stabilized, and, second, there are an electrostatic interaction between the anionic shell and the cation metal inside it. Aihara studied the kinetic stability of free fullerenes and endohedral metallofullerenes using the BRE model.⁵⁶ Kinetic stability means stability against any chemical reaction or decomposition.^{57,58} The BRE, defined in Hückel theory, represents the contribution of a given π bond to the topological resonance energy (TRE) of the molecule.⁵⁹ If the minimum BRE of a given molecule or its molecular ion has a large negative value, it will be kinetically very unstable with chemically reactive sites. Isolable fullerene cages and endohedral metallofullerenes were found to be devoid of reactive C–C bonds with large negative BREs. Aihara demonstrated that kinetically unstable fullerenes tend to form kinetically stable endohedral metallofullerenes. In this way Aihara detected the 15 kinetically unstable fullerene isomers between C_{60} and C_{84} .⁶⁰ Subsequently, they successfully investigated how many electrons must be added to unstable structures if they are to become kinetically stable and correlated this data with the accepted ionic model for endohedral metallofullerenes $M_n@C_k$.⁶⁰ As far as TNT endohedral metallofullerenes were concerned, Aihara concluded that D_3-C_{68} :**6140**, $D_{3h}-C_{78}$:**5**, $D_{5h}-C_{80}$:**6** and I_h-C_{80} :**7** had a minimum BRE, like free fullerenes, but had the impressive capacity to accept six electrons and become extremely kinetically stable.^{60,41} Aihara also corroborated that the complex with a formal charge distribution of $La_3N^{8+}@C_{80}^{8-}$ must be kinetically unstable because it contains the octaanion with minimum BRE. This electronic distribution, therefore, does not explain its relative stabilization. In conclusion, Aihara et al. provided a general explanation for the particular stabilization of some empty fullerene cages encapsulating TNT and other metal units.

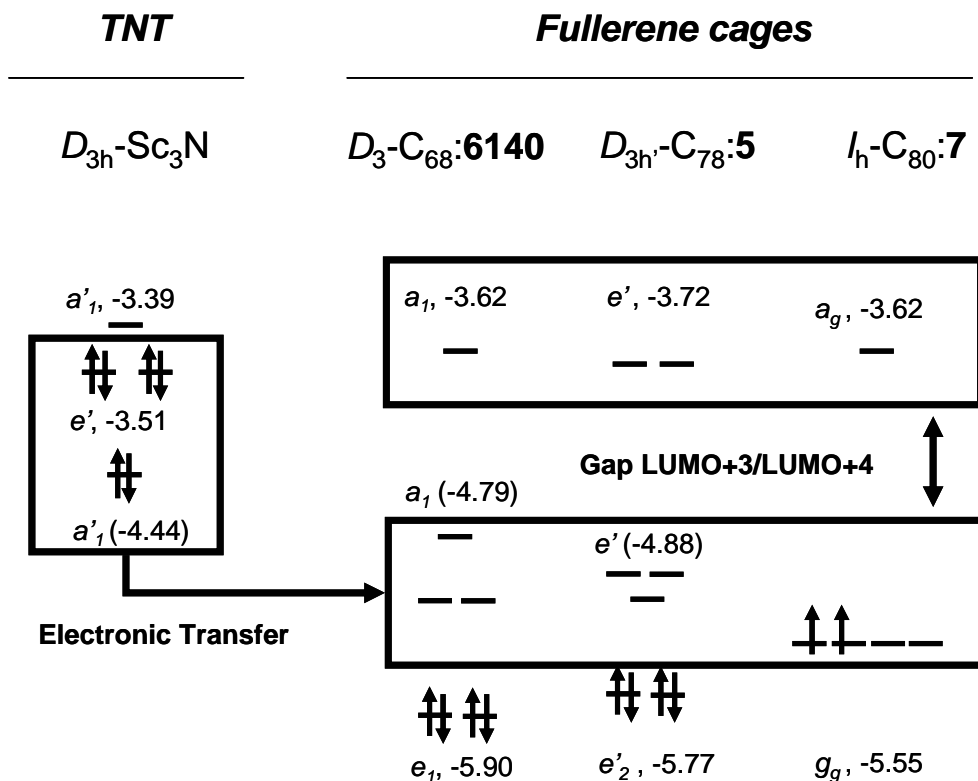


Figure 4.10 The ionic bond between the trimetallic nitride template (TNT) and the fullerene cages: $D_3\text{-C}_{68}$:**6140**, $D_{3h}\text{-C}_{78}$:**5** and $I_h\text{-C}_{80}$:**7**. There is a formal transfer of six electrons of the three highest occupied orbitals of the TNT unit to the three low unoccupied orbitals of the fullerene cages. Consequently, the $M_3N@C_k$ ($k = 68, 78, 80$) complexes are described as $Sc_3N^{6+}@C_k^{6-}$ with a relatively big HOMO–LUMO gap nearly equal to the LUMO+3–LUMO+4 found in the free cages.

4.6.3 LUMO+3–LUMO+4 gap method

We have observed that the three cages studied here — $D_3\text{-C}_{68}$:**6140**, $D_{3h}\text{-C}_{78}$:**5** and $I_h\text{-C}_{80}$:**7**— have three very low-lying LUMOs accompanied with non- or very small HOMO–LUMO gaps. These cage orbitals can easily accommodate the six electrons that come from the three destabilized TNT HOMOs. Note also that these cages have a large energy separation between the LUMO+3 and LUMO+4 as a consequence of the stabilization of the

three LUMOs mentioned above (see the electronic structure described in Figure 4.10). The electronic structure of the empty fullerenes means that it acquires a considerable HOMO–LUMO gap after a six electron transfer. It confers stability. Indeed, the final HOMO–LUMO gap of the TNT endohedral metallofullerenes can be estimated from the gap between LUMO+3 and LUMO+4 in the free cages. The calculated and estimated values are for $\text{Sc}_3\text{N}@C_{68}$: 1.27 / 1.17 eV; for $\text{Sc}_3\text{N}@C_{78:1}$: 1.24 / 1.16 eV and for $\text{Sc}_3\text{N}@C_{80:11}$: 1.18 / 1.93 eV. The main conclusion that can be drawn from this observation is that we can predict which isomers will be capable of encapsulating TNT simply by checking the molecular orbitals (MO) energies. Only the free isomers with a large LUMO+3–LUMO+4 gap will be predisposed to encapsulate TNT units. In order to check if this affirmation can be generalized, we calculated all LUMO+3–LUMO+4 gaps for all the IPR isomers between C_{60} and C_{84} stoichiometries.

There are 51 IPR isomers: 1 of C_{60} , C_{70} , C_{72} and C_{74} ; 2 of C_{76} ; 5 of C_{78} ; 7 of C_{80} ; 9 of C_{82} and 24 of C_{84} .²⁰ The LUMO+3–LUMO+4 gaps were calculated using DFT single point calculations on geometries from the Fullerene Structure Library constructed by Mitsuho Yoshida (Figure 4.11).⁶¹ The result is quite surprising and conclusive: the LUMO+3–LUMO+4 gap for all IPR isomers is lower than 1 eV, except for $D_{3h}\text{-}C_{78:5}$, $D_{5h}\text{-}C_{80:6}$ and $I_h\text{-}C_{80:7}$ isomers which range between 1.16 eV for $D_{3h}\text{-}C_{78:5}$ and almost 1.93 eV for $I_h\text{-}C_{80:7}$. In conclusion, only these isomers can stabilize such highly charged cations as Sc_3N^{6+} . The endohedral metallofullerenes constructed from these empty cages have already been isolated, and according to the present calculations, no more IPR fullerenes that have between 60 and 84 carbons will encapsulate TNT units in the future. The TNT endohedral metallofullerenes of the $D_{3h}\text{-}C_{78:5}^4$ and $I_h\text{-}C_{80:7}^1$ cages were synthesized first, but the minor TNT endohedral metallofullerene of $D_{5h}\text{-}C_{80:6}^9$ cage came later. It was discovered during the purification and isolation process of $\text{Sc}_3\text{N}@C_{80}$ (cage $I_h\text{-}C_{80:7}$). However, we do not exclude that other non-IPR fullerenes such as C_{66} , C_{68} and C_{72} can encapsulate TNT units. In fact, these cages have been isolated as endohedral metallofullerenes. So, non-IPR cages, such as the carbon cage in $\text{Sc}_3\text{N}@C_{68}$, also follow this rule (Figure 4.11).

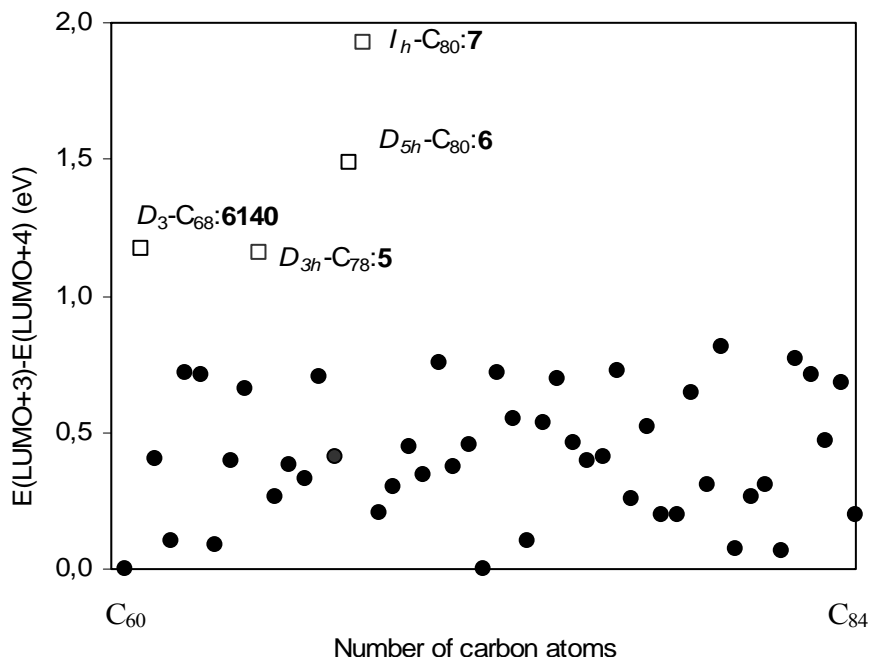


Figure 4.11 Why only D_3 - C_{68} :**6140**, D_{3h} - C_{78} :**5**, I_h - C_{80} :**7** and D_{5h} - C_{80} :**6** encapsulate TNT units. The LUMO+3–LUMO+4 gap for all IPR isomers from C_{60} and C_{84} and also the non-IPR D_3 - C_{68} :**6140** fullerene. Only isomers with the gap higher than 1 eV have been capable of encapsulating TNT units.

4.7 EXOHEDRAL REACTIVITY (I): [4 + 2] CYCLOADDITION

TNT endohedral metallofullerenes have attracted special attention because they engender new spherical molecules with unique electronic properties and structures that are unexpected for empty fullerenes. The successful isolation and purification of these metallofullerenes has encouraged into their physical and chemical properties. It would be of interest to understand how the chemical reactivity is affected by endohedral metal doping and how the electronic properties of TNT endohedral metallofullerenes are affected by reduction, oxidation and chemical functionalization processes.

The remarkable regioselectivity of the addition reactions (including [4 + 2] cycloadditions) to C_{60} and C_{70} , which occur to the 6:6 C–C bonds in C_{60} and to the 6:6 Ca–Cb / Cc–Cc in the C_{70} ,⁶² encouraged us to find out how much the regioselectivity of the C_{68} , C_{78} and C_{80} cages have changed after the TNT encapsulation process. The effect of reduction and oxidation reactions on TNT endohedral metallofullerenes has already been dealt with in section 4.4, so here we will focus on the chemical functionalization of these endohedral complexes in comparison to that of their corresponding empty cages. Dorn and co-workers reported the first organic functionalization product of the endohedral metallofullerene $Sc_3N@C_{80}$ via a Diels-Alder reaction (see below) and recently Taylor obtained the $Sc_3N@C_{80}F_{52}$ compound as a prevalent product via a fluorination reaction (next section 4.8).

4.7.1 Experimental and theoretical considerations

The organic functionalization chemistry of the free C_{60} fullerene has grown exponentially since the molecule was produced in bulky quantities thanks to the Krätschmer-Huffman generator. Although the classical endohedral metallofullerenes were synthesized in low relative yields, this did not prevent these metallofullerenes from being the first to be exohedrally functionalized. The $La_2@C_{80}$ and $Sc_2@C_{84}$ dimetallofullerenes were functionalized by a thermal and photochemical reaction with an excess of 1,1,2,2-tetramesityl-1,2-disilirane to give the $La_2@C_{80}(Mes_2Si)_2CH_2$ and $Sc_2@C_{84}(Mes_2Si)_2CH_2$ adducts, respectively.⁶³ The analogous exohedral derivative of $La@C_{82}$, $La@C_{82}(Mes_2Si)_2CH_2$, was also synthesized. Unlike the first two exohedral compounds, this compound provided the additional valuable information that no multipleaddition occurred.⁶⁴ A carbene derivative of this monometallofullerene, $La@C_{82}$, has also been reported recently.⁶⁵ Kobayashi et al. carried out density functional calculations for two $La_2@C_{80}$ derivatives, $La_2@C_{80}(C_8H_6(OCH_3)_2)$ and $La_2@C_{80}(Si_2H_4CH_2)$. They concluded the attachment of the electron-accepting molecule $C_8H_6(OCH_3)_2$ has no significant effect on the internal rotation in $La_2@C_{80}$, but the random circular motion of two La atoms in $La_2@C_{80}$ can be highly controlled by attaching exohedrally electron-donating molecules such as disilirane ($c-Si_2R_4CH_2$).⁶⁶

Dorn and co-workers have proposed a structure for the first symmetric derivative of the $\text{Sc}_3\text{N}@C_{80}$ TNT endohedral metallofullerene formed when it reacts with the 6,7-dimethoxyisochroman-3-one diene precursor.¹³ The final structure is a Diels-Alder cycloadduct, $\text{Sc}_3\text{N}@C_{80}\text{-C}_8\text{H}_6(\text{OCH}_3)_2$, which is produced via a [4 + 2] cycloaddition mechanistic pathway.⁶⁷ The $\text{Sc}_3\text{N}@C_{80}$ acts as electron-deficient dienophile and the 6,7-dimethoxyisochroman-3-one as an diene precursor. The product has been crystallographically characterized and the ^{13}C NMR suggested that the molecule possesses a plane of symmetry.¹⁴ Unlike C_{60} , the $I_h\text{-C}_{80}:\mathbf{7}$ cage does not have any of the reactive pyracylene C–C bonds (**A** type in Appendix A.1). Instead, the $I_h\text{-C}_{80}:\mathbf{7}$ cage contains only corannulene 6:5 C–C bonds (**D** type) and C–C bonds at 6:6 ring junctions abutted by a hexagon and a pentagon (**B** type). The cycloaddition occurs to the 6:5 C1–C2 bond which is elongated and pulled away from the center of the carbon cage toward the addend. Moreover, a detailed inspection of the geometry shows that the Sc_3N unit is positioned well away from the site of external modification, in a relative position corresponding to that of the $\text{Sc}_3\text{N}@C_{80}:\mathbf{12}$ isomer (section 4.3). It is not surprising to find another isomer of $\text{Sc}_3\text{N}@C_{80}$ instead of the most stable one $\text{Sc}_3\text{N}@C_{80}:\mathbf{11}$ because the free motion of Sc_3N was predicted inside the fullerene cage. Even the high degree of disorder in the crystal structures indicates that the encapsulated entities are highly mobile.

4.7.2 Effects of TNT encapsulation on exohedral reactivity

It is well known that fullerenes can accept electrons and, thus, that they prefer to react with electron-rich reagents. This has been widely confirmed by the electronic nature of the organic and organometallic C_{60} adducts reported so far. And the Diels-Alder reaction is no exception. One of the characteristics of C_{60} is that dienes prefer to attack the shorter 6:6 C–C bonds rather than the longer 6:5 C–C bonds. Thus, as far as chemical reactivity is concerned, two characteristics appear to be determinant. First, regardless of the bond type, short bond lengths (which mean larger π -bond orders and higher π -density) are preferred; and second, additions to 6:6 C–C bond types are favoured by larger pyramidalization of the carbons. In the first step, we analyze how the TNT unit encapsulation affects the electron-

attracting character of the cage, the pyramidalization and the π -bond orders of the C–C bonds. The study is not restricted only to the most stable isomer, $\text{Sc}_3\text{N}@C_{80}$:**11**, but also includes the $\text{Sc}_3\text{N}@C_{80}$:**6** and $\text{Sc}_3\text{N}@C_{80}$:**12** isomers.

Electron-attracting character of the $\text{Sc}_3\text{N}@C_{80}$ dienophile. This character can be evaluated from the EAs. The electronic structure of C_{80} was characterized by the presence of energetically low-lying 4-fold degenerate LUMOs, which enables this fullerene to accept six electrons. This is corroborated by a high EA of 3.75 eV (section 4.4). After the TNT endohedral doping the EA of the new molecule decreases to 2.99 eV for the $\text{Sc}_3\text{N}@C_{80}$:**11** isomer, which indicates that the dienophile is less reactive. Although data are only available for the $\text{Sc}_3\text{N}@C_{80}$:**11** isomer, it is expected that the encapsulation process will modify the EA in the same way for all isomers.

Pyramidalization of carbons. The relationship between the local atomic structure and the chemical reactivity of fullerenes was characterized by Haddon using the pyramidalization angle of carbons (θ_p).⁶⁸ The pyramidalization angle is a simple quantitative measure of the local curvature and strain in carbon systems. The pyramidalization angle is obtained as $\theta_p = \theta_{\sigma\pi} - 90$. In POAV1⁶⁹ theory, the $\theta_{\sigma\pi}$ (π -orbital axis vector) is introduced and defined as that vector which makes equal angles to the three σ -bonds at a conjugated carbon atom. For planar sp^2 carbons the $\theta_{\sigma\pi}$ is 90° while for tetrahedral sp^3 carbons this angle is 109.47° . Consequently, the pyramidalization angle is 0° for sp^2 centers, 19.47° for sp^3 centers and 11.67° for C_{60} . There are other methods of calculating the pyramidalization but POAV1 is conceptually simple and widely used.⁷⁰ For purposes of comparison, we describe the different C–C bond types for each complex in several tables: $\text{Sc}_3\text{N}@C_{80}$:**6** in Table 4.10, $\text{Sc}_3\text{N}@C_{80}$:**11** in Table 4.11 and $\text{Sc}_3\text{N}@C_{80}$:**12** in Table 4.12. The description includes the C–C bond types, bond lengths, pyramidalization angles and bond orders. The equivalent data for the free I_h - C_{80} :**7** can be found in Appendix A.6. The I_h - C_{80} :**7** contains only two types of C–C bonds. The corannulene 6:5 C–C bonds (**D** type) are more highly pyramidalized ($\theta_p = 10.58^\circ$) than the 6:6 C–C bonds ($\theta_p = 9.62^\circ$). Three important conclusions can be drawn from the pyramidalization

angle analysis after the TNT encapsulation: (1) the increases are not severe except in the C–C bonds closest to the Sc atoms; (2) the most pyramidalized C–C bonds are still the corannulene 6:5 C–C bonds; and (3) the highest pyramidalization angle is found in the $\text{Sc}_3\text{N}@C_{80}$:**11** and **12** complexes (13.15° in the set of C67–C68 bonds and 13.09° in the set of C7–C23 bonds, respectively). Unlike the two above mentioned complexes, in the $\text{Sc}_3\text{N}@C_{80}$:**6** complex the Sc atoms face one C_6 ring and two C_5 rings, so none of the C–C bonds are pyramidalized in a particular way. To sum up, in principle the exohedral reactivity is enhanced in the cage regions which face Sc atoms, especially for the $\text{Sc}_3\text{N}@C_{80}$:**11** and **12** isomers. However, this analysis by itself is not conclusive because it also requires bond order considerations.

Mayer bond order (MBO) and bond lengths. The MBO⁷¹ is a measure of the electron density of C–C bonds as a generalization of the Wiberg bond index.⁷² The MBO is related to the number of shared electron pairs between the atoms and is calculated using the density and overlap matrices. The MBO has proved to be an extremely useful, transparent, analytical and interpretative tool for measuring the strength of a chemical bond.⁷³ Bond lengths follow the same trend as MBO. The higher MBO, the shorter bond length. Dienes for [4 + 2] cycloadditions such as 6,7-dimethoxyisochroman-3-one (or 1,3-butadiene) require a C–C bond with high π -density. The MBO analysis finds no significant difference between two different C–C bonds in the free I_h - C_{80} :**7** cage: 1.209 for the 6:6 C–C bonds and 1.194 for the 6:5 C–C bonds. So no conclusive prediction can be made if only this factor is taken into account. To get some idea as to whether the relative differences are significant or not, the MBO can be compared with the C_{60} values. In all cases, the reactivity of these free C–C bonds in I_h - C_{80} :**7** is expected to be lower than that of C_{60} and C_{70} because the MBO are significantly lower than those for C_{60} and C_{70} . The MBO of the 6:6 C–C bond of C_{60} is computed to be 1.342 whereas the 6:6 Ca–Cb bond of C_{70} is computed to be 1.334. A complete description of the C–C bonds of I_h - C_{60} :**1**, D_{5h} - C_{70} :**1** and I_h - C_{80} :**7** is listed in Appendix A.1, A.4 and A.6, respectively.

However, the lack of regioselectivity in the I_h -C₈₀:**7** cage as a consequence of the numerous C–C bonds with similar reactivities deserves more attention. Because the MBOs are equal, the pyramidalization angles will become the most important factor in determining the most reactive site. The highest pyramidalization angle (and the most reactive) is found in the 6:5 C–C bonds, 10.58°, a long way from the value of 9.62° in the 6:6 C–C bonds. On the other hand, the encapsulation of the TNT unit inside the I_h -C₈₀:**7** cage changes the MBOs considerably and, more importantly, this change is extremely sensitive to the relative position of the Sc₃N unit within the cage. Consequently, the most reactive C–C bonds in all the isoenergetic isomers do not coincide with each other. However, one main rule emerges from the MBO analysis: the highest MBOs are never found in the C–C bonds of the cage interacting region which directly faces the Sc atoms. These C–C bonds, which are the most pyramidalized overall, have very low MBO. This makes them not suitable for addition reactions. The MBO for the C67–C68 bond in Sc₃N@C₈₀:**11** isomer is 1.125 and 1.122 for the C7–C23 in the Sc₃N@C₈₀:**12** isomer. The range of MBO for Sc₃N@C₈₀:**6** isomer is 1.226-1.109, for Sc₃N@C₈₀:**11** it is 1.247-1.095 and for Sc₃N@C₈₀:**12** it is 1.246-1.089.

We have marked the three most reactive sites according to the highest MBO and pyramidalization angle of the C–C bonds in a Schlegel diagram for the free I_h -C₈₀:**7**, Sc₃N@C₈₀:**6**, **11** and **12** isomers in Figure 4.12. The most important result is that the *regioselectivity* is considerably better in the TNT endohedral complexes than in the free cage. Each isomer has its own pattern of most reactive sites. These differences between isomers meant that extra computational effort had to be made in an attempt to obtain conclusive results about the most reactive site overall Sc₃N@C₈₀ isomers. On the other hand, it is not possible to predict whether Sc₃N@C₈₀ complexes will be more reactive than the free C₈₀ toward the [4 + 2] cycloadditions just taking into account MBO and pyramidalization angle considerations. The simplicity of C₈₀ is transformed: there is a huge variety of C–C bonds with a wide range of MBOs, pyramidalization angles and C–C bond lengths in the TNT endohedral metallofullerenes. But the electron-attracting character of the TNT endohedral metallofullerene compared with that of the free fullerene suggests that the reactivity will decrease.

Table 4.10 Description of the thirty-four distinct set of C–C bonds of the C_{2v} - $Sc_3N@C_{80}:6$ isomer^a

C–C Bond ^b	Type ^c	Bond lengths	θ_p ^d	MBO ^e
36,47	B	1.424	9.89	1.226
37,38	B	1.426	9.88	1.224
44,64	corann., D	1.434	10.55	1.223
17,18	B	1.428	9.80	1.213
3,4	corann., D	1.438	10.46	1.209
46,47	B	1.423	9.82	1.207
4,18	B	1.429	9.64	1.207
16,17	corann., D	1.438	10.59	1.206
17,37	corann., D	1.438	10.71	1.205
36,37	corann., D	1.439	10.68	1.201
1,9	B	1.427	9.37	1.200
6,20	B	1.427	9.37	1.198
48,49	corann., D	1.434	9.47	1.197
21,22	B	1.428	9.10	1.197
21,40	corann., D	1.439	10.38	1.195
3,15	B	1.429	9.40	1.195
1,2	corann., D	1.439	10.43	1.192
38,49	B	1.434	9.31	1.190
65,66	B	1.435	9.65	1.184
22,53	B	1.432	9.34	1.176
1,5	corann., D	1.441	10.42	1.171
47,48	B	1.434	9.25	1.168
46,65	corann., D	1.447	9.73	1.159
16,35	corann., D	1.442	10.18	1.157
44,45	corann., D	1.444	10.48	1.156
48,67	corann., D	1.452	10.43	1.155
7,23	corann., D	1.452	11.47	1.140
7,8	corann., D	1.453	11.01	1.129
23,24	corann., D	1.461	11.79	1.120
8,9	B	1.448	9.60	1.119
6,7	B	1.451	9.76	1.114
66,67	B	1.447	10.91	1.113
67,68	corann., D	1.459	11.37	1.111
22,23	B	1.450	10.00	1.109

^a Bond lengths in Å and pyramidalization angle in °. The Bond lengths, pyramidalization angle and Mayer bond order (MBO) of the two distinct set of C–C bonds of the free $I_h-C_{80}:7$ are 1.428 Å, 9.62° and 1.209 for the **B** 6:6 C–C bond type and 1.438 Å, 10.58°, 1.194 for the corannulene 6:5 C–C bond type (**D** type). ^b See Appendix A.6 for the systematic numeric system. ^c See Appendix A.1 for a graphical representation of the different C–C bond types. ^d Average pyramidalization angle (θ_p) of each carbon atom in the carbon bond. ^e Mayer bond order (MBO).

Table 4.11 Description of the sixty-four distinct set of C–C bonds of the C_s-Sc₃N@C₈₀:**11** isomer ^a

C–C Bond ^b	Type ^c	Bond lengths	θ_p ^d	MBO ^e
36,47	B	1.422	9.68	1.247
21,22	B	1.423	9.60	1.244
1,9	B	1.423	9.61	1.243
45,46	corann., D	1.432	10.90	1.228
37,38	B	1.424	9.85	1.226
6,20	B	1.424	9.81	1.225
10,11	corann., D	1.433	10.81	1.224
3,15	B	1.424	9.81	1.223
28,59	B	1.425	9.60	1.213
63,64	B	1.424	9.61	1.213
17,18	B	1.430	9.62	1.212
58,59	B	1.430	9.70	1.212
4,18	B	1.430	9.61	1.212
76,77	corann., D	1.437	10.50	1.211
60,61	corann., D	1.437	10.57	1.209
61,62	corann., D	1.438	10.54	1.209
75,76	B	1.431	9.67	1.208
61,75	B	1.427	9.95	1.207
62,63	B	1.426	9.95	1.207
3,4	corann., D	1.437	10.69	1.207
17,37	corann., D	1.437	10.71	1.206
16,17	corann., D	1.438	10.70	1.205
63,77	B	1.427	9.91	1.204
42,62	corann., D	1.440	10.18	1.202
41,60	corann., D	1.440	10.17	1.201
44,64	corann., D	1.440	9.85	1.199
77,78	corann., D	1.441	10.14	1.198
27,28	corann., D	1.441	9.85	1.197
64,65	corann., D	1.441	9.76	1.193
46,47	B	1.426	9.86	1.189
22,53	B	1.427	9.81	1.187
9,10	B	1.427	9.77	1.185
36,37	corann., D	1.441	10.60	1.183

Table 4.11 Continue

16,35	corann., <i>D</i>	1.441	10.57	1.182
1,5	corann., <i>D</i>	1.441	10.57	1.182
65,66	<i>B</i>	1.434	9.40	1.181
43,44	<i>B</i>	1.433	9.32	1.181
26,27	<i>B</i>	1.434	9.38	1.179
21,40	corann., <i>D</i>	1.444	10.52	1.178
1,2	corann., <i>D</i>	1.444	10.49	1.177
38,49	<i>B</i>	1.440	8.87	1.166
6,7	<i>B</i>	1.441	8.92	1.159
44,45	corann., <i>D</i>	1.444	10.27	1.155
10,27	corann., <i>D</i>	1.444	10.23	1.154
46,65	corann., <i>D</i>	1.445	10.17	1.152
48,49	corann., <i>D</i>	1.437	9.07	1.150
26,57	<i>B</i>	1.432	9.35	1.149
42,43	<i>B</i>	1.432	9.30	1.148
7,23	corann., <i>D</i>	1.439	9.29	1.146
7,8	corann., <i>D</i>	1.439	9.33	1.146
66,78	<i>B</i>	1.434	9.49	1.140
48,67	corann., <i>D</i>	1.457	11.29	1.130
8,25	corann., <i>D</i>	1.458	11.45	1.129
23,24	corann., <i>D</i>	1.457	11.40	1.129
24,25	corann., <i>D</i>	1.468	13.08	1.128
67,68	corann., <i>D</i>	1.469	13.15	1.125
47,48	<i>B</i>	1.446	9.12	1.125
22,23	<i>B</i>	1.446	9.22	1.124
8,9	<i>B</i>	1.447	9.27	1.123
41,42	corann., <i>D</i>	1.446	9.60	1.114
78,79	corann., <i>D</i>	1.448	9.60	1.109
66,67	<i>B</i>	1.456	11.27	1.095
25,26	<i>B</i>	1.456	11.10	1.095
24,55	<i>B</i>	1.455	11.04	1.095

^a Bond lengths in Å and pyramidalization angle in degrees. The Bond lengths, pyramidalization angle and Mayer Bond Order (MBO) of the two distinct set of C–C bonds of the free I_h -C₈₀:7 are 1.428 Å, 9.62° and 1.209 for the *B* type and 1.438 Å, 10.58°, 1.194 for the *D* type. ^b See Appendix A.6 for the systematic numeric system. ^c See Appendix A.1 for a graphical representation of the different C–C bond types. ^d Average pyramidalization angle (θ_p) of each carbon atom in the carbon bond. ^e Mayer bond order (MBO).

Table 4.12 Description of the sixty-four distinct set of C–C bonds of the C_s - $Sc_3N@C_{80}:12$ isomer ^a

C–C Bond ^b	Type ^c	Bond lengths	θ_p ^d	MBO ^e
9,10	B	1.422	9.72	1.246
66,67	B	1.421	9.67	1.242
26,27	B	1.422	9.84	1.236
1,2	corann., D	1.430	11.02	1.233
38,49	B	1.426	9.69	1.229
47,48	B	1.425	9.88	1.227
46,65	corann., D	1.433	10.70	1.226
28,59	B	1.425	9.89	1.226
21,22	B	1.425	9.93	1.222
36,37	corann., D	1.434	10.41	1.220
41,60	corann., D	1.435	10.68	1.220
17,18	B	1.426	9.91	1.207
17,37	corann., D	1.438	10.52	1.207
43,44	B	1.422	9.54	1.205
46,47	B	1.428	9.72	1.205
63,64	B	1.430	9.57	1.205
37,38	B	1.432	9.71	1.204
4,18	B	1.427	9.58	1.204
44,64	corann., D	1.437	10.42	1.203
65,66	B	1.428	9.88	1.203
42,62	corann., D	1.438	10.41	1.202
61,75	B	1.430	9.65	1.200
48,49	corann., D	1.440	10.60	1.199
1,9	B	1.426	9.94	1.198
3,4	corann., D	1.440	9.73	1.197
27,28	corann., D	1.440	10.79	1.197
60,61	corann., D	1.441	9.96	1.197
48,67	corann., D	1.439	10.65	1.197
16,17	corann., D	1.441	10.15	1.195
36,47	B	1.430	9.66	1.194
21,40	corann., D	1.443	10.03	1.193
41,42	corann., D	1.442	10.66	1.191
22,53	B	1.433	9.46	1.185
10,27	corann., D	1.441	10.58	1.185
3,15	B	1.434	9.37	1.184

Table 4.12 Continue

45,46	corann., D	1.445	9.93	1.183
10,11	corann., D	1.444	10.58	1.183
64,65	corann., D	1.443	10.75	1.177
67,68	corann., D	1.443	10.45	1.171
62,63	B	1.427	9.17	1.171
26,57	B	1.426	9.97	1.169
25,26	B	1.440	8.90	1.169
8,25	corann., D	1.436	8.95	1.160
58,59	B	1.433	9.32	1.158
1,5	corann., D	1.448	10.26	1.150
24,25	corann., D	1.439	9.16	1.149
78,79	corann., D	1.437	9.18	1.149
44,45	corann., D	1.445	9.78	1.145
66,78	B	1.445	9.04	1.144
77,78	corann., D	1.448	10.27	1.136
23,24	corann., D	1.456	11.36	1.136
42,43	B	1.445	9.03	1.135
6,20	B	1.435	9.45	1.134
7,8	corann., D	1.456	11.15	1.133
8,9	B	1.422	9.03	1.130
24,55	B	1.444	9.25	1.129
61,62	corann., D	1.446	9.61	1.126
76,77	corann., D	1.465	12.58	1.125
7,23	corann., D	1.470	13.09	1.122
16,35	corann., D	1.448	9.65	1.106
63,77	B	1.450	9.94	1.104
6,7	B	1.453	11.17	1.100
22,23	B	1.456	11.33	1.092
75,76	B	1.460	11.53	1.089

^a Bond lengths in Å and pyramidalization angle in degrees. The Bond lengths, pyramidalization angle and Mayer Bond Order (MBO) of the two distinct set of C–C bonds of the free I_h -C₈₀:7 are 1.428 Å, 9.62° and 1.209 for the **B** type and 1.438 Å, 10.58°, 1.194 for the **D** type. ^b See Appendix A.6 for the systematic numeric system. ^c See Appendix A.1 for a graphical representation of the different C–C bond types. ^d Average pyramidalization angle (θ_p) of each carbon atom in the carbon bond. ^e Mayer bond order (MBO).

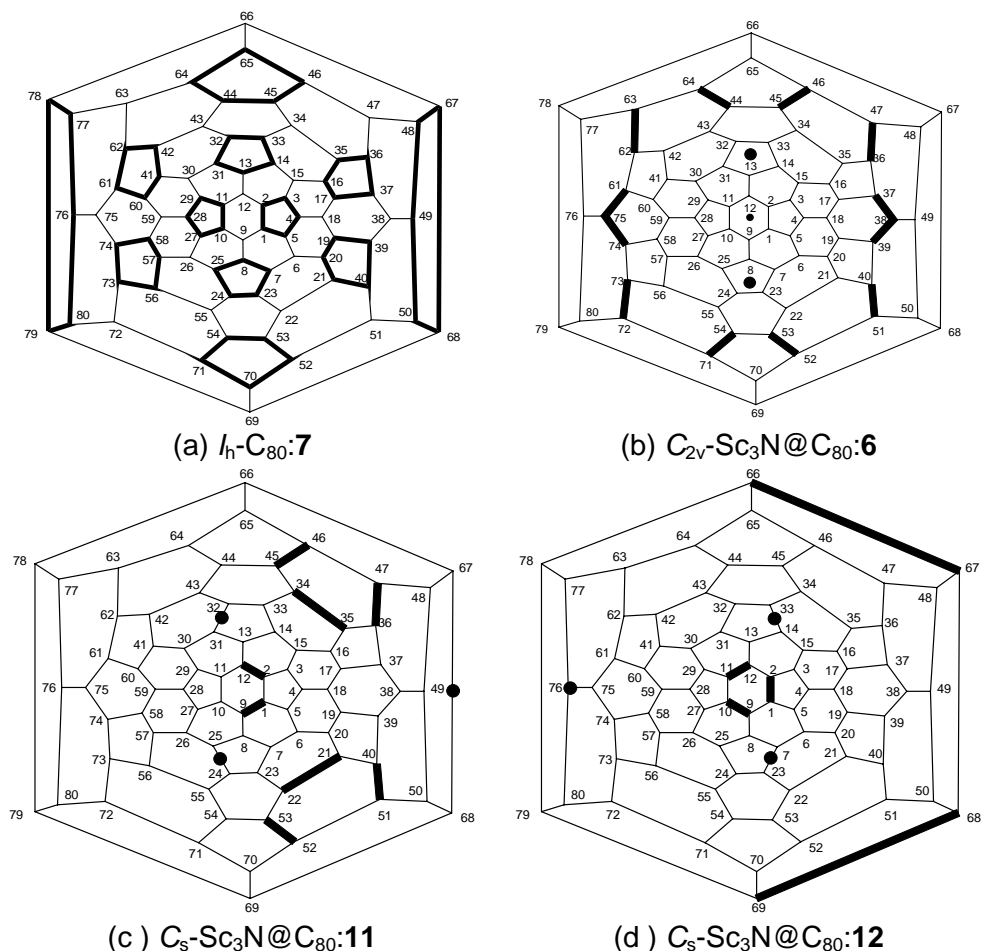


Figure 4.12 Evolution of the three most reactive exohedral sites (bold lines) for $I_h-C_{80}:7$ and $Sc_3N@C_{80}$ isomers according to pyramidalization angle (θ_p) and Mayer bond order (MBO) analysis drawn in the Schlegel diagram of $I_h-C_{80}:7$. The Sc atoms of the TNT unit are facing endohedrally the fullerene surface in the circle positions. The **B** 6:5 C–C bond types have been marked for free $I_h-C_{80}:7$ in (a), the set of the C36–C47, C37–C38 and C44–C64 bonds for $C_{2v}-Sc_3N@C_{80}:6$ in (b), the set of the C36–C47, C21–C22, C1–C9 and C45–C46 bonds for $C_s-Sc_3N@C_{80}:11$ in (c) and finally the set of the C9–C10, C66–C67 and C1–C2 bonds for $C_s-Sc_3N@C_{80}:12$ in (d). The C–C bonds equivalents to C36–C47 in (b) are: C72–C73, C62–C63 and C40–C51; equivalents to C37–C38 in (b) are: C38–C39, C61–C75 and C74–C75; equivalents to C44–C64 are: C54–C71, C45–C46 and C52–C53;

Figure 4.12 Continue

equivalent to C36–C47 in (c) is: C40–C51; equivalent to C21–C22 in (c) is C34–C35; equivalent to C1–C9 in (c) is C2–C12; equivalent to C45–C46 in (c) is C52–C53; equivalent to C9–C10 in (d) is C11–C12; equivalent to C66–C67 in (d) is C68–C69; C1–C2 in (d) is unique. Also the equivalent C–C bonds are marked in the Schlegel diagrams. The experimental structure for $\text{Sc}_3\text{N}@C_{80}\text{-C}_8\text{H}_6(\text{OCH}_3)_2$ corresponds to adduct formation to the C1–C2 bond in the $\text{Sc}_3\text{N}@C_{80}$:**12** isomer (Schlegel diagram d). The characterization of the marked C–C bond types are (MBO, θ_p): $I_h\text{-C}_{80}$:**7** 6:5 (1.194, 10.58°); $\text{Sc}_3\text{N}@C_{80}$:**6** C36–C47 (1.226, 9.89°), C37–C38 (1.224, 9.88°), C44–C64 (1.223, 10.55°); $\text{Sc}_3\text{N}@C_{80}$:**11** C36–C47 (1.247, 9.68°), C21–C22 (1.244, 9.60°), C1–C9 (1.243, 9.61°); C45–C46 (1.228, 10.90°); $\text{Sc}_3\text{N}@C_{80}$:**12** C9–C10 (1.246, 9.72°), C66–C67 (1.242, 9.67°), C1–C2 (1.233, 11.02°).

4.7.3 [4 + 2] cycloaddition on $\text{Sc}_3\text{N}@C_{80}$

Once the various factors affecting the exohedral reactivity had been analyzed, we chose the most reactive sites that had been predicted to perform a cycloaddition reaction of 1,3-butadiene on the free $I_h\text{-C}_{80}$:**7** fullerene and also on the above mentioned isomers of $\text{Sc}_3\text{N}@C_{80}$. The experimental stoichiometry of the Diels-Alder cycloadduct $\text{Sc}_3\text{N}@C_{80}\text{-C}_8\text{H}_6(\text{OCH}_3)_2$ was modelled as $\text{Sc}_3\text{N}@C_{80}\text{-C}_4\text{H}_{10}$. The isomers that are to be calculated must be selected: otherwise it would be impossible to compute the 32 different C–C bonds for $\text{Sc}_3\text{N}@C_{80}$:**6** and the 64 for isomers **11** and **12** of $\text{Sc}_3\text{N}@C_{80}$. Moreover, most of them have no symmetry. As found experimentally, adducts adopt a boat conformation facing to the side where Sc atoms are connected to the carbon cage.

First we analyze the reactivity of the $\text{Sc}_3\text{N}@C_{80}$:**12** isomer because experimentalists have proposed that it is the $\text{Sc}_3\text{N}@C_{80}$ isomer found in the $\text{Sc}_3\text{N}@C_{80}\text{-C}_8\text{H}_6(\text{OCH}_3)_2$ functionalized complex. According to the MBO analysis, four C–C bonds are the most reactive: the C66–C67, C9–C10 and C26–C27 bonds have the highest overall MBO but a low pyramidalization angle (*ca.* 9.7°), while the C1–C2 bond has the fourth highest MBO but the highest pyramidalization angle (11.0°). Calculations corroborate that the most reactive site coincides with the sites found experimentally: the formation of the adduct in the corannulene 6:5 C1–C2 bond is approximately 0.5 eV more stable than the formation in the 6:6 C66–C67,

Table 4.13 Geometric properties and relative energies (REs) for Sc₃N@C₈₀-C₄H₆ and C₈₀-C₄H₆ isomers

	Reac. C–C bond ^b	Sym.	Sc ₃ N@C ₈₀ / C ₈₀			Sc ₃ N@C ₈₀ -C ₄ H ₆ / C ₈₀ -C ₄ H ₆	
			Bond lengths	Initial θ _p ^c	MBO	Final θ _p ^c	RE
Sc ₃ N@C ₈₀ : 12	1,2*	C _s	1.430	11.02	1.233	20.68	0.00 ^d
	9,10	C ₁	1.422	9.72	1.246	18.97	0.48
	66,67	C ₁	1.421	9.67	1.242	18.85	0.52
	26,27	C ₁	1.422	9.84	1.236	18.80	0.61
Sc ₃ N@C ₈₀ : 11	45,46*	C ₁	1.432	10.90	1.228	20.70	0.02
	36,47	C ₁	1.422	9.68	1.247	19.03	0.46
	21,22	C ₁	1.423	9.60	1.244	19.09	0.48
	1,9	C ₁	1.423	9.61	1.243	19.02	0.48
Sc ₃ N@C ₈₀ : 6	1,2*	C _s	1.444	10.49	1.177	20.03	0.58
	1,2*	C _s	1.439	10.43	1.192	20.86	0.16
Sc ₃ N@C ₈₀ : 7	1,2*	C ₁	1.441	10.09	1.188	20.59	0.28
Sc ₃ N@C ₈₀ : 8	1,2*	C ₁	1.448	9.76	1.162	20.34	0.51
Sc ₃ N@C ₈₀ : 10	1,2*	C _s	1.440	10.62	1.193	19.87	0.52
Sc ₃ N@C ₈₀ : 9	1,2*	C _s	1.444	10.49	1.177	19.88	0.71
I _h -C ₈₀ : 7	1,2*	C _s	1.438	10.58	1.194	19.91	0.00 ^e
	1,9	C _s	1.428	9.62	1.209	18.74	0.70

^a Bond lengths in Å, angles in ° and energies in eV. ^b Reactive C–C bond. All are **B** 6:6 C–C bond types except those with *, which indicate that the considered C–C bonds is a 6:5 corannulene type (**D** type). See Figure A.1 for a graphical representation of the different C–C bond types. ^c Pyramidalization angle (θ_p) for the carbons attached to the diene. ^d Energy reaction of Sc₃N@C₈₀:**12** + 1,3-butadiene → Sc₃N@C₈₀-C₄H₆ is computed to be –0.54 eV. ^e Energy reaction of I_h-C₈₀:**7** + 1,3-butadiene → C₈₀-C₄H₆ is computed to be –1.04 eV.

C9–C10 and C26–C27 bonds (Table 4.13). We have also calculated the four most predicted reactive sites of the Sc₃N@C₈₀:**11** isomer which is slightly more stabilized than the Sc₃N@C₈₀:**12** isomer (0.01 eV, see section 4.3). Any functionalized compound from isomer **11** gives a more stable isomer although the reaction through the C45–C46 bond would be a serious

Table 4.14 Crucial geometric parameters which change during the derivatization via a [4 + 2] cycloaddition reaction on Sc₃N@C₈₀:**12** isomer^a

	Sc ₃ N@C ₈₀ : 12 ^b	Sc ₃ N@C ₈₀ -C ₄ H ₆ ^b	Sc ₃ N@C ₈₀ -C ₈ H ₆ (OCH ₃) ₂ ^c
Sc–N bond lengths ^d	2.008-2.019	2.010-2.019	2.021-2.032
Sc–C bond lengths ^e	2.258	2.268	2.244
Cage radius	4.118	4.122	4.098
C1–C2 θ _p	11.02	20.68	21
C1–C2 bond lengths	1.430	1.632	1.626

^a Distances in Å and angles in °. ^b DFT calculations. ^c X-ray data from reference 13. ^d Range of Sc–N bond lengths. ^e Contact distances between Sc and the nearest neighbour carbons.

competitive site. The C45–C46 bond is also a corannulene 6:5 C–C bond type with the highest pyramidalization angle. The results are quite significant: the reaction through the corannulene 6:5 C1–C2 bond of the Sc₃N@C₈₀:**12** isomer appears to be the most favorable of all the calculated cycloaddition adducts because this site is the most pyramidalized of the C–C bonds with high MBO. In conclusion, the reaction through the C1–C2 bond of the Sc₃N@C₈₀:**12** isomer is a compromise between a high MBO and a high pyramidalization angle. The REs, MBOs and some geometrical parameters (bond lengths, initial θ_p, final θ_p) of the cycloaddition adducts are listed in Table 4.13. The correlation between the final pyramidalization angle (final θ_p) in the cycloaddition adducts and the RE indicates that if both fragments are to be bound efficiently, pyramidalization angle must be high. So, the isomers that most facilitate the pyramidalization of carbons will tend to be more stable.

For the most stable cycloaddition adduct, the C1–C2 distance (1.632 Å) is considerably longer than the average C1–C2 distance at the unaltered site (1.430 Å). The experimental value was 1.626 Å. The carbons C1 and C2 are pulled away from the center up to a maximum pyramidalization angle of 20.7° (experimental value of 21°). The average of the five Sc–C contacts is computed to be 2.283 Å, quite close to the experimental value of 2.272 Å and longer than the computed value for the free Sc₃NC₈₀:**12** (2.276 Å). The Sc₃N unit is planar and positioned well away from the site of external modification. The mean Sc–N distances (2.016 Å calculated and 2.027

measured) are slightly longer than those in the free $\text{Sc}_3\text{NC}_{80}$:**12** (2.012 Å). Finally, it should be noted that the cycloaddition increases the cage radius again, from 4.118 Å for $\text{Sc}_3\text{N@C}_{80}$:**12** to 4.122 Å for $\text{Sc}_3\text{N@C}_{80}\text{-C}_4\text{H}_6$. In conclusion, the computed geometry for the functionalized structure of $\text{Sc}_3\text{NC}_{80}$ matches perfectly the experimental geometry proposed by Balch and co-workers. For purposes of comparison the above mentioned structures are drawn in Figure 4.13 and some geometrical parameters are listed in Table 4.14.

Finally, we computed the cycloaddition of 1,3-butadiene to the C1–C2 bond of all the $\text{Sc}_3\text{N@C}_{80}$ isomers to investigate whether Sc_3N can rotate inside the carbon cage after the cycloaddition reaction or whether, on the other hand, it is set in one specific position. Except for $\text{Sc}_3\text{N@C}_{80}$:**12**, for the other isomers the C1–C2 bonds are not very reactive because the MBO has intermediate values of 1.177–1.192 (Table 4.13). The main conclusion is that movement is more hindered after the cycloaddition of the diene. The REs of the Sc_3N motion within $\text{C}_{80}\text{-C}_4\text{H}_6$ increase significantly more than those found for the Sc_3N motion within C_{80} . Only isomer **6** decreases the RE from 0.23 eV to 0.16 eV. The other isomers increase the REs: 0.06 to 0.28 eV for isomer **7**, 0.08 to 0.51 eV for isomer **8**, 0.07 to 0.71 eV for isomer **9**, 0.04 to 0.52 eV for isomer **10** and 0.00 to 0.58 eV for isomer **11** (Figure 4.7 and Table 4.13). Thus, the exohedral derivatization helps to fix the endohedral position of the TNT unit.

To demonstrate the decrease in the exohedral reactivity of TNT endohedral metallofullerenes, we performed a series of calculations of 1,3-butadiene cycloaddition to the free C_{80} . These results are listed at the bottom of Table 4.13. As expected, the most stable isomer comes from the addition to the 6:5 C1–C2 bond. The energy involved in the addition reaction to the free C_{80} is almost twice that of the addition reactions to $\text{Sc}_3\text{N@C}_{80}$:**12** (–1.04 eV and –0.54 eV, respectively). We calculated the addition reaction as the energy reaction of $\text{Sc}_3\text{N@C}_{80}$:**12** + 1,3-butadiene \rightarrow $\text{Sc}_3\text{N@C}_{80}\text{-C}_4\text{H}_6$ which was –0.54 eV and the energy reaction of $I_h\text{-C}_{80}$:**7** + 1,3-butadiene \rightarrow $\text{C}_{80}\text{-C}_4\text{H}_6$ which was –1.04 eV. The numerical results also confirm that the TNT encapsulation improves the exohedral regioselectivity of the $I_h\text{-C}_{80}$:**7** fullerene surface: in $I_h\text{-C}_{80}$:**7** there are 60 C–C bonds with equal reactivity whereas in the TNT $\text{Sc}_3\text{N@C}_{80}$:**12** complex just 7 C–C bonds are the most reactive sites (Figure 4.12).

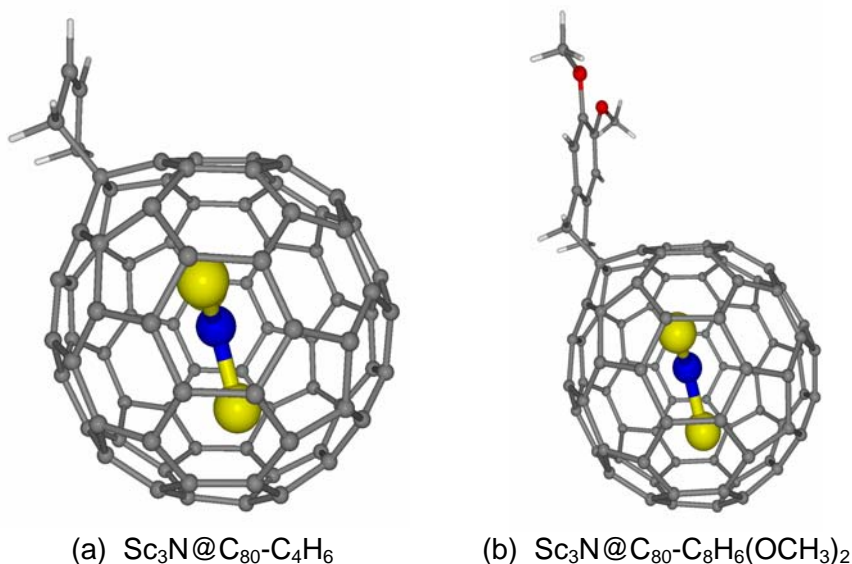


Figure 4.13 Structures for the most stable $\text{Sc}_3\text{N}@C_{80}\text{-C}_4\text{H}_6$ isomer (a) and for the X-ray of $\text{Sc}_3\text{N}@C_{80}\text{-C}_8\text{H}_6(\text{OCH}_3)_2$ (b).

4.7.4 Clues about $[4 + 2]$ cycloaddition on $\text{Sc}_3\text{N}@C_k$ ($k = 68, 78$)

The significant results obtained above in predicting the most reactive exohedral sites of $\text{Sc}_3\text{N}@C_{80}$ prompted us to investigate the $[4 + 2]$ cycloaddition to other known TNT endohedral metallofullerenes: $\text{Sc}_3\text{N}@C_{68}$ and $\text{Sc}_3\text{N}@C_{78}$. The task seemed easier because there is only one possible isomer for these TNT endohedral complexes. We used the same strategy: we localized the most pyramidalized C–C bonds with the highest MBO in the TNT endohedral metallofullerenes of C_{68} and C_{78} . Table 4.15 lists the bond lengths, the pyramidalization angles and the MBOs of the different sets of C–C bonds of the free $D_{3h}\text{-C}_{78}:\mathbf{5}$ and $\text{Sc}_3\text{N}@C_{78}$ while Table 4.16 lists the values for the free C_{68} and $\text{Sc}_3\text{N}@C_{68}$. Here, the MBO analysis suggests that the C–C bonds of the TNT endohedral metallofullerenes are less reactive than the corresponding C–C bonds of the free fullerenes. As was expected the MBO of the C–C bonds near the scandiums decreases and the pyramidalization angle increases significantly.

Table 4.15 Change of the characteristics of the thirteen different set of C–C bonds from free D_{3h} -C₇₈:**5** (initial) to Sc₃N@C₇₈:**1** (final)^a

C–C Bond ^b	Type ^c	Initial Bond lengths	Final bond lengths	Initial θ_p ^d	Final θ_p ^d	Initial MBO ^e	Final MBO ^e
8,24	B	1.424	1.403	9.48	10.05	1.214	1.280
7,21	B	1.419	1.429	9.63	9.51	1.283	1.271
1,2	A	1.392	1.403	11.67	11.28	1.392	1.267
23,44	D	1.470	1.427	10.31	9.20	1.090	1.208
1,6	D	1.443	1.441	11.67	11.28	1.158	1.176
1,9	D	1.446	1.437	11.15	10.95	1.129	1.173
23,24	B	1.423	1.434	9.56	8.98	1.221	1.165
7,8	D	1.443	1.453	10.39	10.98	1.195	1.163
22,23	D	1.414	1.447	10.49	9.68	1.293	1.150
22,42	D	1.451	1.455	10.57	12.02	1.111	1.137
10,11	C	1.470	1.469	8.63	8.36	1.163	1.118
10,26	B	1.436	1.454	9.65	9.26	1.205	1.097
27,28	A	1.372	1.441	10.47	13.88	1.373	1.086

^a Bond lengths in Å and pyramidalization angle in °. ^b See Appendix A.5 for the systematic numeric system extracted from reference: Taylor, R. *J. Chem. Soc., Perkin Trans. 2* **1993**, 813. ^c See Appendix A.1 for a graphical representation of the different C–C bond types (A–D). ^d Average pyramidalization angle (θ_p) of each carbon atom in the C–C bond. ^e Mayer bond order (MBO).

The free D_{3h} -C₇₈:**5** isomer has 13 distinct set of C–C bonds and is one of the fullerenes in which the four possible C–C bond types for IPR fullerenes are present: pyracylene (**A** type), **B** type, pyrene (**C** type) and corannulene (**D** type) (Appendix A.1). The two distinct set of pyracylene C–C bonds are expected to be the most reactive sites for the free C₇₈: C1–C2 and C27–C28. Both C–C bonds have a commonly high MBO (1.392 and 1.373, respectively) which predict a high reactivity and regioselectivity across cycloadditions reactions. Even, these C–C bonds have higher MBOs than those of the 6:6 C–C bonds in C₆₀ and the Ca–Cb in C₇₀. After Sc₃N encapsulation (scandiums are facing the set of C27–C28 bonds), only three distinct C–C bonds (C1–C2, C7–C21 and C8–C24) appear as the most reactive sites, the others being completely discarded because of their lower

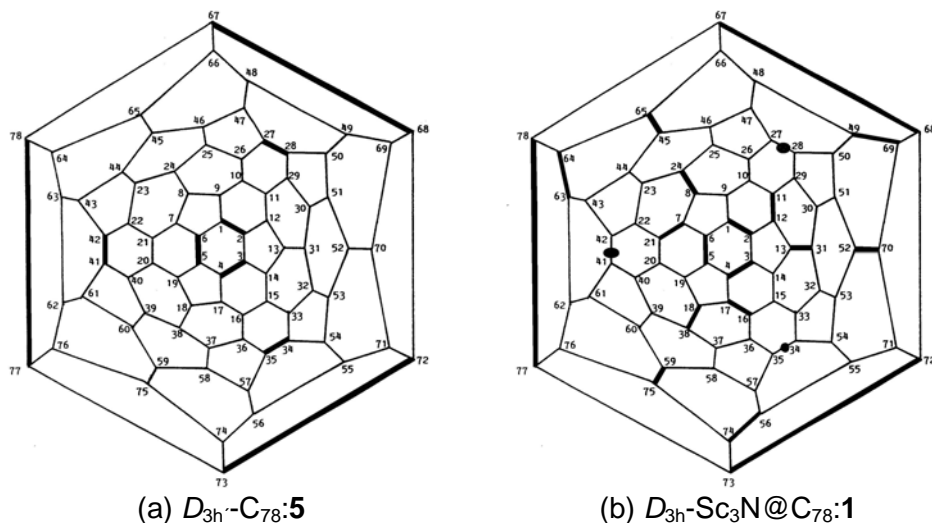


Figure 4.14 The three most reactive exohedral sites for $D_{3h}\text{-C}_{78}:5$ (a) and $\text{Sc}_3\text{N@C}_{78}:1$ (b) drawn in the Schlegel diagram. Sc atoms are facing the fullerene surface in the circle positions. The set of C1–C2 and C27–C28 bonds have been marked (bold lines) for the free $D_{3h}\text{-C}_{78}:5$ in (a), the set of C8–C24, C7–C21 and C1–C2 bonds for $D_{3h}\text{-Sc}_3\text{N@C}_{78}$ in (b). The C–C bonds equivalents to C1–C2 are: C3–C4, C5–C6, C67–C68, C72–C73; equiv. to C27–C28 are: C34–C35, C41–C42, C77–C78; equiv. to C7–C21: C11–C12, C16–C17, C49–C69, C63–C64, C56–C74; equiv. to C8–C24: C13–C31, C18–C38, C45–C65, C52–C70, C59–C75. Description of the marked C–C bonds (MBO, θ_p): (1) $D_{3h}\text{-C}_{78}:5$ C1–C2 (1.392, 11.67°), C27–C28 (1.373, 10.47°) and (2) $D_{3h}\text{-Sc}_3\text{N@C}_{78}$ C8–C24 (1.280, 10.05°), C7–C21 (1.271, 9.51°), C1–C2 (1.267, 11.28°).

MBOs. Special calculations would be necessary to determine the most reactive site because the **B** type 6:6 C7–C21 and C8–C24 have the highest MBO of 1.271 and 1.280, respectively, but a low pyramidalization angle of *ca.* 10° while the set of C1–C2 bonds also has a high MBO with a considerable pyramidalization angle of 11.28°.

Dorn and co-workers derivatized the $\text{Sc}_3\text{N@C}_{78}$ with a ^{13}C -labeled reagent and obtained mono-, di- and triadducts.¹⁷ The ^{13}C and ^1H NMR data of the monoadduct support the idea that addend addition takes place at an asymmetric site (C7–C21 bond) on the C_{78} cage and so we discard the reaction in the C1–C2 and C8–C24 bonds because these would give symmetric structures. It is important to remark that $\text{Sc}_3\text{N@C}_{78}$ is predicted

Table 4.16 Change of the characteristics of the eighteen different set of C–C bonds from free $D_3\text{-C}_{68}$:**6140** (initial) to $\text{Sc}_3\text{N}@C_{68}$ (final) ^a

C–C bond ^b	Patch type ^c	Initial bond lengths	Final bond lengths	Initial θ_p ^d	Final θ_p ^d	Initial MBO ^e	Final MBO ^e
14,24	B	1.429	1.437	9.71	9.97	1.252	1.219
2,13	D	1.449	1.439	10.14	10.35	1.159	1.218
1,2	B	1.431	1.432	9.58	9.55	1.215	1.201
2,3	D	1.433	1.439	10.90	10.69	1.210	1.199
24,25	C	1.488	1.462	8.58	9.01	1.118	1.196
13,14	D	1.443	1.449	10.54	10.58	1.194	1.182
12,13	B	1.413	1.43	9.72	9.43	1.247	1.178
14,15	D	1.438	1.436	10.80	10.67	1.133	1.167
11,12	B	1.433	1.443	10.48	9.76	1.235	1.164
15,27	A	1.396	1.416	11.52	11.56	1.266	1.152
3,15	D	1.447	1.448	11.27	10.65	1.165	1.146
21,42	E	1.436	1.445	16.20	16.69	1.156	1.144
26,27	D	1.458	1.451	11.78	11.44	1.136	1.143
21,22	F	1.421	1.456	13.77	14.66	1.224	1.138
22,23	D	1.45	1.467	11.31	11.40	1.199	1.131
12,22	B	1.446	1.445	10.27	10.63	1.151	1.129
23,24	B	1.418	1.454	9.93	9.60	1.257	1.123
20,21	F	1.424	1.446	14.49	14.70	1.185	1.123

^a Bond lengths in Å and pyramidalization angle in °. ^b See Appendix A.3 for the systematic numeric system. ^c See Appendix A.1 for a graphical representation of the different C–C bond types (**A-F**). ^d

Average pyramidalization angle (θ_p) of each carbon atom in the carbon bond. ^e Mayer bond order (MBO).

to be the most reactive molecule in the cycloaddition reactions: it has the highest MBO of all the TNT endohedral metallofullerenes studied although several positions are possible for the cycloaddition.

According to MBO analysis the most reactive sites in the non-IPR $D_3\text{-C}_{68}$:**6140** fullerene are the **B** type 6:6 C–C bonds: C19–C31, C29–C30 and C18–C28 (Table 4.16 and Figure 4.15). When the Sc_3N is encapsulated, the most reactive sites move to the C5–C6, C6–C7, C18–C19 and C6–C17 bond types but in general the reactivity is substantially reduced. It would be

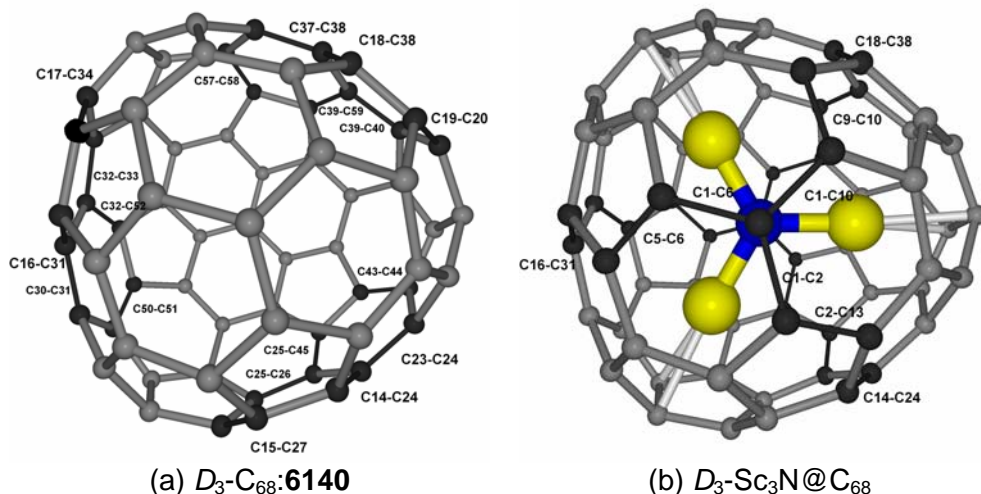


Figure 4.15 The three most reactive exohedral sites for $D_3\text{-C}_{68}\text{:6140}$ (a) and $\text{Sc}_3\text{N@C}_{68}$ (b). The set of C15–C27, C23–C24 and C14–C24 bonds have been marked (bold lines) for the free $D_3\text{-C}_{68}\text{:6140}$ in (a), the set C14–C24, C2–C13 and C1–C2 bonds for $D_3\text{-Sc}_3\text{N@C}_{68}$ in (b). The C–C bonds equivalents to C15–C27 are: C43–C44, C19–C20, C57–C58, C17–C34, C50–C51; equivalents to C23–C24 are: C25–C26, C37–C38, C39–C40, C32–C33, C30–C31; equivalents to C14–C24: C25–C45, C18–C38, C39–C59, C16–C31, C32–C52; equivalents to C2–C13: C9–C10, C5–C6, C46–C63, C60–C67, C53–C65; equivalents to C1–C2: C1–C6, C1–C10, C67–C68, C65–C68 and C63–C68. Description of the marked C–C bonds (MBO, θ_p): (1) $D_3\text{-C}_{68}\text{:6140}$; C15–C27 (1.266, 11.52 °), C23–C24 (1.257, 9.93 °), C14–C24 (1.252, 9.71 °) and (2) $D_3\text{-Sc}_3\text{N@C}_{68}$; C14–C24 (1.219, 9.97 °), C2–C13 (1.218, 10.35 °), C1–C2 (1.201, 9.55°).

interesting to know the reactivity of the 5:5 C15–C46, 6:5 C25–C26 and C24–C25 bond types, which have the highest final pyramidalization angles of 16.69°, 14.66° and 14.70°, respectively.

In conclusion, the study of the electron-attracting character and the analysis of the pyramidalization angle and MBO have shown that the endohedral doping of free fullerenes changes the exohedral reactivity of the fullerene surface in two ways: (1) it reduces and changes the reactivity of the most reactive sites, principally those around the carbon region that the scandiums are facing and (2) it improves the regioselectivity for C_{80} , which showed a very poor character, but does not improve it for C_{78} and C_{68} . In

general, however, TNT encapsulation is a new tool for controlling the regioselectivity of additions to the fullerene surface.

4.8 EXOHEDRAL REACTIVITY (II): FLUORINATION OF $\text{Sc}_3\text{N@C}_{80}$

4.8.1. Experimental

Preliminary data for hydrogenation of a very small quantity (*ca.* 1 mg) of $\text{Sc}_3\text{N@C}_{80}$ (mainly I_h but containing *ca.* 10% of the D_{5h} isomer) showed in two separate samples, the addition of 60 H and 68 H.¹⁶ Subsequent investigation of fluorination of $\text{Sc}_3\text{N@C}_{80}$ using a larger sample gave a number of products that contained, in varying relative concentrations, between 42 and 64 fluorines. Because of the larger sample used, we consider that the fluorination results are the more reliable, and in all the fluorinated fractions $\text{Sc}_3\text{N@C}_{80}\text{F}_{52}$ was present, being the dominant species in a number of them.⁷⁴ Because of the presence of the minor isomer (which is less soluble in toluene than the main one) and possibly others, we believe that further and meaningful experimental investigations of polyaddition can only be undertaken with larger quantities of the pure isomers, should these become available. We have therefore carried out theoretical calculations to predict stabilities of derivatives of various addition levels, and to consider the stabilities in particular of various isomers at the X_{52} ($X = \text{H}, \text{F}$) addition level, both with and without incarcerated Sc_3N . Because of the difficulty accompanying calculations for large highly polyfluorinated fullerenes, for the incarcerated Sc_3N derivatives we have used the isostructural hydrogenated species as models *cf.* reference 75.

4.8.2 Hydrogenation binding energies (HBE) for $I_h\text{-C}_{80}:7$

As a first step we determined the most stable structures for compounds C_{80}H_x ($x = 2, 4, 16, 36, 44, 48, 52, 72, 76, 78, 80$), thereby covering low ($x = 2, 4$), intermediate ($x = 16, 36, 44, 48, 52$) and high ($x = 72, 76, 78, 80$) addition levels. Each group has a particular rule for their stabilization. Previously, a large number of isomers, including non-symmetric structures, have been examined with the AIMPRO program to

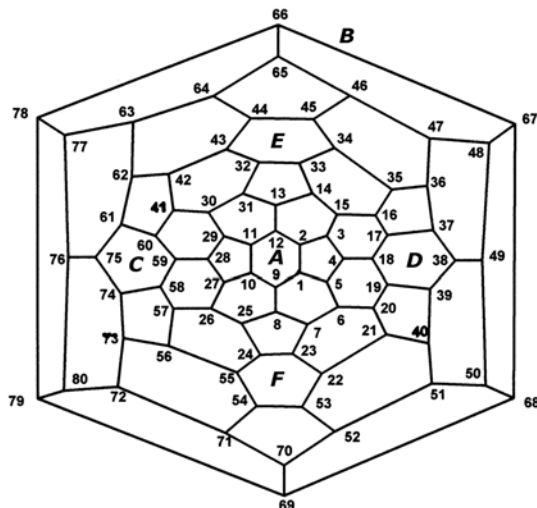


Figure 4.16 Schlegel diagram for the I_h -C₈₀:7 fullerene showing numbering. The capital letters represent the position of the benzenoid rings.

obtain indications as to the most stable of them. The AIMPRO self-consistent density functional code running at the local spin density approximation (LSDA) level, allows an economic calculation as a first step.⁷⁶ With AIMPRO we found that non-symmetric structures for some stoichiometries are almost isoenergetic compared with the analogous symmetric structures presented in Table 4.17.⁷⁷ The description of the most stable isomers of each stoichiometry is given in Table 4.17, which shows the aromatic benzenoid rings, C=C bonds, symmetry, and the hydrogenation binding energies (HBE) for the process $C_{80} + nH_2 \rightarrow C_{80}H_{2n}$. Specifically, we computed the HBE per added H₂ (referred to as HBE/*n*) above the C₈₀ surface because this BE allows us to compare all stoichiometries with each other. There are only two possibilities for the first addition to the C₈₀ surface, either 6:5 C1–C2 or 6:6 C1–C9 bonds (see Figure 4.16 for numbering and position of the benzenoid rings) but we expect the most pyramidalized with a high MBO 6:5 C1–C2 bond ($\theta_p = 10.58^\circ$ and MBO = 1.194) to be the most reactive site (HBE = -1.25 eV). The product of H₂ addition across the 6:6 C1–C9 bond is 0.61 eV less stable.

Table 4.17 Hydrogenation binding energies (HBE/ n , eV) per added H₂ of the most stable C₈₀H _{x} and Sc₃N@C₈₀H _{x} isomers ^a

x	H atom locations ^a	Benzenoid rings ^b	C=C bonds ^b	Sym. ^c	HBE/ n for C ₈₀ H _{x} ^d	HBE/ n for Sc ₃ N@C ₈₀ H _{x} ^e
2	1,2	0	--	C _s	-1.25	--
4	1,2,7,23	0	--	C _{2v}	-1.24	--
16	3-8, 25-31, 13-15	A	--	C _{2v}	-1.04	--
36	^f	A, C, D	--	C ₂	-1.05	--
44	--	A, B, C, D, E, F	--	T _h	-1.08	-0.64
48	--	A, B, C, D	18,19; 37,38, 58,59; 61,75	C _s	-0.92	-0.53
52:1	--	A, B, C, D	23,24; 32,33	C _{2v}	-0.83	-0.47
52:5	--	A, B, C, D	22,23; 33,34	C _s	-0.82	-0.49
72	--	0	1,2; 39,40; 41,60; 78,79	C _s	-0.35	-0.10
76	--	0	1,2; 78,79	C _s	-0.20	--
78	--	0	1,2	C _s	-0.13	--
80	--	0	--	I _h	-0.06	--

^a Up to the 36 H level the description is with respect to the hydrogenated carbons. Above the 16 H level it is with respect to benzenoid rings and the hydrogen-free C₂ bond atoms. ^b See Figure 4.16 for numbering. ^c Symmetry of C₈₀H _{x} molecule. ^d HBE per H₂ added to C₈₀, HBE/ n = $\Delta E/n$, $n = x/2$, where ΔE = reaction energy for C₈₀ + n H₂ → C₈₀H _{$2n$} . ^e HBE per H₂ added to Sc₃N@C₈₀, HBE/ n = $\Delta E/n$, $n = x/2$, where ΔE = reaction energy for Sc₃N@C₈₀ + n H₂ → Sc₃N@C₈₀H _{$2n$} . ^f 3-8, 13-16, 20, 21, 25-31, 35, 36, 40-42, 48, 49, 56, 57, 62, 73, 76, 80.

Formation of C₈₀H₄ is predicted to involve addition of H₂ to C₁–C₂ bond followed by addition to the 6:5 C₇–C₂₃ bond. By contrast, addition to the opposed remote C₇₈–C₇₉ or neighbouring 6:5 C₄–C₅ bonds gives isomers that are less stable by 0.38 and 1.20 eV, respectively. This suggests

that it is profitable to investigate additions fairly near to C–C bonds that have already undergone addition. The most stable isomers of $C_{80}H_x$ ($x = 16, 36, 44, 48, 52$) involve hydrogen addition so as to produce aromatic (benzenoid) rings, as is the case in the formation of $C_{60}Y_x$ ($Y = H, F; x = 18, 36$).^{78, 79} $C_{80}H_{16}$ has only one benzenoid ring (A), whereas $C_{80}H_{44}$ has the maximum number of six (A-F). The latter structure adopts a ‘cubic’ shape due to the six planar aromatic faces together connected with twenty-two hydrogenated C–C bonds (Figure 4.17). $C_{80}H_{48}$ and $C_{80}H_{52}$ add the additional H_2 units to the E and F rings of $C_{80}H_{44}$ and consequently retain four benzenoid rings. In the higher stoichiometries, ($x = 72, 76, 78$) there are no benzenoid rings, and the remaining free 6:5 bonds are separated as far possible from each other. Thus the two unhydrogenated C=C bonds in $C_{80}H_{76}$ are located in the opposite hemispheres at C1–C2 and C78–C79. Location of the sole unhydrogenated bond in $C_{80}H_{78}$ across a 6:5 C1–C2 bond is marginally (0.11 eV) favoured over a 6:6 C1–C9 bond. Full sphericity is restored in $C_{80}H_{80}$, the cage radius being 4.502 Å compared with 4.103 Å for C_{80} , due to C–C bond lengthening arising from strong H–H steric repulsions rather than to rehybridization effects.⁸⁰

We have also analyzed the bond between the C_{80} cage and the H_2 units using the extended transition method developed by Ziegler and Rouk (an extension of the decomposition scheme of Morokuma). According to this method, the BE between two fragments can be dissected into two main contributions: $BE = \Delta E_{DE} + \Delta E_{INT}$. In our specific case, ΔE_{DE} comprises only the deformation energy of C_{80} , *i.e.* the energy difference between the free C_{80} and C_{80} with the geometry of the particular $C_{80}H_x$ compound. ΔE_{INT} , the interaction energy, represents the energy involved in the interaction between the deformed C_{80} fullerene and the nH_2 units. ΔE_{DE} is always > 0 *i.e.* destabilising, whereas ΔE_{INT} can be $>$ or < 0 . An exothermic reaction requires $\Delta E_{INT} < 0$ and $|\Delta E_{INT}| > |\Delta E_{DE}|$. More details about this decomposition can be found in subsection 4.2.4. Recently this method has been used very satisfactorily, to rationalise the metal- C_{60} bonding in organometallic derivatives of C_{60} .⁴⁸ The components of the HBE are collated in Table 4.18.

There is a relatively small variation in the HBE/ n between $C_{80}H_2$ and $C_{80}H_{44}$, (-1.25 and -1.08 eV per added H_2 , respectively), but at higher hydrogenation levels the stabilities rapidly decrease, and $C_{80}H_{80}$ is only

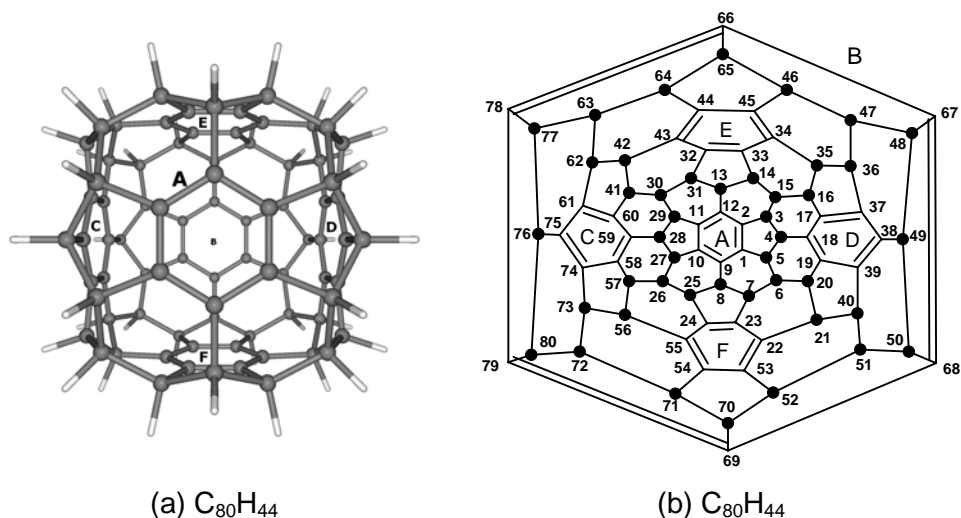


Figure 4.17 Optimized structure (a) and Schlegel diagram (b, ● = H) for $C_{80}H_{44}$. The benzenoid rings are located in both for comparison.

marginally stabilized (-0.06 eV per added H_2). This trend can be clearly seen in Figure 4.18 (circles). A parallel observation was found for C_{60} and C_{70} in that hydrogenation and fluorination led to maximum addend levels only of *ca.* 52 and 56 respectively.⁸¹ A significant feature is that $C_{80}H_{44}$ possesses six benzenoid rings, the aromaticity of the latter arising from the presence of three sp^3 hybridised carbons in the two pentagons adjacent to each, thereby allowing delocalization without strain.⁸² From $C_{80}H_2$ to $C_{80}H_{52}$ the ΔE_{DE} values increase gradually from 1.40 to 1.62 eV but thereafter reduce substantially to 1.01 eV for $C_{80}H_{80}$. This trend is closely related to the deformation of the cage; at hydrogenation levels above $C_{80}H_{52}$ the C_{80} geometry becomes increasingly spherical again up to $C_{80}H_{80}$. The ΔE_{INT} values also increase slightly up to $C_{80}H_{44}$ but thereafter decrease even more rapidly than the ΔE_{DE} values due to the lack of reactivity of the remaining C=C bonds towards H_2 . The C–C bonds at high $C_{80}H_x$ stoichiometries are long and have low π -bond character. This seems to be the important factor in determining the notable change in HBE/*n* at around $C_{80}H_{44}/C_{80}H_{52}$ stoichiometry (Figure 4.18). For this reason, the $C_{80}H_{52}$ stoichiometry is particularly important, and in the next section we focus on the encapsulation of Sc_3N nitride in several isomers of $C_{80}H_{52}$ in order to find the most stable

Table 4.18 Deformation (ΔE_{DE}) and interaction energy (ΔE_{INT}) components of the hydrogenation binding energies per added H_2 (HBE/n) for the most stable isomers of $C_{80}H_x$ ^a

x	$\Delta E_{DE}/n$ ^b	$\Delta E_{INT}/n$ ^c	HBE/n ^d
2	1.40	-2.65	-1.25
4	1.42	-2.66	-1.24
16	1.67	-2.71	-1.04
36	1.59	-2.64	-1.05
44	1.60	-2.68	-1.08
48	1.62	-2.54	-0.92
52: 1	1.62	-2.45	-0.83
52: 5	1.59	-2.41	-0.82
72	1.31	-1.66	-0.35
76	1.16	-1.36	-0.20
78	1.08	-1.21	-0.13
80	1.01	-1.07	-0.06

^a Energies in eV. ^b $\Delta E_{DE}/n = [E(C_{80}^* \text{ geometry fixed at } C_{80}H_x) - E(C_{80} \text{ optimized})]/n$. ^c $\Delta E_{INT}/n = [E(C_{80}^* + n H_2 \rightarrow C_{80}H_{2n})]/n$. ^d $HBE/n = \Delta E_{DE}/n + \Delta E_{INT}/n$.

one. Tables 4.17 and 4.18 present only a brief summary of the $C_{80}H_{52}$ study: the values for the most stable empty cage $C_{80}H_{52}$:**1**, and for the empty $C_{80}H_{52}$:**5** cage that produces the most stable $Sc_3N@C_{80}H_{52}$:**5** complex.

4.8.3 HBE for $Sc_3N@C_{80}$

Cages $C_{80}H_x$ ($x = 44, 48, 52, 72$) selected for encapsulation with Sc_3N are completely deformed, consequently there is only one possible position where the nitride can be stabilized (see below). The nitride is planar in $Sc_3N@C_k$ ($k = 68, 78, 80$), but is pyramidal in most $Sc_3N@C_{80}H_{52}$ studied isomers and $Sc_3N@C_{80}H_{72}$ as it is a free molecule. We compare HBE/n for $C_{80}H_{2n}$ and $Sc_3N@C_{80}H_{2n}$ to determine the difference in the values arising from adding H_2 units to the corresponding parents (last two columns of Table 4.16). The data for the endohedral complexes parallel those for the empty cages, except that the BE disadvantage on going to higher addition levels is even larger (see squares compared with circles in Figure 4.18). For

Table 4.19 Decomposition of the hydrogenation (HBE) and encapsulation (EBE) binding energies for $\text{Sc}_3\text{N}@C_k$ ($k = 78, 80$) and $\text{Sc}_3\text{N}@C_{80}\text{H}_x$ ($x = 44, 48, 52, 72$)^a

Compound	ΔE_{DE}	ΔE_{INT}	HBE ^b	ΔE_{DE}		ΔE_{INT}	EBE ^c
				Sc_3N	Cage		
$\text{Sc}_3\text{N}@C_{78}:\mathbf{1}$	--	--	--	0.72	1.49	-11.91	-9.70
$\text{Sc}_3\text{N}@C_{80}:\mathbf{11}$	--	--	--	0.79	0.58	-12.97	-11.60
$\text{Sc}_3\text{N}@C_{80}\text{H}_{44}$	35.20	-58.96	-23.76	0.53	1.47	-5.69	-3.69
$\text{Sc}_3\text{N}@C_{80}\text{H}_{48}$	38.95	-60.98	-22.03	0.57	1.84	-6.34	-3.93
$\text{Sc}_3\text{N}@C_{80}\text{H}_{52}:\mathbf{5}$	41.29	-62.56	-21.27	0.28	2.62	-7.83	-4.93
$\text{Sc}_3\text{N}@C_{80}\text{H}_{72}$	47.09	-59.65	-12.56	0.34	2.55	-7.09	-4.20

^a Energies in eV. ^b Hydrogenation binding energies (HBE) for the reaction $C_{80} + n\text{H}_2 \rightarrow C_{80}\text{H}_{2n}$; HBE = $\Delta E_{DE} + \Delta E_{INT}$. ^c Encapsulation binding energies (EBE) for the reactions $C_k + \text{Sc}_3\text{N} \rightarrow \text{Sc}_3\text{N}@C_k$ ($k = 78, 80$) and $C_{80}\text{H}_x + \text{Sc}_3\text{N} \rightarrow \text{Sc}_3\text{N}@C_{80}\text{H}_x$ ($x = 44, 48, 52, 72$); EBE = $\Delta E_{DE} + \Delta E_{INT}$.

example, the addition of 22 H_2 to empty C_{80} produces an energy of *ca.* 1.08 per added H_2 , whereas the same addition to $\text{Sc}_3\text{N}@C_{80}$ gives an energy of only 0.64 eV per added H_2 . Encapsulation of Sc_3N is a strongly exothermic process that is accompanied by a formal transfer of six electrons from the scandiums to the fullerene cage, thereby making hydrogen addition less favourable. In large stoichiometries such as $\text{Sc}_3\text{N}@C_{80}\text{H}_{72}$ the lack of reactivity of the remaining C–C bonds also disfavours addition, and the HBE/ n is reduced to only -0.10 eV.

4.8.4 Sc_3N encapsulation in free cages vs. hydrogenated fullerenes cages

The comparison (Table 4.19) between $\text{Sc}_3\text{N}@C_k$ ($k = 78, 80$) and $\text{Sc}_3\text{N}@C_{80}\text{H}_x$ ($x = 44, 48, 52, 72$) provides a measure of the energy involved in the encapsulation and hydrogenation processes. The EBE for $C_k + \text{Sc}_3\text{N} \rightarrow \text{Sc}_3\text{N}@C_k$ accounts -11.60 and -9.70 eV for $k = 80$ and 78, respectively. The deformation energy component (ΔE_{DE}) of EBE comprises the deformation produced in the Sc_3N nitride and the cage, both of which are small components, *e.g.* 1.37 eV in total for $k = 80$. The much more significant contributor to the EBE is the favourable interaction energy (ΔE_{INT}) arising from the electron transfer from nitride to fullerene cage, and which for $x = 80$ is -12.97 eV. Whereas for $\text{Sc}_3\text{N}@C_k$ complexes, only

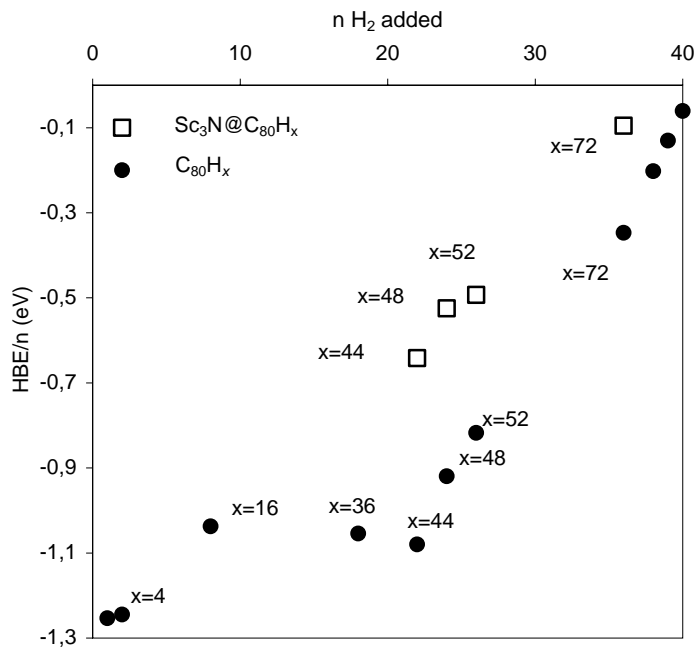


Figure 4.18 Hydrogenation binding energy per added H₂ (HBE/*n*) for series C₈₀H_{*x*} (*x* = 2, 4, 16, 36, 44, 48, 52, 72, 76, 78 and 80), circles, and Sc₃N@C₈₀H_{*x*} (*x* = 44, 48, 52, 72), squares.

computation of encapsulation is required, Sc₃N@C₈₀H_{*x*} requires computation of both encapsulation and hydrogenation, for which two sequences exist. To simplify the calculations involved in finding the most stable structures of Sc₃N@C₈₀H_{*x*} we first narrow down the hydrogenated possibilities (in order to make the computations manageable) and then determine energies for placing Sc₃N inside them. Note that this simplification is based on the difference of the absolute EBE and HBE. HBE for C₈₀H_{*x*} (*x* = 44, 48, 52) are *ca.* -22 eV, almost double the EBE involved in formation of Sc₃N@C₈₀ (-11.6 eV). Consequently, hydrogenation rather than encapsulation will determine the selection of the most stable isomers, so that this energy difference validates our procedure. The HBE for C₈₀H_{*x*} are dominated by the favourable ΔE_{INT} between the cages and the H₂ units, and decrease in the order C₈₀H₄₄ > C₈₀H₄₈ > C₈₀H₅₂ > C₈₀H₇₂. The EBE in these hydrogenated cages decrease drastically from –

11.6 for $\text{Sc}_3\text{N}@C_{80}$ to *ca.* -4 for $\text{Sc}_3\text{N}@C_{80}\text{H}_x$ ($x = 44, 48, 52, 72$) complexes due to an increase of ΔE_{DE} of the fullerene cage, but above all due to a decrease of the ΔE_{INT} between the hydrogenated cage and the nitride *i.e.* -12.97 eV for $\text{Sc}_3\text{N}@C_{80}$ compared to *ca.* -7 for $\text{Sc}_3\text{N}@C_{80}\text{H}_x$ ($x = 44, 48, 52, 72$) complexes. This less effective interaction may reflect electron transfer from the nitride to the hydrogenated cage being less facilitated due to the lower acceptor character of the unoccupied orbitals of the hydrogenated cage compared to those of C_{80} . The decrease in the in-cage space and consequent increase in steric repulsion between the nitride and cage is involved in the ΔE_{INT} diminution.

The highest HBE is found for $C_{80}\text{H}_{44}$ and the highest EBE for $\text{Sc}_3\text{N}@C_{80}\text{H}_{52}$:**5**. The EBE is favoured by having a suitable in-cage space to incarcerate Sc_3N , the largest space being found in $\text{Sc}_3\text{N}@C_{80}\text{H}_{52}$ among $\text{Sc}_3\text{N}@C_{80}\text{H}_x$ ($x = 44, 48, 52, 72$). Note that the only marginally stabilized H_2 addition to $\text{Sc}_3\text{N}@C_{80}$ at higher addition levels is caused by HBE rather than EBE, as exemplified by $\text{Sc}_3\text{N}@C_{80}\text{H}_{72}$ (-0.10 eV). Compared to $\text{Sc}_3\text{N}@C_{80}\text{H}_{44}$ the HBE decreases from -23.76 to -12.56 eV, whereas the EBE are closely similar (-3.69 and -4.20 eV respectively).

4.8.5 Stabilities of $C_{80}\text{H}_{52}$ and $C_{80}\text{F}_{52}$ isomers

A common experimental occurrence of a 52-addend level for hydrogenation and fluorination of $\text{Sc}_3\text{N}@C_{80}$, prompted a deeper investigation to find the most stable isomers of $C_{80}\text{H}_{52}$, $C_{80}\text{F}_{52}$, and $\text{Sc}_3\text{N}@C_{80}\text{H}_{52}$ and the stabilising factors affecting their REs. Following the procedure in subsection 4.8.4, the most stable structures obtained from hydrogenation were determined and then Sc_3N was encapsulated. Fourteen isomers of $C_{80}\text{H}_{52}$ are collated in Table 4.20 showing the number of benzenoid rings, C=C bonds and REs. Isomers **1-8** are the most stable, the stabilities differing by only 0.35 eV overall, with **1** being the most stable. These isomers uniquely each possess four benzenoid rings (A, B, C, D) and two C=C bonds in hexagons E and F *i.e.* on opposite sides of the cage (Figure 4.16 and Table 4.20). Isomers **9** and **10** also have four benzenoid rings but here the C=C bonds are not located in hexagons **E** and **F** and this is seen to have a marked difference on the calculated stabilities. The calculated energies for isomers **9-14** are also high due evidently to the lower

Table 4.20 Description and relative energies (RE) of $C_{80}H_{52}$, $C_{80}F_{52}$ and $Sc_3N@C_{80}H_{52}$ isomers ^a

<i>Iso.</i>	<i>Benzenoid rings</i> ^b	<i>C=C bond</i> ^c	<i>Sym.</i> _d	$C_{80}H_{52}$	$C_{80}F_{52}$	$Sc_3N@C_{80}H_{52}$
1	A, B, C, D	23,24; 32,33	C_{2v}	0.00	0.00	0.00
2	A, B, C, D	23,24; 44,45	C_{2h}	0.03	0.05	-0.39
3	A, B, C, D	22,53; 32,33	C_1	0.18	--	--
4	A, B, C, D	22,23; 32,33	C_2	0.32	0.51	0.43
5	A, B, C, D	22,23; 33,34	C_s	0.31	0.50	-0.55
6	A, B, C, D	22,23; 32,43	C_2	0.35	0.55	-0.25
7	A, B, C, D	22,23; 34,45	C_2	0.32	0.51	0.44
8	A, B, C, D	22,23; 44,45	C_i	0.35	0.58	--
9	A, B, C, D	7,23; 14,33	C_s	1.73	2.21	1.77
10	A, B, C, D	21,22; 42,43	C_2	2.26	3.07	--
11	A, B	17,37; 19,39; 22,23; 24,55; 32,43; 33,34; 58,74; 60,61	C_s	1.39	0.19	--
12	A, B	17,18; 22,23; 24,55; 32,43; 33,34; 38,39; 58,59; 61,75	C_2	1.44	0.79	0.49
13	--	^e	C_s	5.24	5.22	--
14	--	^f	C_{2v}	3.58	4.04	2.90

^aEnergies in eV. Description with respect to hydrogen-free carbons, benzenoid rings, and C_2 free bonds. ^b See Figure 4.16. ^c Double bond locations, either 6:6 or 6:5 bonds. ^d Symmetry of $C_{80}H_{52}$ and $C_{80}F_{52}$ isomers. ^e 1,5; 7,23; 10,27; 14,33; 17,37; 19,39; 31,32; 44,64; 45,46; 50,68; 52,53; 58,74; 60,61; 79,80. ^f 4,18; 8,9; 12,13; 22,23; 24,55; 28,59; 32,43; 33,34; 36,47; 40,51; 62,63; 65,66; 69,70; 72,73.

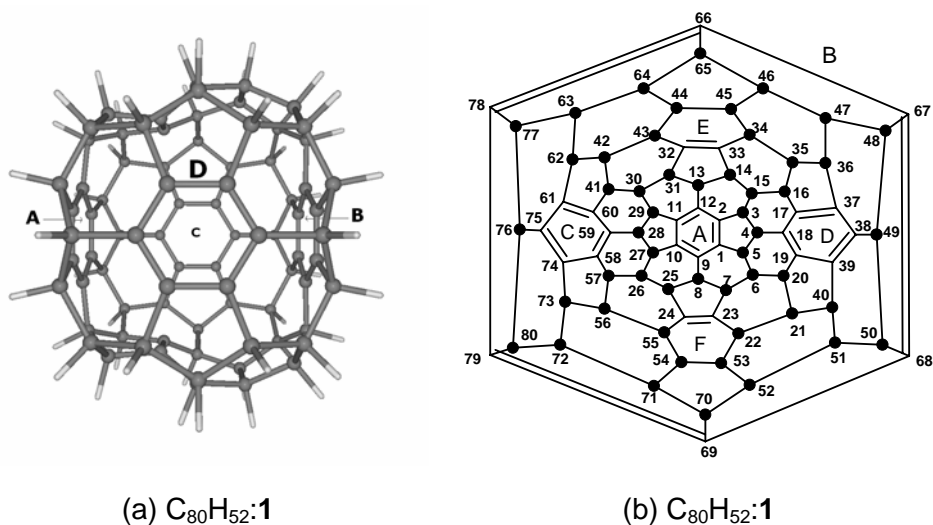
number of benzenoid rings in the structures, and thus the least stable isomers **13** and **14** have no benzenoid rings, the fourteen C=C bonds being spread around the cage.

The Schlegel diagram and optimized structure of $C_{80}H_{52}$:**1** are shown in Figure 4.19. The lengths of the C–C bond in the aromatic benzenoid rings are calculated to vary only from 1.377 to 1.386 Å, the aromaticity being

confirmed also by the calculated planarity. This parallels the structural situation found experimentally for $C_{60}H_{36}$ isomers.⁷⁹ The lengths of the isolated C=C bonds are calculated as 1.335 Å. The resultant structure resembles a cube with four planar faces and two wrinkled ones which contain the C=C bonds, and notably, the hydrogenation of 26 C–C bonds in C_{80} produces a major distortion of the original shape. The C–C bond lengths for the other isomers differ little from the above values. Results for fluorination are similar, except that isomer **11** is relatively more stable than the hydrogenated counterpart. The C–F distances for the most stable isomer **1** are calculated to range from 1.367–1.396 Å which parallels the values found for $C_{60}F_{48}$ (1.362–1.395 Å)⁸³ and $C_{60}F_{18}$ (1.361–1.396 Å).⁸⁴ This indicates that the present level of computing is very satisfactory. The similar results for H and F atoms allow us to use with some confidence, hydrogen as a model for calculating the energies of the *incar* Sc_3N derivatives.

4.8.6 Stabilities of $Sc_3N@C_{80}H_{52}$ isomers

To construct the $Sc_3N@C_{80}H_{52}$ isomers we encapsulated the Sc_3N unit retaining some symmetry properties such as symmetry plane or C_2 axis and also orientating the Sc atoms over the C=C bonds and the benzenoid rings. These requirements and the space limitation of the fullerene restrict the stabilising orientation of the nitride in each $C_{80}H_{52}$ isomer to one possibility only. By contrast, in $Sc_3N@C_{80}$ the Sc_3N unit is not trapped in a specific position and free rotation is expected. The preference for Sc atoms to be close to the free C atoms is expected because the latter can use their p_z orbitals to make Sc–C bonds. Moreover, to accomplish these requirements, Sc_3N adopts a pyramidal structure in most of the isomers. Isomers of $Sc_3N@C_{80}H_{52}$ were optimized from $C_{80}H_{52}$ isomers **1**, **2**, **4-7**, **9** that have four benzenoid rings, and also isomers **12** and **14** that have two and no benzenoid rings, respectively; lack of symmetry precluded calculations on isomers **3**, **8**, **10** and **11**. The REs show significant differences from those of their empty-cage counterparts (see last column of Table 4.20), but the most stable $Sc_3N@C_{80}H_{52}$ isomers come from the first eight most stable $C_{80}H_{52}$ isomers. Isomers $Sc_3N@C_{80}H_{52}$:**2**, **5**, and **6** are predicted to be more stable than isomer $Sc_3N@C_{80}H_{52}$:**1** (derived from the most stable $C_{80}H_{52}$ isomer)



Figures 4.19 Optimized structure (a) and the Schlegel diagram (b, ● = H) for $C_{80}H_{52}:1$. Structure (a) is rotated relative to the Schlegel diagram. The benzenoid rings are located in both for comparison.

with $Sc_3N@C_{80}H_{52}:5$ the most stable overall; both isomers are displayed in Figures 4.20 and 4.21.

The substantial alteration of the REs as a result of encapsulation of Sc_3N arises from different interaction between the nitride and the relevant hydrogenated cage, together with the different number and strength of the Sc–C bonds. This argument is developed further in section 4.3. The geometric and electronic structure of the most stable isomer $Sc_3N@C_{80}H_{52}:5$ is considered first, followed by determination of the factors that affect the stabilization of the $Sc_3N@C_{80}H_{52}$ isomers.

4.8.7 Geometric and electronic structure of $Sc_3N@C_{80}H_{52}:5$

Some values of the HOMO-LUMO gap in eV (a measure of stability) are: I_h-C_{80} , 1.93; $C_{80}H_{52}:5$, 3.96; $Sc_3N@C_{80}:11$, 1.18; $Sc_3N@C_{80}H_{52}:5$, 0.23. The latter thus appears to be the least stable amongst this family of complexes. When Sc_3N is encapsulated by $C_{80}H_{52}:5$, there is significant local distortion in the hydrogenated cage. In this isomer, two Sc atoms face the two isolated C=C bonds (C22–C23 and C33–C34) and the other faces benzenoid ring D and two atoms of B (Figure 4.20b). This

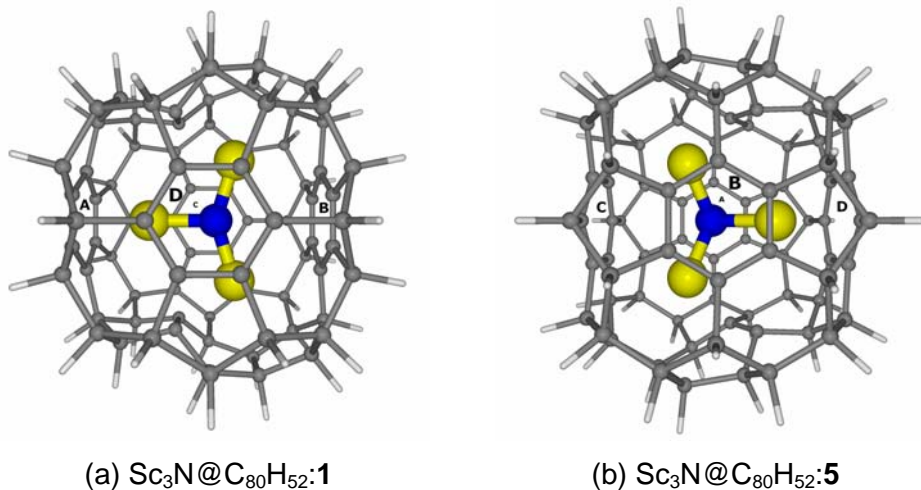


Figure 4.20 Optimized structures for $\text{Sc}_3\text{N}@C_{80}\text{H}_{52}:1$ (a) and $\text{Sc}_3\text{N}@C_{80}\text{H}_{52}:5$ (b). For comparison, the benzenoid rings are located in each picture.

distortion results in inward movement of the non-hydrogenated carbons until they attain bonding Sc–C distances. The benzenoid ring B is moved substantially inward. The pyramidal Sc_3N unit (Sc–N distance of 1.921 Å, *cf.* 1.957 Å in the free molecule, Table 4.21) is unable to either rotate or fluctuate *i.e.* it is completely fixed in this orientation. The cage otherwise retains the overall structure of the $\text{C}_{80}\text{H}_{52}:5$ precursor (Figure 4.21). Hence hydrogenation determines the main geometric features of the cage, whilst encapsulation produces modification. During the geometrical optimization process, the contacts between Sc and free C atoms become favoured and maximized. The average distance between Sc and the eight carbons of benzenoid ring D and two of ring B decrease to a bonding distance of 2.391 Å. The aromaticity of these two rings is broken and the range of C–C distances within them is increased (1.384–1.446 Å). The other non-bonded benzenoid rings (A and C) retain their aromaticity. The shortest Sc–C distances (2.293 Å) are found between the other two Sc atoms and one of the carbons of the two C=C bonds. Due to these Sc–C₂ bonds the C=C bond lengths of the cage are increased by 0.085 Å.

These Sc–C distances fall within the range of values obtained in an exploration of 73 examples in the Cambridge Structural Database, where the mean is 2.430 Å and the shortest 2.204 Å. Both experimental (2.170 Å) and

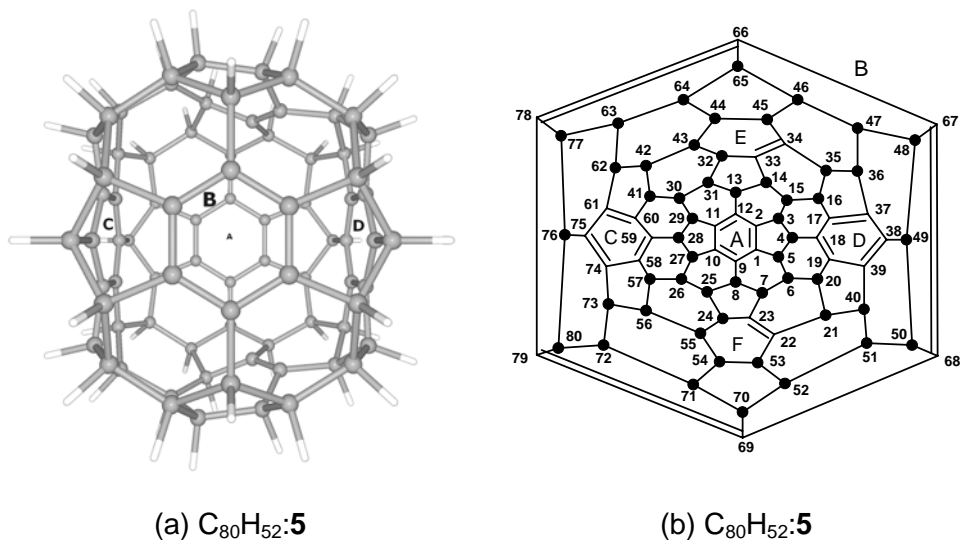


Figure 4.21 Optimised molecular structure (a) and Schlegel diagram (b, ● = H) for $C_{80}H_{52}:5$. The benzenoid rings are located in both for comparison.

theoretical (2.276 Å) distances for $Sc_3N@C_{80}$ were shorter than the calculated Sc–C distances in $Sc_3N@C_{80}H_{52}:5$. The presence of bonding Sc–C distances and the potential for trapping of Sc_3N in a specific position, prompted us to investigate the possibility of strong Sc–C bonds between the Sc_3N unit and the hydrogenated cage. However, $Sc_3N@C_{80}$ may be *formally* described by the $Sc_3N^{6+}@C_{80}^{6-}$ ionic model involving the transfer of six electrons from the three nitride highest occupied orbitals to the three lowest unoccupied orbitals of C_{80} , and free rotation of Sc_3N unit. The electronic structure of $Sc_3N@C_{80}H_{52}:5$ is characterized not only by the ionic interaction but also by orbital interactions of both fragments which incarcerate the Sc_3N in a specific position. Likewise, there is formal transfer of six electrons from the three highest occupied orbitals of Sc_3N unit to the three lowest unoccupied orbitals of $C_{80}H_{52}:5$ molecule, which become the three HOMOs of the new $Sc_3N@C_{80}H_{52}:5$ complex. These cage orbitals, which represent π^* C–C orbitals of $C_{80}H_{52}:5$ also become highly stabilized due to bonding interactions with empty *d* metal orbitals, so explaining the strong link between Sc atoms and the free C atoms of the cage. The three bonding orbitals are displayed in Figure 4.22.

Table 4.21 Optimized distances for Sc₃N@C₈₀H₅₂ isomers ^a

<i>Iso.</i>	<i>Mean Sc–N distance</i> ^a	<i>No. of Sc–C₂ connections</i>	<i>Mean Sc–C distance</i> ^b	<i>No. of Sc–C₆ connections</i>	<i>Mean Sc–C distances</i>
1	1.879	4	2.224	6	2.361
2	1.895	4	2.326	6	2.387
4	1.884	4	2.391	6	2.366
5	1.921	4	2.423	8	2.391
6	1.897	4	2.313	6	2.437
7	1.891	4	2.363	6	2.371
9	1.903	2	2.269	8	2.388
12	1.877	6	2.318	--	--
14	1.920	4	2.364	--	--

^aDistances in Å. ^b Calculated as 1.957 Å in Sc₃N. ^c Calculated as 2.276 Å in Sc₃N@C₈₀.

4.8.8 Factors affecting the stabilization energies

The REs were analyzed in terms of their components in order to determine the origin of the differences amongst the Sc₃N@C₈₀ isomers (Table 4.22). To aid this analysis, the Sc–N bond lengths and the different type of Sc-cage connections with their respective lengths are collated in Table 4.21. The main contributions to the RE (HBE and EBE), can each be dissected into the deformation energy (ΔE_{DE}) and the interaction energy (ΔE_{INT}). As seen from Table 4.22, EBE but not HBE is the crucial component of the RE and determines the stability order of the Sc₃N@C₈₀H₅₂ isomers. Thus whilst Sc₃N@C₈₀H₅₂:**5**, the most stable isomer, does not have the highest HBE, it has the highest EBE of –4.93 eV. For the first eight most stable C₈₀H₅₂ isomers the relative HBE ranges between 0.00 and 0.35 eV whereas the relative EBE between 0.44 and –0.55 eV. So the differences in the interaction between Sc₃N and the different C₈₀H₅₂ cages determine the final RE of Sc₃N@C₈₀H₅₂ isomers. This isomer is therefore the most favourable because Sc₃N unit is encapsulated favouring Sc–C contacts,

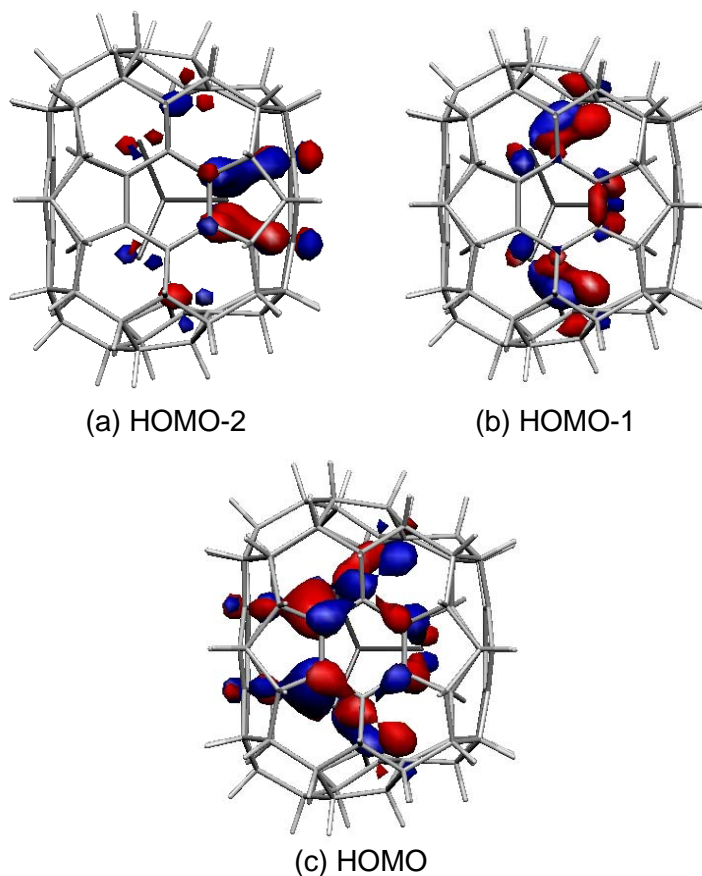


Figure 4.22 The three highest occupied molecular orbitals (MO) of $\text{Sc}_3\text{N}@C_{80}\text{H}_{52}:5$. The orbitals represent the bonding between (a) Sc atom and the 6 carbons of D benzenoid ring, (b) two Sc atoms and the two C=C bonds (C22–C23, C33–C34) and (c) Sc atom and the B benzenoid ring. All orbitals comprise the empty Sc *d*-orbitals and π^* C–C orbitals of $C_{80}\text{H}_{52}:5$.

shown by the maximum interaction term ($\Delta E_{\text{INT}} = -7.83$ eV) and minimum deformation of Sc_3N ($\Delta E_{\text{DE}} = 0.28$ eV) compared to the other isomers.

Unlike isomers $\text{Sc}_3\text{N}@C_{80}\text{H}_{52}:1$, **2**, **4**, **6** and **7**, which have at least four Sc–C₂ type and six Sc–C₆ type interactions, the most stable isomer $\text{Sc}_3\text{N}@C_{80}\text{H}_{52}:5$ has the advantage of two additional Sc–C₆ type interactions. Moreover these two additional bonding interactions are

Table 4.22 Relative binding energies (RE[HBE] and RE[EBE]) for the most stable $\text{Sc}_3\text{N}@C_{80}\text{H}_{52}$ isomers ^a

<i>Iso.</i> ^b	ΔE_{DE}	ΔE_{INT}	<i>HBE</i> ^c	$\frac{RE}{[HBE]}$	ΔE_{DE}	ΔE_{INT}	<i>EBE</i> ^d	$\frac{RE}{[EBE]}$	<i>Total RE</i> _e
1*	42.02	-63.58	-21.56	0.00	2.87	-6.94	-4.07	0.00	0.00
2°	42.04	-63.57	-21.53	0.03	3.13	-7.62	-4.49	-0.42	-0.39
4°	41.41	-62.64	-21.23	0.33	3.15	-7.12	-3.97	0.10	0.43
5*	41.30	-62.55	-21.25	0.31	2.90	-7.83	-4.93	-0.86	-0.55
6°	41.12	-62.33	-21.21	0.35	3.10	-7.77	-4.67	-0.60	-0.25
7°	41.41	-62.65	-21.24	0.32	3.03	-6.98	-3.95	0.12	0.44
9*	--	--	-19.83	1.73	--	--	-4.03	0.04	1.77
12°	--	--	-20.12	1.44	--	--	-5.02	-0.95	0.49
14^a	--	--	-17.98	3.58	--	--	-4.75	-0.68	2.90

^a Energies in eV. The binding energy of $\text{Sc}_3\text{N}@C_{80}\text{H}_{52}$ isomers comprise the energy required to hydrogenate C_{80} to the $C_{80}\text{H}_x$ isomers (HBE) and the energy of incarcerating Sc_3N (EBE). This necessarily differs from the experimental sequence involving encapsulation followed by hydrogenation. ^b * = C_{5s} ; ° = C_2 and ^a = C_{2v} . Symmetry of $\text{Sc}_3\text{N}@C_{80}\text{H}_{52}$ which in some cases is reduced from corresponding symmetry of $C_{80}\text{H}_{52}$ isomers. ^c Hydrogenation binding energy (HBE), ΔE for $C_{80} + 26 \text{H}_2 \rightarrow C_{80}\text{H}_{52}$. $\text{HBE} = \Delta E_{DE} + \Delta E_{INT}$. ^d Encapsulation binding energy (EBE), ΔE for $C_{80}\text{H}_{52} + \text{Sc}_3\text{N} \rightarrow \text{Sc}_3\text{N}@C_{80}\text{H}_{52}$. $\text{EBE} = \Delta E_{DE} + \Delta E_{INT}$. $\Delta E_{DE} = \Delta E_{DE}(\text{Sc}_3\text{N}) + \Delta E_{DE}(\text{cage})$. ^e Total RE = RE[HBE] + RE[EBE].

obtained with only minor distortion of the Sc_3N unit. Finally, it is noteworthy that for encapsulation of Sc_3N unit inside isomers $C_{80}\text{H}_{52}$:**12** and **14** the EBE is not enough to counteract the destabilization produced by the HBE. This is important because it deters searching for $\text{Sc}_3\text{N}@C_{80}\text{H}_{52}$ with a HBE for C_{80} destabilized more than 1 eV (the highest relative EBE found has been -0.95 eV for $\text{Sc}_3\text{N}@C_{80}\text{H}_{52}$:**12**).

In conclusion, the most stable $\text{Sc}_3\text{N}@C_{80}\text{H}_{52}$ isomer is that in which the Sc_3N unit can be hosted to allow the highest number of bonding interactions between the Sc atoms and the 28 free carbons, provided the destabilization produced by the HBE is not too high. This has allowed us to predict the most stable isomers for $\text{Sc}_3\text{N}@C_{80}\text{H}_x$ ($x = 44, 48, 72$) complexes.

4.9 CONCLUDING REMARKS

The experimental results illustrate that a wide range of new endohedral metallofullerenes that contain four atoms can be prepared in reasonably high yields and purity. The unique structure, chemistry and reactivity of these new encapsulated molecules will clearly provide new directions in host-guest chemistry. The fact that the internal atomic or molecular species (*e.g.* Er, Sc, Gd, etc. as well as mixed metals), the number of caged atoms and the fullerene cage size (*e.g.* C₆₈, C₇₈, C₈₀) can be controlled separately in TNT endohedral metallofullerenes means that considerably more variations may be found in the near future. The TNT process for the production of endohedral metallofullerenes opens up new vistas for developing and understanding how the properties are determined by metal encapsulation and for exploiting these unique materials in a wide range of electronic, optoelectronic, magnetic, catalytic, nanomechanical and medical applications.

Experimental advances. A new family of trimetallic nitride template (TNT) endohedral metallofullerenes have been synthesized and fully characterized recently in yields that are relatively higher than the classical endohedral metallofullerenes with a formula of A_{3-n}B_nN@C_k (*n* = 0-3; A and B = group III, IV and rare-earth metals, *k* = 68, 78, 80). The archetypal examples are: Sc₃N@C₈₀, Sc₃N@C₇₈ and Sc₃N@C₆₈. The high yields produced by the modified Krätschmer-Huffman method have enabled these new endohedral metallofullerenes to be fully characterized by X-ray and spectroscopic techniques. It is interesting to see that the IPR fullerene cages encapsulating the TNT units (*D*_{3h}-C₇₈:**5**, *I*_h-C₈₀:**7**) are not the most stable IPR isomers for each stoichiometry. The theoretically most stable and experimentally isolable isomers are the *C*_{2v}-C₇₈:**3** and *D*_{5d}-C₈₀:**1** fullerene isomers. Even the TNT encapsulation can stabilize non-IPR cages such as *D*₃-C₆₈:**6140**. Finally, the exohedral functionalization via cycloaddition and fluorination addition reactions has been carried out successfully, mostly in the Sc₃N@C₈₀ complex.

Ionic bond. Sc₃N@C_k (*k* = 68, 78, 80) complexes may be formally described by the ionic model Sc₃N⁶⁺@C_k⁶⁻. A total of six electrons formally

go from the three highest occupied orbitals to three low-lying unoccupied cage orbitals. The resulting endohedral complex has a relatively high HOMO-LUMO gap, which confers stability. We have shown that the final HOMO-LUMO gap of these TNT endohedral metallofullerenes can be estimated from the LUMO+3-LUMO+4 gap found in the free cages, which corresponds to the hypothetical anion when six additional electrons are added to the free cage, C_k^{6-} . The search for high LUMO+3-LUMO+4 gaps in the 51 IPR isomers of the cages between C_{60} and C_{84} revealed that only D_{3h} - C_{78} :**5**, D_{5h} - C_{80} :**6** and I_h - C_{80} :**7** provide an electronic structure that is suitable for encapsulating the TNT units. Moreover, the non-IPR D_3 - C_{68} :**6140** cage was similarly stabilized by the formal six electron charge transfer. Indeed, only these cages have been detected experimentally to encapsulate TNT units. Two conclusions can be drawn the electronic structure of TNT endohedral metallofullerenes: (1) the IPR cannot be applied to charged fullerenes, and (2) so far only endohedral metallofullerenes have been capable of producing non-IPR fullerenes and non-stabilized IPR fullerene cages.

$Sc_3N@C_{78}$. In the endohedral $Sc_3N@C_{78}$ the Sc_3N unit lies planar unlike the free Sc_3N and the scandium ions are strongly linked to pyracylene 6:6 C–C bonds. This bond does not allow the Sc_3N unit to rotate freely inside the fullerene. Steric repulsion forces the C_2 units closest to the Sc ions to be pushed away from the fullerene surface, a feature that the original X-ray characterization of $Sc_3N@C_{78}$ did not show. The consequence is an increment in the cage radius and an elongation of the pyracylene 6:6 C–C bonds. However, re-examination of the crystallographic data using the computed structure for $Sc_3N@C_{78}$ shows that this model provides a better fit to the data than the rigid C_{78} cage used previously. The EBE for this TNT endohedral metallofullerene is computed to be -9.70 eV, rather large stabilization energy. Although $Sc_3N@C_{78}$ may also be *formally* described by the $Sc_3N^{6+}@C_{78}^{6-}$ ionic model, the difference of 1.11 eV between the most and least stable isomers ($Sc_3N@C_{78}$:**1** and $Sc_3N@C_{78}$:**3**, respectively), constructed by the hypothetical Sc_3N rotation, is basically due to an *orbital* effect.

$Sc_3N@C_{80}$. In essence, the bond between the Sc_3N unit and the icosahedral isomer of C_{80} is comparable to the analogous bond in C_{78} , but the lack of any pyracylene C–C bond in I_h-C_{80} :**7** makes the two endohedrals ($Sc_3N@C_{78}$ and $Sc_3N@C_{80}$) different. In the latter, the scandium ions are not trapped in a specific position in the fullerene. This was confirmed experimentally by (1) the numerous Sc_3N orientations in complexes with the $Sc_3N@C_{80}$ unit; and (2) the ^{13}C NMR spectrum which preserves the I_h symmetry of the cage. The majority of the isomers are less stable than the most stable isomer—where the Sc atoms are facing three corannulene 6:5 C–C bonds—by only 0.01–0.08 eV. The EBE is somewhat higher for the larger cluster, a fact that may be attributed to the smaller steric repulsion.

$Sc_3N@C_{68}$. All isomers of C_{68} are non-IPR fullerenes but isomer $D_{3h}-C_{68}$:**6140** has the minimum number of destabilising fused pentagon pairs, which means that it has an advantage over the other isomers with a higher number of this kind of C–C bonds. The nitride donates six electrons to the C_{68} cage, so the resulting closed-shell electronic structure with a high HOMO-LUMO gap is formally described as the $Sc_3N^{6+}@C_{68}^{6-}$ ionic model. It is noteworthy that only endohedral encapsulation is capable of producing non-IPR fullerene cages since these cages would be very unstable as free fullerenes. This fullerene is significantly different from the other fullerenes whose endohedral complexes are detected. $D_{3h}-C_{78}$:**5** and I_h-C_{80} :**7** are spherical with a cage radius of 4.052 Å and 4.103 Å, respectively, but C_{68} not only has a smaller cage radius (3.783 Å) but also a distorted cage with only one plane which can accommodate the host. In this plane, where the planar Sc_3N is directly connected to 5:5 ring junctions, there is enough space to encapsulate the TNT unit because the distances between the fullerene surface and the cage-center are similar to those found in C_{78} and C_{80} fullerene cages. Only one Sc_3N orientation is possible for the $Sc_3N@C_{68}$ complex. The EBE and its decomposition is similar to those found in C_{80} . Although C_{68} has a higher steric repulsion term because it is smaller, the highest stabilization in the orbital interaction compensates for this destabilization.

Extended family. The geometry and electronic structure of the encapsulation of the Y_3N and La_3N TNT units inside the D_{3h} - C_{78} :**5** and I_h - C_{80} :**7** cages were studied. The TNT unit maintains a pyramidal shape because the ionic radius of the Y and La atoms increases. This prevents the unit from being planarized. Although the electron charge transfer to the cage in these new members of the TNT endohedral metallofullerenes is expected to be higher, the formal electronic structure can also be described as $M_3N^{6+}@C_k^{6-}$ ($M = Y$ and La , $k = 78, 80$). This observation disagrees with the electronic structure for $La_3N@C_{80}$ proposed by Kobayashi, who theorizes about an eight electron charge transfer from the TNT unit to the cage. In our studies, this electron charge transfer is not observed because it involves the removal of highly stabilized electrons from the p nitrogen orbitals. It is expected that encapsulation of TNT units containing a variety of metals will extend and enrich the research area of TNT endohedral metallofullerenes.

Physical properties. The formal transfer of six electrons from the TNT unit to the cage reduces the electron affinity (EA) of the TNT endohedral metallofullerenes with respect to the analogous free cages. This behavior differs from that of the classical endohedral metallofullerenes, the EA of which increases after the metal unit is encapsulated. However, these TNT endohedrals still retain relatively large EAs, which suggests that their redox properties are similar to those of C_{60} . The ionization potentials (IPs) are calculated to be slightly smaller. This is because the HOMOs in the TNT endohedral metallofullerenes are less stable than in the empty cages. In conclusion, TNT endohedral metallofullerenes are better electron donors and worse electron acceptors than the corresponding free fullerenes.

Exohedral reactivity: [4 + 2] cycloaddition. $Sc_3N@C_{80}$ and $Sc_3N@C_{78}$ complexes have already been exohedrally functionalized via cycloaddition reactions. The TNT endohedral metallofullerenes of C_{80} , C_{78} and C_{68} have demonstrated that endohedral doping of the free fullerenes changes the exohedral reactivity of the fullerene surface in two ways: (1) it reduces and changes the reactivity of all C–C bonds, principally those around the carbon region that scandiums are facing; and (2) it improves the regioselectivity in the case of C_{80} , the character of which was very poor but

does not improve it in the cases of C_{68} and C_{78} . In general, TNT encapsulation is a new tool for the regioselectivity in the addition reactions to fullerenes. The combination of the analysis of the MBO and the pyramidalization angle of the C–C bonds is a general tool for predicting the most reactive site. The most pyramidalized C–C bonds with the highest MBO appear to be the most reactive in the [4 + 2] cycloaddition of 1,3-butadiene.

Exohedral reactivity: hydrogenation and fluorination of $Sc_3N@C_{80}$. We calculated the stabilities of the highly hydrogenated and fluorinated $I_h-C_{80}:7$ fullerene cages, both of which are empty and contain the Sc_3N molecule. We also confirmed that the hydrogenation of the free fullerene is more favourable than the hydrogenation of the $Sc_3N@C_{80}$ metallofullerene. The addition of 44 hydrogen atoms to C_{80} and $Sc_3N@C_{80}$ is predicted to be the most favourable addition pattern because of the formation of six octahedrally-located aromatic benzenoid rings, whilst the addition of up to 52 atoms (consistent with preliminary fluorination data) gives a structure that is stabilized by four aromatic benzenoid rings. The hydrogenation binding energy per added hydrogen (HBE/ n) remains constant for the addition of up to 52 atoms but at higher hydrogenation levels the HBE/ n reduces drastically because of the unreactivity of the remaining C–C bonds, which increase in length and have a low π bond order. The most stable isomers at this addition level were determined, and the relative stabilities of a number of $C_{80}H_{52}$, $C_{80}F_{52}$, and $Sc_3N@C_{80}H_{52}$ species were calculated. From the geometrical point of view, the Sc_3N molecule is planar in the parent C_{80} but is calculated to be pyramidal in some of the hydrogenated/fluorinated derivatives, where it also has fixed locations due to orbital interactions caused by the deformation of the cage and the presence of localized double bonds.

REFERENCES AND NOTES

- ¹ Stevenson, S.; Rice, G.; Glass, T.; Harich, K.; Cromer, F.; Jordan, M.R.; Craft, J.; Hadju, E.; Bible, R.; Olmstead, M. M.; Maltra, K.; Fisher, A. J.; Balch, A. L.; Dorn, H. C. *Nature*, **1999**, 401, 55.
- ² Stevenson, S.; Fowler, P. W.; Heine, T.; Duchamps, J. C.; Rice, G.; Glass, T.; Harich, K.; Hajdu, E.; Bible, R.; Dorn, H. C. *Nature* **2000**, 408, 428.
- ³ Jacobs, H. O.; Tao, A. R.; Schwartz, A.; Gracias, D. H.; Whitesides, G. M. *Science* **2002**, 296, 323.
- ⁴ Olmstead, M. M.; Bettencourt-Dias, A.; Duchamp J. C.; Stevenson, S.; Marcui, D.; Dorn, H. C.; Balch, A. L. *Angew. Chem., Int. Ed. Engl.* **2001**, 40, 1223.
- ⁵ Stevenson, S.; Dorn, H. C.; Burbank, P.; Harich, K. *Anal. Chem.* **1994**, 66, 2675.
- ⁶ (a) Olmstead, M. M.; Costa, D. A.; Maitra, K.; Noll, B. C.; Philips, S. L.; Van Calcar, P. M.; Balch, A. L. *J. Am. Chem. Soc.* **1999**, 121, 7090. (b) Boyd, P. D. W.; Hodgson, M. C.; Rickard, C. E. F.; Oliver, A. G.; Chaker, L.; Brothers, P. J.; Bolskar, R. D.; Tham, F. S.; Reed, C. A. *J. Am. Chem. Soc.* **1999**, 121, 10487. (c) Dunsch, L.; Bartl, A.; Georgi, P.; Kuran, P. *Synth. Met.* **2001**, 121, 1113.
- ⁷ Krause, M.; Kuzmany, H.; Georgi, P.; Dunsch, L.; Vietze, K.; Seifert, G. *J. Chem. Phys.* **2001**, 115, 6596.
- ⁸ Dunsch, L.; Krause, M.; Noack, J.; Georgi, P. *J. Phys. Chem. Sol.* **2004**, 65, 309.
- ⁹ Duchamp, J. C.; Demortier, A.; Fletcher, K. R.; Dorn, D.; Iezzi, E. B.; Glass, T.; Dorn, H. C. *Chem. Phys. Lett.* **2003**, 375, 655.
- ¹⁰ Kroto, H. *Nature* **1987**, 329, 529. (b) Smalz, T. G.; Seitz, W. A.; Klein, D. J.; Hite, G. E. *J. Am. Chem. Soc.* **1988**, 110, 1113.
- ¹¹ Olmstead, M. M.; Bettencourt-Dias, A.; Duchamp, J. C.; Stevenson, S.; Dorn, H. C.; Balch, A. L. *J. Am. Chem. Soc.* **2000**, 122, 12220.
- ¹² Iezzi, E. B.; Ducamp, J. C.; Fletcher, K. R.; Glass, T. E.; Dorn, H. C. *Nano Lett.* **2002**, 2, 1187.
- ¹³ Iezzi, E. B.; Ducamp, J. C.; Harich, K.; Glass, T. E.; Lee, H. M.; Olmstead, M. M.; Balch, A. L.; Dorn, H. C. *J. Am. Chem. Soc.* **2002**, 124, 524.
- ¹⁴ Lee, H. M.; Olmstead, M. M.; Iezzi, E.; Duchamp, J. C.; Dorn, H. C.; Balch, A. L. *J. Am. Chem. Soc.* **2002**, 124, 3494.
- ¹⁵ Iezzi, E. B.; Cromer, F.; Stevenson P.; Dorn, H. C. *Synth. Metals* **2002**, 128, 289.
- ¹⁶ Darwish, A. D.; Dorn, H. C.; Taylor, R. unpublished work.
- ¹⁷ Iezzi, E. B. Ph. D. Dissertation *Exohedral Functionalization and Applications of the Trimetallic Nitride Endohedral Metallofullerenes*, Virginia Tech, 2003.
- ¹⁸ Gillan, E. G.; Yerezian, C.; Min, K. S.; Alvarez, M. M.; Whetten, R. L.; Kaner, R. B. *J. Phys. Chem.* **1992**, 96, 6869.

-
- ¹⁹ Fowler, P. W.; Zerbetto, F. *Chem. Phys. Lett.* **1995**, *243*, 36.
- ²⁰ Fowler, P. W.; Manolopoulos, D. E. *An Atlas of Fullerenes*, Oxford University Press, Oxford, **1995**.
- ²¹ (a) Hennrich, F. H.; Michel, R. H.; Fischer, A.; Richard-Schneider, S.; Gilb, S.; Kappes, M. M.; Fuchs, D.; Bürk, M.; Kobayashi, K.; Nagase, S. *Angew. Chem. Int. Ed.* **1996**, *35*, 1732. (b) Wang, C. R.; Sugai, T.; Kai, T.; Tomiyama, T.; Shinohara, H. *Chem. Commun.* **2000**, 557.
- ²² Kobayashi, K.; Nagase, S.; Akasaka, T. *Chem. Phys. Lett.* **1995**, *245*, 230.
- ²³ Cao, B.; Hasegawa, M.; Okada, K.; Tomiyama, T.; Okazaki, T.; Kazutomo, S.; Shinohara, H. *J. Am. Chem. Soc.* **2001**, *123*, 9674.
- ²⁴ Kobayashi, K.; Sano, Y.; Nagase, S.; *J. Comput. Chem.* **2001**, *22*, 1353.
- ²⁵ Akasaka, T.; Nagase, S.; Kobayashi, K.; Wälchli, M.; Yamamoto, K.; Funasaka, H.; Kako, M.; Hoshino, T.; Erata, T. *Angew. Chem., Int. Ed. Engl.* **1997**, *36*, 1643.
- ²⁶ (a) Zhang, B. L.; Wang, C. Z.; Ho, K. M. *Chem. Phys. Lett.* **1992**, *193*, 225. (b) Slanina, Z.; Francois, J. P.; Bakowies, D.; Thiel, W. *J. Mol. Struct. (THEOCHEM)* **1993**, *279*, 213. (c) Bühl, M.; van Wüllen, C. *Chem. Phys. Lett.* **1995**, *247*, 63. (d) Osawa, E.; Ueno, H.; Yoshida, M.; Slanina, Z.; Zhao, X.; Nishiyama, M.; Saito, H. *J. Chem. Soc. Perkin Trans 2* **1998**, 943. (e) Sun, G.; Kertesz, M. *J. Phys. Chem. A* **2000**, *104*, 7398. (f) Heine, T.; Seifert, G.; Fowler, P. W.; Zerbetto, F. *J. Phys. Chem.* **1999**, *103*, 8738.
- ²⁷ (a) Diederich, F.; Whetten, R. L.; Thielgen, C.; Ettl, R.; Chao, I.; Alvarez, M. M. *Science* **1991**, *254*, 1768. (b) Kikuchi, K.; Nakahara, N.; Wakabayashi, T.; Suzuki, S.; Shiromaru, H.; Miyake, Y.; Saito, K.; Ikemoto, I.; Kainosho, M.; Achiba, Y. *Nature*, **1992**, *357*, 142. (c) Taylor, R.; Langley, J. G.; Dennis, T.J.S.; Kroto, H. W.; Walton, D. R. M. *J. Chem. Soc. Chem. Commun.* **1992**, 1043.
- ²⁸ Akasaka, T.; Nagase, S. *Endofullerenes: a new family of carbon clusters, Developments in fullerene science*, Kluwer Academic Publishers, Dordrecht, 2002, chapter 4 and 5.
- ²⁹ David, W. I. F.; Ibberson, R. M.; Mattewman, J. C.; Prassides, K.; Dennis, T. J. S.; Hare, P. J.; Kroto, H. W.; Taylor, R.; Walton, D. R. M. *Nature* **1991**, *252*, 1160.
- ³⁰ Hedberg, K.; Hedberg, L.; Bethune, D.S.; Brown, C.A.; Dorn, H.C.; Johnson, R. D.; de Vries, M. *Science* **1991**, *254*, 410.
- ³¹ Balch, A.; Olmstead, M. M. *Chem. Rev.* **1998**, *98*, 2123.
- ³² Campanera, J. M.; Bo, C.; Olmstead, M. M.; Balch, A. L.; Poblet, J. M. *J. Phys. Chem. A* **2002**, *106*, 12356.

-
- ³³ Nishibori, E.; Takata, M.; Sakata, M.; Inakuma, M.; Shinohara, H. *Chem. Phys. Lett.* **1998**, *298*, 79.
- ³⁴ Takata, M.; Nishibori, E.; Umeda, B.; Sakata, M.; Yamamoto, E.; Shinohara, H. *Phys. Rev. Lett.* **1997**, *78*, 3330.
- ³⁵ Kobayashi, K.; Nagase, S. *Chem. Phys. Lett.* **1998**, *282*, 325.
- ³⁶ Olmstead, M. M.; Lee, H. M.; Duchamp, J. C.; Stevenson, S.; Marciu, D.; Dorn, H. C.; Balch, A. L. *Angew. Chem. Int. Ed.* **2003**, *42*, 900.
- ³⁷ Kobayashi, K.; Nagase, S.; Yoshida, M.; Osawa, E. *J. Am. Chem. Soc.* **1997**, *119*, 12693.
- ³⁸ Nagase, S.; Kobayashi, K.; Akasaka, T. *J. Mol. Struct. (Theochem)* **1999**, *97*, 161.
- ³⁹ Dorn, H. C.; Stevenson, S.; Burbank, P.; Harich, K.; Sun, T.; Glass, T.; Anderson, A.; Bethume, D. S.; Sherwood, M. *Recent Advances in the Chemistry and Physics of Fullerenes and Related Materials* Kadish, K. M. and Ruoff, R. S., Eds., Pennington, The Electrochemical Society, Inc., 1998, p. 990.
- ⁴⁰ Wang, C.; Kai, T.; Tomiyama, T.; Yoshida, T.; Kobayashi, Y.; Nishibori, E.; Takata, M.; Sakata, M.; Shinohara, H. *Nature* **2000**, *408*, 426.
- ⁴¹ Aihara, A. *Chem. Phys. Lett.* **2001**, *343*, 465.
- ⁴² (a) Fowler, P. W.; Heine, T.; Manolopoulos, D. E.; Mitchell, D.; Orlandi, G.; Schmidt, R.; Seifert, G.; Zerbetto, F. *J. Phys. Chem.* **1996**, *100*, 6984. (b) Fowler, P. W.; Manolopoulos, D. E.; Orlandi, G.; Zerbetto, F. *J. Chem. Soc., Faraday Trans.* **1995**, *91*, 1421. (c) Fowler, P. W.; Heine, T.; Manolopoulos, D. E.; Mitchell, D.; Orlandi, G.; Schmidt, R.; Seifert, G.; Zerbetto, F. *J. Chem. Soc., Faraday Trans.* **1996**, *92*, 2203.
- ⁴³ Lee, S. L.; Sun, M. L.; Slanina, Z. *Int. J. Quantum Chem.* **1996**, *60*, 355.
- ⁴⁴ Coppens, P.; Hall, M. B. *Electron Distributions and the Chemical Bond* Eds. Plenum Press, New York, **1981**.
- ⁴⁵ (a) Roszak, S.; Balasubramanian, K. *J. Phys. Chem. A* **1997**, *101*, 2666. (b) Benard, M.; Rohmer, M. M.; Poblet, J. M. *Chem. Rev.* **2000**, *100*, 495. (c) Li, X.; Wang, L. S. *J. Chem. Phys.* **1999**, *111*, 8389.
- ⁴⁶ (a) Ziegler, T.; Rauk, A. *Teor. Chim. Acta* **1977**, *46*, 1. (b) Ziegler, T.; Rauk, A. *Inorg. Chem.* **1979**, *18*, 1558.
- ⁴⁷ (a) Morokuma, K. *J. Chem. Phys.* **1971**, *55*, 1236. (b) Kitaura, K.; Morokuma, K. *Int. J. Quantum Chem.* **1976**, *10*, 325.
- ⁴⁸ Nunzi, F.; Sgamelloti, A.; Re, N.; Floriani, C. *Organometallics* **2000**, *19*, 1628.
- ⁴⁹ Gonzalez-Blanco, O.; Branchadell, V. *Organometallics*, **1997**, *16*, 5556.
- ⁵⁰ In structures **6-12** the four atoms of the Sc₃N fragment are not strictly coplanar but the deviation from the planarity is very small.

-
- ⁵¹ Yang, S. H.; Pettiette, C. L.; Conceicao, J.; Cheshnowsky, O.; Smalley, R. E. *Chem. Phys. Lett.* **1987**, *139*, 233.
- ⁵² Brink, C.; Andersen, L. H.; Hvelplund, P.; Mathur, D.; Voldstad, J. D. *Chem. Phys. Lett.* **1995**, *233*, 52.
- ⁵³ Ioffe, I. N.; Boltalina, O. V.; Sidorov, L. N.; Dorn, H. C.; Stevenson, S.; Rice, G. *Fullerenes: Recent Advances in the Chemistry and Physics of Fullerenes and Related Materials*; Kadish, K. M.; Ruoff, R. S., Eds., Electrochemical Society, Pennington, **2000**; p. 166.
- ⁵⁴ Dorn, H. C.; Stevenson, S.; Craft, J.; Cromer, F.; Duchamp, J.; Rice, G.; Glass, T.; Harich, K.; Fowler, P. W.; Heine, T.; hajdu, E.; Bible, R.; Olmstead, M.M.; Maitra, K.; Fisher, A. J.; Balch, A. L. Proc IWEPNM2000 Conf 2000, 135.
- ⁵⁵ Shinohara, H. *Rep. Prog. Phys.* **2000**, *63*, 843.
- ⁵⁶ (a) Aihara, J. *J. Am. Chem. Soc.* **1995**, *117*, 4130. (b) Aihara, J. *J. Phys. Chem.* **1995**, *99*, 12739. (c) Aihara, J.; Oe, S.; Yoshida, M.; Osawa, E. *J. Comput. Chem.* **1996**, *17*, 1387. (d) Aihara, J. *Bull. Chem. Soc. Jpn.* **1999**, *72*, 7 (e) Aihara, J. *Phys. Chem.* **2001**, *3*, 1427. (f) Aihara, J. *Chem. Phys. Lett.* **2001**, *343*, 465.
- ⁵⁷ Manolopoulos, D. E.; May, J. C.; Down, S. E. *Chem. Phys. Lett.* **1991**, *181*, 105.
- ⁵⁸ Minkin, V. I. *Pure Appl. Chem.* **1999**, *71*, 1919
- ⁵⁹ (a) Aihara, J. *J. Am. Chem. Soc.* **1976**, *98*, 2750. (b) Gutman, I.; Milun, M.; Trinajstić, N. *J. Am. Chem. Soc.* **1977**, *99*, 1692.
- ⁶⁰ Aihara, J. *J. Phys. Chem. A* **2002**, *106*, 11371.
- ⁶¹ <http://www.cochem2.tutkie.tut.ac.jp/Fuller/Fuller.html>
- ⁶² (a) Solà, M.; Duran, M.; Mestres, J. *J. Am. Chem. Soc.* **1996**, *118*, 8920. (b) Mestres, J.; Duran, M.; Solà, M. *J. Phys. Chem.* **1996**, *100*, 7449.
- ⁶³ Akasaka, T.; Nagase, S.; Kobayashi, K.; Suzuki, T.; Kato, T.; Kikuchi, K.; Achiba, Y.; Yamamoto, K.; Funasaka, H.; Takahashi, T. *Angew. Chem., Int. Ed. Engl.* **1995**, *34*, 19.
- ⁶⁴ Takeshi, A.; Kato, T.; Kobayashi, K.; Nagase, S.; Yamamoto, K.; Funasaka, H.; Takahashi, T. *Nature* **1995**, *374*, 600.
- ⁶⁵ Maeda, Y.; Matsunaga, Y.; Wakahara, T.; Takahashi, S.; Tsuchiya, T.; Ishitsuka, O.; Hasegawa, T.; Akasaka, T.; Liu, M. T. H.; Kokura, K.; Horn, E.; Yoza, K.; Kato, T.; Okubo, S.; Kobayashi, K.; Nagase, S.; Yamamoto, K. *J. Am. Chem. Soc.* **2004**, *126*, 6858.
- ⁶⁶ Kobayashi, K.; Nagase, S.; Maeda, Y.; Wakahara, T.; Akasaka, T. *Chem. Phys. Lett.* **2003**, *374*, 562.
- ⁶⁷ (a) Belik, P.; Gügel, A.; Kraus, A.; Spickermann, J.; Enkelmann, V.; Frank, G.; Müllen, K. *Adv. Mater.* **1993**, *5*, 854. (b) Belik, P.; Gügel, A.; Kraus, A.;

-
- Spickermann, J.; Enkelmann, V.; Frank, G.; Müllen, K. *Angew. Chem., Int. Ed. Engl.* **1993**, *32*, 78.
- ⁶⁸ (a) Haddon, R. C.; Scott, L. T. *Pure Appl. Chem.* **1986**, *58*, 137. (b) Haddon, R. C. *J. Am. Chem. Soc.* **1986**, *108*, 2837. (c) Haddon, R. C.; Chow, S. Y. *J. Am. Chem. Soc.* **1998**, *120*, 10494.
- ⁶⁹ Haddon, R. C. *Acc. Chem. Res.* **1988**, *21*, 243.
- ⁷⁰ (a) Rabideau, P. W.; Sygula, A. *Acc. Chem. Res.* **1996**, *29*, 235. (b) Abdourazak, A. H.; Marcinow, Z.; Sygula, A.; Sygula, R.; Rabideau, P. W. *J. Am. Chem. Soc.* **1995**, *117*, 6410.
- ⁷¹ (a) Mayer, I. *Chem. Phys. Lett.* **1983**, *97*, 270. (b) Mayer, I. *J. Quantum Chem.* **1984**, *26*, 151.
- ⁷² Wiberg, K. A. *Tetrahedron* **1968**, *24*, 1083.
- ⁷³ Bridgeman, A. J.; Cavigliasso, G. *Faraday Discussions* **2003**, *124*, 239.
- ⁷⁴ Darwish, A. D.; Avent, A. G.; Boltalina, O. V.; Stevenson S.; Taylor, R. unpublished work.
- ⁷⁵ Fowler, P. W.; Sandall, J. P. B.; Taylor, R. *J. Chem. Soc., Perkin Trans. 2* **1997**, 419.
- ⁷⁶ Jones, R.; Briddon, P. R. *Semicond. Semimet.* **1998**, *51A*, 287.
- ⁷⁷ Some of the structures reported here could eventually be saddle points corresponding to hydrogen transfer between two minima. The characterization would require the calculation of the vibrational frequencies but this still requires a huge computational effort.
- ⁷⁸ (a) Darwish, A. D.; Avent, A. G.; Taylor, R.; Walton, D. *J. Chem. Soc., Perkin Trans. 2*, **1996**, 2051. (b) Boltalina, O. V.; Markov, V. Yu.; Taylor, R.; Waugh, M. P. *Chem. Commun.* **1996**, 2549. (c) Boltalina, O. V.; Street, J. M.; Taylor, R. *J. Chem. Soc., Perkin Trans. 2* **1998**, 649. (d) Nossal, J.; Saini, R. K.; Sadana, A. K.; Bettinger, H. F.; Alemany, L. B.; Scuseria, G. E.; Billups, W. E.; Saunders, M.; Khong, A.; Weisemann, R. *J. Am. Chem. Soc.* **2001**, *123*, 8482.
- ⁷⁹ (a) Hitchcock, P. B.; Taylor, R. *Chem. Commun.* **2002**, 2078. (b) Avent, A. G.; Clare, B. W.; Hitchcock, P. B.; Kepert, D. L.; Taylor, R. *Chem. Commun.* **2002**, 2370.
- ⁸⁰ Cioslowski, J. *Chem. Phys. Lett.* **1991**, *181*, 68.
- ⁸¹ For collation of data and leading references see (a) Taylor, R.; Langley, G. J.; Holloway, J. H.; Hope, E. G.; Brisdon, A. K.; Kroto, H. K.; Walton, D. R. M. *J. Chem. Soc., Perkin Trans. 2* **1995**, 181. (b) Darwish, A. D.; Abdul-Sada, A. K.; Langley, G. J.; Kroto, H. W.; Taylor, R.; Walton, D. R. M. *J. Chem. Soc., Perkin Trans. 2* **1995**, 2359.

-
- ⁸² (a) Taylor, R. *Philos. Trans. R. Soc. London, A* **1993**, 343, 87. (b) Austin, S. J.; Batten, R. C.; Fowler, P. W.; Redmond, D. B.; Taylor, R. *J. Chem. Soc., Perkin Trans. 2* **1993**, 1383.
- ⁸³ Troyanov, S. I.; Troshin, P. A.; Boltalina, O. V.; Ioffe, I. N.; Sidorov, L. N.; Kemnitz, E. *Angew. Chem., Int. Ed. Engl.* **2001**, 40, 2285.
- ⁸⁴ Neretin, I. S.; Lyssenko, K. A.; Antipin, M. Yu.; Slovokhotov, Yu. L.; Boltalina, O. V.; Troshin, P. A.; Lukonin, A. Yu.; Sidorov, L. N.; Taylor, R. *Angew. Chem., Int. Ed. Engl.* **2000**, 39, 3273.

